AFAL-TR-76-34

AD A042073

AN ELECTRICAL, CHEMICAL, AND STRUCTURAL STUDY OF THE Ge(100)/Cs/O PHOTOSURFACE

UNIVERSITY OF MINNESOTA

APRIL 1977

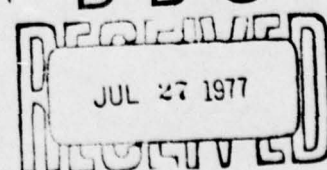TECHNICAL REPORT AFAL-TR-76-34
JULY 1, 1972 - MAY 31, 1975

AIR FORCE AVIONICS LABORATORY
AIR FORCE WRIGHT AERONAUTICAL LABORATORIES
AIR FORCE SYSTEMS COMMAND
WRIGHT-PATTERSON AIR FORCE BASE, OHIO 45433
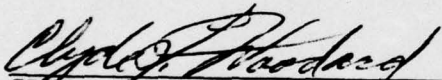
D D C

JUL 27 1977

F

NOTICE

When Government drawings, specifications, or other data are used for any purpose other than in connection with a definitely related Government procurement operation, the United States Government thereby incurs no responsibility nor any obligation whatsoever; and the fact that the Government may have formulated, furnished, or in any way supplied the said drawings, specifications, or other data, is not to be regarded by implication or otherwise as in any manner licensing the holder or any other person or corporation, or conveying any rights or permission to manufacture, use, or sell any patented invention that may in any way be related thereto.
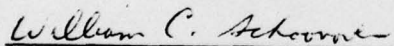
This technical report has been reviewed and is approved for publication.

This report has been reviewed by the Information Office (OI) and is releasable to the National Technical Information Service (NTIS). At NTIS, it will be available to the general public, including foreign nations.

CLYDE L. WOODARD, Chief
Electro-Optic Detectors Group
Electro-Optics Technology Branch

FOR THE COMMANDER

WILLIAM C. SCHOONOVER, Chief
Electro-Optics Technology Branch
Electronic Technology Division

Copies of this report should not be returned unless return is required by security considerations, contractual obligations, or notice on a specific document.

Technical rept. 1 Jul 72 -
31 May 75,

REPORT DOCUMENTATION PAGE		READ INSTRUCTIONS BEFORE COMPLETING FORM
1. REPORT NUMBER AFAL-TR-76-34	2. GOVT ACCESSION NO.	3. RECIPIENT'S CATALOG NUMBER
4. TITLE (and Subtitle) AN ELECTRICAL, CHEMICAL AND STRUCTURAL STUDY OF THE Ge(100)/Cs/O PHOTOSURFACE		5. TYPE OF REPORT & PERIOD COVERED TECHNICAL REPORT 7-1-72 - 5-31-75
		6. PERFORMING ORG. REPORT NUMBER
7. AUTHOR(s) Richard Edward Erickson		8. CONTRACT OR GRANT NUMBER(s) F33615-72-C-2105
9. PERFORMING ORGANIZATION NAME AND ADDRESS University of Minnesota Dept of Electrical Engineering Minneapolis, Minn. 55455		10. PROGRAM ELEMENT, PROJECT, TASK AREA & WORK UNIT NUMBERS 62204F 2001-03-31
11. CONTROLLING OFFICE NAME AND ADDRESS AFAL/DHO-3 Wright-Patterson AFB, Ohio 45433		12. REPORT DATE April 1977
		13. NUMBER OF PAGES 104
14. MONITORING AGENCY NAME & ADDRESS(if different from Controlling Office)		15. SECURITY CLASS. (of this report) UNCLASSIFIED
		15a. DECLASSIFICATION/DOWNGRADING SCHE

16. DISTRIBUTION STATEMENT (of this Report)

Approved for public release; distribution unlimited.

17. DISTRIBUTION STATEMENT (of the abstract entered in Block 20, if different from Report)

18. SUPPLEMENTARY NOTES

19. KEY WORDS (Continue on reverse side if necessary and identify by block number)

Photocathode   Electron Emission
Auger Spectroscopy   Work Function Leed
Photosurface

20. ABSTRACT (Continue on reverse side if necessary and identify by block number)

The Ge(100)/Cs/O photosurface and surfaces at intermediate stages of
activation are characterized in terms of photoemission, work function, Auger
electron spectroscopy (AES), low energy electron diffraction (LEED), and
elastic specular electron reflectivity (ESER). An electrical and structural
model is proposed for Ge/Cs/O which is consistent with this data. A number

233520

of experiments are reported which investigate the sensitivity of
the Ge/Cs/O surface to deviations from chemical and structural
perfection.

PREFACE

The research described in this report was carried out in the
Physical Electronics Laboratory of the University of Minnesota,
Minneapolis, Minnesota 55455 under Contract No. F33615-72-C-2105 -
Project 2001, Task 03, Work Unit 31,between July 1, 1972 and May
31, 1975. The work was supervised by W. T. Peria, Professor of
Electrical Engineering, University of Minnesota, Minneapolis,
Minnesota. The project monitor is W. H. Nelson, AFAL/ DHO Air
Force Avionics Laboratory, Wright-Patterson Air Force Base, Ohio.

iii

TABLE OF CONTENTS

LIST OF ILLUSTRATIONS

I. INTRODUCTION

Alkali-covered semiconductors have been studied with increasing frequency in recent years at least in part because of the potential of these materials as efficient photoelectron emitters.[1] These systems have also been used to examine semiconductor energy band structure by photoemission because of the considerable lowering of the surface barrier which takes place upon alkali adsorption. The reduced electron affinity effectively increases the escape probability for photoexcited electrons and extends the long wavelength photoelectric threshold. The same efficient photoemission is not exhibited by alkali-covered metals because of the high optical reflectivity and the short photoelectron path length due to strong electron-electron interactions.

Much of the early alkali-semiconductor effort was devoted to germanium and silicon. But as III-V semiconductor technology began to develop in the 1960's, these studies were gradually extended to the III-V materials. Out of this work came the GaAs/Cs negative electron affinity photocathode (Scheer and van Laar, 1965)[2] and subsequently a whole new class of III-V compound photocathodes which operated on the negative electron affinity (or NEA) principle. The NEA photocathode, unlike its predecessors, had effectively no surface barrier to prohibit the escape of bulk photoelectrons. Consequently, NEA devices were considerably more sensitive than cathodes of earlier design.

The operation of an NEA emitter is compared to that of a conventional "hot electron" emitter in Fig. 1. In both devices, electrons which are photoexcited into the conduction band rapidly "thermalize" to the conduction band minimum by giving energy to the crystal lattice. For a single electron this involves a large number of small energy losses over a fairly short path length (several hundred Å). A thermalized electron remains at the conduction band minimum until it has the opportunity to recombine with a valence band hole. The path length for such an event is typically hundreds of times longer than that for thermalization. Consequently, a photoexcited electron that has thermalized to the conduction band minimum may diffuse several microns before recombining across the gap. The internal energy distribution of photoelectrons (shown by the dotted line in Fig. 1) is therefore peaked near the conduction band minimum.

In the hot electron device, only those electrons which are very near the surface (100-1000 Å) are able to escape into vacuum. Electrons which have thermalized to the conduction band minimum are trapped within the solid by the surface barrier. In the NEA device, however, there is effectively no surface barrier for bulk electrons, and even those electrons which have thermalized several microns beneath the surface are able to diffuse to the surface and escape into vacuum. The escape depth is, in fact, the minority carrier (or electron) diffusion length, a factor of 100 to 1000 greater than the escape depth in the hot electron device. Consequently, the photoelectric sensitivity is greatly enhanced,

1

especially in the threshold region. This property is particularly useful in infrared or low light level applications.

It is evident from the diagram of Fig. 1 that for NEA to occur, the semiconductor must be doped heavily p-type. The p-type doping raises the bulk energy bands with respect to the surface bands because the position of the latter is determined independently by the surface state distribution. The resulting band-bending ensures that bulk valence band electrons are photoexcited into energy states as high as possible with respect to the vacuum level.

The density of the doping determines the width of the bent-band region. The density must be high enough that the bulk electrons are able to pass through this region to the surface without appreciable energy loss by phonon production, and yet low enough that electron transport in the bulk is not impaired by impurity scattering.

After the GaAs/Cs NEA photocathode was discovered in 1965, the cathode was not applied immediately to a practical device because it could be produced only with the best available materials and only in ultra-high vacuum. These difficulties were overcome when it was discovered that a lower work function could be generated with cesium oxide than with cesium alone,[3] permitting more reliable photoemission to be obtained from GaAs. This process also allowed NEA to be achieved on lower band gap III-V materials with the resultant extension of the infrared response. InGaAs/Cs-O[4], one of these devices, promises to replace the well-established S-1 photocathode (AgOCs) for infrared detection. In addition to a lower photoelectric threshold (~0.8 eV) and greater sensitivity, InGaAs/Cs-O also has a dark current smaller by several orders of magnitude.

In 1970, Martinelli[5] demonstrated that NEA could also be achieved on silicon upon activation with cesium and oxygen. Silicon appeared to offer advantages over its III-V counterparts in the area of transmission-mode devices. These devices require large-area self-supporting layers no thicker than the mean escape depth for photoelectrons. Silicon, with its long diffusion length and advanced materials technology, had obvious advantages in this application.

It was evident quite early that there were considerable differences between the silicon cathode and the III-V devices. Silicon, for example, could be activated by a single application of cesium and oxygen ("two-step process") rather than by a series of applications ("yo-yo process") which had to be used for the III-V materials. Only the (100) surface could be activated, whereas several faces could be activated for any of the III-V semiconductors. Low energy electron diffraction (LEED) indicated that the cesium and oxygen atoms occupied specific sites on the silicon surface, while no such ordering of the cesium oxide layer was observed for any of the III-V materials. Finally, the silicon photocathode had a much higher dark current (factor of 10^6) than any of the III-V NEA photocathodes.

All of these observations point to fundamental differences in the physical structure of the cesium oxide layer. These differences

2

have been discussed at length in recent publications by Levine[6], Goldstein[7], and Martinelli[8,9] of RCA laboratories and by J. R. Howorth, et al.[10] of the English Electric Valve Company. Levine proposes a structural model for Si/Cs/0 which attributes much of the photoelectric behavior to the silicon surface geometry rather than to the properties of cesium oxide. Martinelli lends considerable support to the Levine model with his report of achieving nearly identical emission characteristics using rubidium instead of cesium in the surface layer.

The present experiment is an extension of the silicon work to germanium. It was determined from earlier work in this laboratory by R. L. Erickson[11] that Ge(100) activates similarly to Si(100) with cesium and oxygen. The purpose of the present study was to add more insight into the Si/Cs/0 work while at the same time to determine whether NEA could be achieved with germanium. Apart from the photoelectric and work function measurements, emphasis was placed upon structural and chemical data, because of the sensitivity of Si/Cs/0 to these factors[12,13]. It was assumed that the same sensitivity would carry over to germanium, because of the identical clean surface structure.

Measurements of low energy electron diffraction (LEED) were used to link this work with Goldstein's Si/Cs/0 study, while measurements of elastic specular electron reflectivity (ESER) were used to provide a more quantitative probe of structural quality. Auger electron spectroscopy (AES) was used to detect surface contamination (sensitive to 1% monolayer of most elements) and to determine relative amounts of cesium and oxygen in the surface layer. Besides characterizing the Ge/Cs/0 surface at various stages of formation and formulating a surface model, an effort was made to understand those factors most critical to the photoelectric optimization process.

In the discussion to follow, the final photosurface produced by the two-step process will be referred to as the "activated" or the "optimized" surface. Adhering to the convention of Levine, it will be denoted by the symbol Ge/Cs/0. In the same manner, the "fully cesiated" or "cesium-saturated" surface will be denoted by Ge/Cs. Only these two particular surface designations will be written with the "slash" notation. Other surfaces, such as those at intermediate stages of formation, will be designated with the more general "dash" symbolism, e.g. Ge-Cs or Ge-Cs-0.

II. EXPERIMENTAL TECHNIQUES AND APPARATUS

The Ge/Cs/0 photosurface, like Si/Cs/0, is formed by reacting roughly "monolayer" quantities of cesium and oxygen on the atomically clean (100) crystalline surface. The cathode is very reactive and can only be successfully formed and maintained in ultrahigh vacuum. Goldstein[12] has found that for the similar Si/Cs/0 cathode, a well-ordered and chemicaly clean initial surface is important for successful activation. Consequently, considerable emphasis was placed in the present experiment upon the procurement of structural and chemical data.

The desired structural information was obtained by means of low energy electron diffraction (LEED) and measurements of elastic specular electron reflectivity (ESER), while surface chemical information was obtained by means of Auger electron spectroscopy (AES). Measurements of work function and photoelectric emission were used both to characterize the various surfaces under study and to gauge the performance of the final activated surface. The principal aim of the experiment was to understand the photocathode formation process in terms of appropriate electrical, chemical, and structural parameters. Particular emphasis was placed upon the discovery of those factors leading to optimum photoelectric response.

This section deals primarily with the various experimental techniques used in the investigation rather than with a detailed description of the experimental apparatus. All of the apparatus has been used before in this laboratory and is discussed at length in other sources. Reference to these sources is made in the text where appropriate. A rudimentary description of each technique is given here, along with a discussion of the information which could be extracted via that technique. The assumptions associated with each measurement are examined, as well as limitations and possible sources of error.

1. Vacuum System

The vacuum system used in the activation study was a 12-inch diameter stainless steel chamber (Ultek model TNB) equipped with ion pumping (100 liters/sec) and titanium sublimation pumping. An overall view of the system is shown in Fig. 2. After baking and processing, the background pressure always reached less than 1×10^{-10} Torr as measured with a Bayard-Alpert ionization gauge. The system was equipped with an EAI 150A quadrupole mass spectrometer for residual gas analysis. A typical mass trace is shown in Fig. 3. The principal background gases were CO, CO_2, Ar, and CH_4, none of which, in the quantities present, had a marked effect on any of the surfaces studied. Even freshly cesiated surfaces, after reaching coverage equilibrium, were chemically and structurally stable for periods of at least several days in the vacuum used.

A cross-section of the vacuum system is shown in Fig. 4. The Ge sample was situated at the center and could be rotated via the sample manipulator to any of several processing or measurement stations. It was mounted securely to a tantalum block which was

heated by an internal filament. Distributed about the center of the system were pieces of apparatus for performing various surface treatments and for obtaining relevant electrical, chemical, and structural measurements.

A sputtering chamber was used to clean the sample by argon ion bombardment. Controlled amounts of cesium were deposited with an aluminosilicate source and ion gun or by means of a valved molecular source. Oxygen was introduced from a separate gas admission system through a high vacuum valve. At the other stations were devices for measurement of photoelectric yield, work function, elastic specular electron reflectivity (ESER), low energy electron diffraction (LEED), and for Auger electron spectroscopy (AES). Each of these measurements is discussed separately below in relation to the goals of the experiment.

2. Apparatus for Sample Preparation

The germanium sample was cleaned in vacuum by a combination of argon ion bombardment and heating.[13] This method of surface preparation is commonly referred to as the sputter-anneal process. The argon bombardment was used to remove surface contamination and damaged layers, while heating served both to outgas the sample and to reorder (or anneal) the surface following the argon sputtering. Between successive activations the sample was simply heated to 550°C to remove the cesium oxide layer.

The sputtering chamber was identical to that described by Riach[14] and was capable of producing current densities of 5 to 50 $\mu a/cm^2$ in argon pressures of 1 to 2 microns. The sputtering chamber and associated circuitry are shown in Fig. 5. Relatively low ion energies (100 to 200 eV) were typically used in order to avoid ion focusing at the sample surface. This ensured reasonably uniform surface removal.

The argon for sputtering was admitted into the vacuum system via a two-stage admission system from a one liter flask of spectrographically pure argon. The gas was further purified by a combination of cataphoresis[15] and exposure to freshly sputtered titanium. Inside the vacuum system the argon purity was maintained by titanium sublimation pumping.

The only problem associated with the sputtering process was the contamination of the sample surface with slight amounts of tantalum during bombardment. The tantalum was believed to originate at the sample holder by sputter removal and to be subsequently transported to the sample surface by gas scattering. The amount of tantalum contamination was held to less than 1% of a monolayer by using lower argon pressures and higher sputtering energies and by minimizing exposure of the sample holder to the plasma by proper sample placement.

The sample was outgassed and annealed by thermal contact with the sample holder, which itself was heated by an internal filament. The contact was poor enough that the sample could only be heated to 550°C without raising the block temperature above the melting point

of germanium (953°C). Higher sample temperatures were achieved with additional electron bombardment heating at the sample surface using the sputtering chamber filament. Long periods of electron bombardment were avoided in order to minimize the cracking of background gases (especially CO) on the surface. The CO was found to originate from the sputtering chamber housing by outgassing during the electron bombardment.

3. Apparatus for Surface Chemical Analysis

During sample cleaning and subsequent cathode formation, AES was used to determine the chemical composition of the surface layer. This technique, when properly calibrated, can be used in a quantitative as well as in a qualitative fashion, and is capable of detecting less than 1% of a monolayer of most elements.[16] The beauty of the technique is that it is sensitive to only the uppermost two or three atomic layers.

Basically, the measurement consists of analyzing the energy distribution of electrons backscattered from the sample under the influence of electron bombardment. A certain fraction of the backscattered electrons occurs as peaks in the energy distribution at energies characteristic of inner atomic energy level spacings of the various surface atoms. In practice, the derivative of the energy distribution is recorded because the characteristic peaks are more outstanding in these curves. Details of the AES technique are described in Ref. 16.

Estimates of the amounts of surface contaminants or cathode constituents were derived from the peak-to-peak magnitudes of the Auger peaks in the derivative spectra. For a given element there was typically a choice of several peaks depending upon the total number of energy levels involved. The most prominent peak was usually used unless it occurred at the same energy as one of the peaks of another of the surface constituent. Such was the case in the present experiment for germanium and cesium. Since both had prominent peaks near 45eV, the next largest cesium peak (near 565eV) had to be used to gauge cesium coverage.

The absolute quantity of a particular element was determined by comparing the peak-to-peak Auger magnitude with that from a known amount of that element, assuming a linear relationship between Auger magnitude and coverage. The assumption of linearity is generally a good approximation to first order, at least up to a coverage of one monolayer. The main problem associated with measuring the absolute coverage of a particular element was the difficulty in obtaining a known amount for calibration. This was not a problem in the case of cesium because of the ability to deposit from an ion source. The situation was different, however, for carbon and tantalum. The sensitivity for these elements was calibrated by measuring the Auger signal from a thick layer and assuming the peak to represent a coverage of 3 monolayers or approximately the Auger electron escape depth. The differing backscattering coefficients were not taken into account.

AES was used in the present experiment together with ESER and LEED (the structural indicators) to judge the quality of the clean

6

germanium surface prior to cathode formation. AES was also used
to gauge cesium and oxygen coverage during the activation process.
The 0:KLL(520eV) and Cs:$M_{4,5}N_{4,5}$(565,580eV) transitions were used
for this purpose.

All of the AES data in the experiment was obtained with a
four-grid hemispherical LEED-Auger analyzer. The source of ex-
citation was typically a 2000 eV, 50 μa electron beam of 1 to 2 mm
diameter, amounting to an incident current density never greater
than 5 ma/cm^2. This bombardment was not particularly damaging to
the clean surface, except that carbon would build up on the surface
over a period of time due to dissociation of adsorbed background
gases. The same effect was observed on cesium- and cesium oxide-
covered surfaces, in addition to some slight rearrangement and/or
desorption of the cesium and oxygen. None of the bombardment effects
was very serious, in that no significant degradation of the photo-
electric yield was observed for any surface over the course of time
of a normal measurement.

4. Cesium Deposition

During the activation of the germanium sample with cesium and
oxygen, cesium was deposited by one of two methods. The method
used most frequently was that of ionic deposition. The other method,
that of molecular adsorption, was used chiefly to circumvent some
of the undesirable aspects of the ion technique. Each of these
methods is described separately below.

Ionic deposition

The source used for ionic deposition was an aluminosilicate
source (ion-exchanged Linde type A zeolite) identical to that
described by Weber and Cordes.[17] An ion gun (Fig. 6) consisting
of a control grid, cylindrical Einzel lens, and mask was used to
control the deposition. The gun produced a semi-focused ion beam
capable of providing reasonably uniform and rapid deposition over
the area of the sample.

The chief advantage of the ion beam technique was the ability
to measure the amount of cesium deposited by integrating the ion
flux. This was accomplished by measuring the voltage across a capac-
itor placed in series with the target lead. The main disadvantage
of the technique was the inability to achieve reliably uniform ce-
sium deposition because of partial focusing of the ion beam. This
was not a problem on fully cesiated surfaces (~1m cesium) because
there was no coverage variation once saturation was achieved.
Partially cesiated surfaces were generally not uniform but the varia-
tion across the sample was never worse than 15%. Even this amount
was not particularly troublesome, because it was always possible
to examine several areas of the sample (usually with work function)
and find a region of roughly "average" coverage.

Another potentially serious problem associated with the ion
deposition technique was the apparent evolution of oxygen by the
source during operation. The oxygen was thought to arise from
the same solid-state electrolytic process which produced the cesium
ions, since the evolution of oxygen proceeded only while cesium ions

were being extracted.[18] The consequences were especially objection-
able for the formation of the Ge/Cs/0 photosurface, since it was
desirable to examine cesium and oxygen adsorption separately.

The amount of oxygen liberated by the cesium source was reduced
considerably by preheating the source for one minute at 50-100°C
above the normal operating temperature and by depositing the cesium
in 0.2 monolayer steps, operating the gun in the cutoff condition
(control grid 30 volts positive) for one minute between steps. The
gun potentials were also set so that cesium would be deposited as
rapidly as possible. This minimized the length of exposure of the
sample to the oxygen. Using this procedure, oxygen contamination
as determined by AES was kept to a level less than 10% of that
present on the final optimized surface. The effect of this amount
of oxygen on the electrical properties of the cesiated and optimized
surfaces is discussed in Sec. III. 4.

Typical cesium ion flux during deposition was 1.5 x 10^{12} ions/sec
over the 0.5 cm^2 sample area. This high rate made it possible to
deposit one monolayer of cesium in about 3 1/2 minutes, excluding
the pauses between the steps. Approximate operating potentials are
shown in Fig. 6 along with the sketch of the ion gun.

One of the prime considerations of the ion deposition technique
was the accuracy of the coverage measurement. It was important
to know the actual cesium coverage in order to understand the phys-
ical structure of the adsorbed layer. There were several factors
which directly influenced the relationship between the measured
and the actual coverage. One of these factors, deposition uniformity,
has already been discussed (earlier this section). Another factor,
the deposition area, is equally important. The area uncertainty
arises because of the oxide border left around the sample edges
after sputtering. A 10% coverage error could arise if the adsorp-
tion characteristics of the oxide differed significantly from those
of the clean germanium (<.2mm border assumed). If the oxide adsorb-
ed cesium less readily, the measured coverage would appear less
than the actual coverage since the maximum sample area was used
in the coverage calculation. Finally, long-range surface migra-
tion like that observed by Cordes[19] for Ge(111)-Na might potential-
ly have been a factor but was not observed here for Ge(100)-Cs.

All of the other factors affecting the coverage measurement
involve the arrival or ejection of particles (neutral or charged)
other than the incident cesium ions. Such events would appear as
errors in the initial assumption of proportionality between inte-
grated charge and actual coverage.

The most important of these events would be the evolution
of neutral cesium atoms away from the sample during deposition.
This could occur either by spontaneous desorption or by sputter-
ing by the incident ions. The former is the basis of the concept
of sticking probability and is discussed in some detail in sec.
IV. 3. b. The outcome of this discussion is that the sticking
probability most likely does not deviate from unity until the notice-
ably rapid change at coverage saturation (near 1 monolayer). De-
sorption by sputtering was considered insignificant because the

incident ion energy (<3 eV) was much less than typical sputtering thresholds (>20 eV).

Another event which would affect the coverage measurement is the evolution of neutral atoms from the ion gun by re-evaporation from the ion gun electrodes. This was measured from time to time by biasing the target positively during operation to repel the ionic portion of the cesium beam, and then measuring the work function after a period of time to determine the change in cesium coverage. The neutral component was never found to be greater than 1% of the total ion flux and was therefore considered negligible.

Another event which would affect the coverage measurement is the ejection of secondary electrons during deposition. This type of event would cause the measured cesium coverage to appear greater than the actual coverage. Such errors were considered negligible on the basis of the secondary electron emission coefficients reported by Hagstrum.[20]

Molecular deposition

The molecular cesium source consisted of a bulk source and heater as shown in the lower portion of Fig. 6. The cesium was admitted to the vacuum system through a valve. The design was similar to that described by Klein[21], with the addition of a drift tube and mask inside the vacuum system to collimate the cesium beam. The heater was used only during the initial outgassing process, since cesium deposition occurred at a reasonable rate (approximately .01 monolayer/minute) at room temperature once the inner surfaces of the valve and drift tube were saturated with cesium.

A large amount of argon was evolved from the cesium ampule (99.95% pure, A. D. Mackay) during the initial outgassing process, but the argon diminished later and was obscured by other gases, notably CH_4 and C_2H_6. The latter gases were never completely eliminated, and small amounts were observed whenever the valve was opened, even when the cesium had not been heated. The occasional presence of these gases in the vacuum system appeared to contribute to a buildup of carbon on those surfaces upon which AES was performed.

The molecular source was used primarily to check on some of the difficulties associated with the ion technique. The ability to deposit uniformly and without oxygen contamination made it ideal for this purpose. The molecular technique also made it possible to compare the results of thermal deposition with the more energetic ion deposition. The results of these studies are described in sec. III. 3. d. The chief disadvantage of the molecular deposition was the inability to measure the cesium flux or even to control accurately the rate of deposition.

5. Oxygen Admission

Oxidation of the cesiated surface during the activation process was accomplished by backfilling the vacuum chamber with oxygen from

a two-stage admission system. The source was a one liter flask of spectrographically pure oxygen obtained from Airco. The admission was controlled by two Granville-Phillips Type C valves and the pressure in the intermediate stage was approximately 2 Torr.

The entire gas admission system was thoroughly processed before opening the oxygen flask in order to prevent the oxygen from being contaminated by outgassing materials. Mass spectrometer analysis during a typical admission indicated an oxygen purity of approximately 80%. The other principal gases were CO, CO_2, CH_4, and inert species. Evidently the additional mass peaks did not reflect the actual gas constituency, or these foreign gases did not adsorb as readily as oxygen on the cesiated surface, since carbon was never observed by AES on optimized surfaces. It is likely that the additional gases were regurgitated by the ion pumps during oxygen admission.

6. Low Energy Electron Diffraction

It was assumed at the onset of the Ge activation study that the cesium oxide layer would be ordered and that the structural quality of the clean Ge(100) surface and of subsequent surfaces would be important to the ultimate performance of the cathode. This assumption was based on earlier results of Goldstein for Si/Cs/O.[13] This was the reason for the inclusion of LEED and ESER among the various experimental techniques. LEED (visual display method) was used to determine surface periodicity and symmetry and to provide a link with Goldstein's published work on Si/Cs/0.[7] ESER (00 beam intensity) was used as a quantitative gauge of structural perfection. The latter measurement is described in sec. II. 7.

The LEED data was obtained with the 4 1/2-inch diameter four-grid hemispherical LEED-Auger analyzer shown in Fig. 4. With this apparatus it was possible to bombard the sample with a nearly monoenergetic beam of low energy electrons (0-200 eV) and to selectively display the elastic portion of the backscattered electrons. The resultant "diffraction pattern" was viewed through the front window of the vacuum system and was usually photographed to provide a permanent record. Patterns observed at incident electron energies of less than 50 eV were usually slightly distorted because of the operation of the electron gun in the "retarding mode". This method of operation allowed the gun to be operated at a higher voltage while maintaining a low incident energy. This was necessary in order to compensate for poor gun efficiency at low voltage (<50 volts).

In the retarding mode, electrons exit from the gun at a greater energy than that with which they eventually strike the target. The difference is made up by a retarding voltage (45 volts in this case) applied between the gun and the target. The protruding electron gun "snout" distorts the nearly radial field surrounding the sample and alters the electron trajectories. The beams most severely affected are those which pass nearest the snout, and the

end result is the crowding together of those spots nearest the center of the diffraction pattern. Although some distortion was noticeable in all of the photographs, the effect was never severe enough to interfere with the identification of the beams.

The LEED display technique is most useful in detecting ordered surface structures and in determining the periodicity of these structures. The technique is a relatively poor indicator of structural perfection because it is generally not very sensitive to deviations from ideal surface periodicity. Neither is it an indicator of surface cleanliness, since contamination can exist in an ordered fashion in almost any amount and not severely affect the normal LEED pattern. Combined with AES, however, LEED is an extremely useful technique and can be used quite reliably to arrive at a clean, well-ordered, and reproducible surface for surface studies.

LEED is also quite useful in studies of adsorption.[22] The technique is especially powerful when combined with some sort of quantitative measurement of the adsorbed species as, for example, ionic deposition. It was used in conjunction with ionic cesium deposition in the present experiment to investigate cesium adsorption on Ge(100).

LEED is most helpful in identifying ordered adsorption. The periodicity of an adsorbate with respect to the substrate net, for example, can be identified by means of the extra or "fractional-order" beams that appear in the LEED pattern. Certain types of disorder are also readily identified and analyzed. A partial filling of surface sites (with or without long-range order), for example, may produce streaky or enlarged beams or may alter beam intensities. Adsorption into domains or "islands" which are smaller than the effective coherence diameter of the electron beam (100-1000 Å in a typical LEED apparatus) will also affect beam profiles. If the adsorbate forms domains which are out of phase with each other, some of the diffraction beams may become streaky or enlarged or may even remain distinct but split into multiple beams depending upon the orientation and regularity of the subdomain boundaries. Non-coincidence of the adsorbate and substrate nets may cause satellite peaks to occur about some of the substrate spots.

7. Elastic Specular Electron Reflectivity

Measurements of elastic specular electron reflectivity (ESER) were used to supplement the structural information obtained from the LEED patterns. These measurements provided a semi-quantitative estimate of the structural quality of the surface. The ESER data itself is very nearly the absolute 00 beam intensity vs. primary energy at normal electron incidence, with the possible exception of a slight additional smoothly-varying inelastic background. As such, the data was found to be extremely sensitive to surface order. It was possible, for example, to detect quantities of cesium as small as 0.3% of a monolayer on the clean Ge(100) surface via this technique. Disordering the surface by argon sputtering caused the clean surface peaks to disappear almost completely.

11

The ESER data was obtained with a slightly modified version of the instrument described by Zollweg[23]. The details of the operation of the present instrument have been discussed by Cordes[19]. The principal feature of the Zollweg gun is the orthicon-type deflection system which separates the incident and reflected beams. This makes it possible to use normal electron incidence and yet detect the 00 beam. The Zollweg gun also utilizes an ac modulation scheme to provide a sufficiently "monoenergetic" electron beam for good energy resolution.

The gun structure and associated circuitry are shown in Fig. 7. The gun is divided roughly into two sections, the electron lens and the collector-deflector assembly. Each section is discussed separately below. The entire assembly is immersed in a uniform axial magnetic field of 100 gauss produced by two 30-inch diameter coils in the Helmholz configuration. The magnetic field not only forms part of the deflection system, but also serves to collimate the electron beam.

The electron lens consists of a series of five circular apertures designed to produce a low energy electron beam (~2 eV) having a small ac component superimposed upon a larger dc component. Only the ac signal is detected during the reflectivity measurement. Electrons produced at the filament are accelerated by the first electrode (accelerator) into a retarder and energy filter consisting of three electrodes. All three electrodes are operated at the same dc potential but the center electrode has an additional .05 volt 1 KHz negative-going square wave superimposed upon the dc level. This ac potential alternately transmits and reflects electrons in a narrow energy range while allowing more energetic electrons to be transmitted. The final electrode accelerates the beam into the collector-deflector assembly. The ac component of the emerging beam has an energy spread of .05 eV.

The collector-deflector assembly consists of two collector electrodes separated by deflector plates, and a suppressor grid between the collector and the target. The operation of this section can be best understood with the aid of the lower portion of Fig. 7, which shows the electron trajectories. The beam first enters the deflection region through an aperture in the main collector, where it encounters crossed electric and magnetic fields. If the deflector voltage is adjusted properly, the beam is deflected away from the gun axis just enough so that it passes through the apertures in the second collector and suppressor. Both apertures are displaced approximately 3 mm from the gun axis in the direction of deflection. After the beam leaves the deflection region it again follows the magnetic field lines because the transverse electric field is zero. This allows the beam to strike the target with normal incidence.

After the beam is reflected from the target, it follows the magnetic field lines until it reaches the deflection region, where the transverse electric field once again deflects it away from the gun axis. This deflection causes the beam to strike the main

12

collector (C_1) rather than to pass back up the gun. Electrons which are reflected from the main collector are deflected to the second collector (C_2), etc. so that all of the reflected electrons are eventually collected.

When re-entering the collector from the target region, the reflected beam passes through a suppressor grid. The potential of this grid is set so that only those electrons which have been reflected without energy loss are able to reach the collector. The actual adjustment during the experiment was made for minimum background in the reflectivity curves. The total current reflected into the collector was also a minimum (or very nearly so) at this setting. If the suppressor was made more negative than the optimum value, part of the incident beam was reflected directly back into the collector without ever reaching the target. If, on the other hand, the suppressor was made more positive, some unwanted inelastic current was reflected back into the collector along with the elastic current. This caused an undesirable increase in the background current.

The curves obtained with the Zollweg instrument were termed "specular" because only the 00 or specular reflected beam is represented in the collector current. The other diffracted beams are excluded because of the planar suppressor geometry. This type of geometry allows only those electrons having sufficient velocity normal to the target surface to actually penetrate the suppressor grid and reach the collector. Consequently, even elastic electrons which are scattered at angles greater than some critical angle measured with respect to the surface normal are excluded. In the present experiment this critical angle was less than 5° for primary energies greater than approximately 10 eV. The excluded electrons include a major portion of the elastic current and all of the non-specular diffracted beams.

The useful (or 1 KHz) portion of the collector signal was detected by a frequency selective amplifier (Electronics, Missiles, and Communications, Inc., Model RJB). The output of the amplifier was connected to the Y-axis of an X-Y recorder, and the target voltage was applied to the X-axis (Fig. 7). The X axis zero was adjusted so that the rapid change in reflection coefficient occurred at the zero of kinetic energy. The recorder plotted the reflection coefficient directly because the total beam current remained constant over the range of target voltages used.

The energy resolution of the instrument was limited by the energy spread of the electron beam. This was measured as < .10eV from the width of the electron reflectivity data near zero kinetic energy. The spatial resolution was limited by the diameter of the electron beam and was estimated to be ~1.5 mm from the deflection characteristics. The filament was always operated at a dc emission current of 1μa. A major portion of this current actually reached the target because of the magnetic collimation of the beam.

Because of the constant current feature of the electron gun, ESER data obtained from a given surface was extremely reproducible.

13

The data was also not a strong function of sample position. Peak magnitudes could be reproduced to within 3% and energy positions to within 1%. Peak magnitudes were typically used to gauge the structural quality of a particular surface or to compare several surfaces differing slightly in formation or initial preparation. The value of this procedure was enhanced by the extreme sensitivity of the data to structural changes. The ESER data also served as a valuable "fingerprint" technique for identifying particular surfaces or stages of cathode formation.

The ESER data was not considered valuable as LEED intensity data because of the inability to determine the origin of the diffraction peaks from basic principles. This stems from the prevalence of multiple scattering among top layer atoms in the energy range of interest (0-25 eV). If such low energy data were readily interpretable, information concerning actual atomic positions of the scatterers could ultimately be derived. At the present state of diffraction theory, this would require, at a minimum, data for several diffraction beams at a number of angles of incidence and detection.

8. Work Function

Work function measurements were used along with photoelectric measurements to determine the surface potential at various stages of cathode formation (the surface potential here is defined as the difference between the Fermi level and the uppermost valence band level at the surface). The work function measurements were also used as the major indicator of cathode performance. In a few instances these measurements were also used to determine cesium coverage when no other coverage indicator was available. This required the use of a previous calibration of work function vs. cesium coverage. Examples of the use of work function for coverage determination include measurements of deposition uniformity and the determination of absolute coverage on molecularly-deposited surfaces.

All of the work function measurements were obtained by means of a retarding potential technique using the Zollweg gun described in Sec. II. 7. The ac component of the target current was plotted as a function of the target voltage to obtain the retarding characteristics. The gun potentials were the same as for the ESER measurement, but the target rather than the collector was connected to the tuned filter and lock-in amplifier (Fig. 8). This method proved to be very attractive in terms of energy resolution. The electron beam was sufficiently monoenergetic that the I-V characteristics were never more than 100 mv. wide. This allowed work function shifts as small as .02eV to be measured. The spatial resolution was ~1.5 mm as limited by the electron beam diameter.

Since only changes in the work function of the sample could be measured, the retarding potential curves had to be calibrated in order to determine absolute values. This was accomplished by comparing the measured curves with the retarding characteristic for a Ta-Cs surface, having first determined the work function of the latter by photoelectric means. The result agreed with a less accurate method using the work function of the gold-plated retarding

14

electrode (zero of kinetic energy for those electrons that provide the ac component of the beam).

9. Photoelectric Emission

Measurements of photoelectric emission were used in conjunction with work function determinations to characterize the Ge/Cs/0 emission processes and determine changes in surface potential as a function of cathode formation. The photoelectric data was of two types, the total photoelectric yield and the energy distribution of photoemitted electrons, both as functions of photon energy. The yield measurements were obtained by illuminating the sample with monochromatic radiation of known wavelength and intensity, and measuring the target current as a function of the wavelength of the radiation. The energy distribution measurements were obtained by dc-differentiating the retarding potential characteristic between the sample and a cylindrical collector at various photon energies. The photoemission apparatus is described briefly below.

The optical system used for all of the photoelectric measurements is shown in Fig. 9. The system was designed and built by Riach and has been discussed in considerable detail in ref. 14. The primary feature of the system is its high spectral purity, which was considered necessary in order to obtain reliable data in regions of relatively low yield. The high spectral purity was achieved by using a Bausch and Lomb model 33-86-25 high intensity grating monochromator in series with a Bausch and Lomb 33-86-40 250 mm focal length grating monochromator. Filters were inserted near the output in order to eliminate higher order dispersions and further reduce the scattered light content.

The light source used with the optical system was a 150 watt xenon arc lamp obtained from Engelhard Hanovia, Inc., chosen because of its smooth high intensity spectral output (except for several lines between 1.0 and 1.5 eV). Quartz beam splitters at the monochromator output were used to reflect a small portion of the light to either of two photocells for intensity measurement. An RCA type 917 photocell was used for photon energies in the range 1.2 to 3.1 eV and an RCA type 935 photocell was used in the range above 3.1 eV. The optical system was calibrated with a vacuum thermopile (Epply 4100) which had (C-631) obtained from the National Bureau of Standards.

Before the final photoelectric measurements were taken, the 917 photocell had to be recalibrated because of a slight increase (as much as 80% at one point) in the photocell output. The error was apparently caused by a change in the position of the photocell with respect to the incident light. The recalibration was accomplished by comparing the yield data from a stable uniform Ge/Cs/0 surface to that obtained with a more recently calibrated optical system. Because of the intermediate step associated with the recalibration, yield measurements were expected to be within 20% of absolute instead of the 5% figure quoted by Riach. The 20% uncertainty was not expected to affect any of the photoelectric

15

threshold values, since these were determined from the extrapolation of photocurrent data ranging over several orders of magnitude within a small range of photon energies.

The range of photon energies used in the experiment was 1.2 eV to 3.5 eV. The low energy constraint was the response limitation of the 917 photocell. The high energy constraint was the transparency cutoff of the viewport (Corning 7056 glass) which occurred near 4 eV. The high energy limitation made it impossible to obtain any clean surface photoelectric data. A decision was made not to replace the viewport with an ultraviolet window because the interest was primarily in the photoelectric threshold data from low work function surfaces. The photoelectric results of Jeanes and Mularie[18] were used for the clean and partially-cesiated surfaces. In the limited energy range of the data of the experiment, the optical system was found to have an energy accuracy of $\pm.015$ eV and an energy bandwidth of about .04 eV.

The cylindrical collector used for collection and energy analysis of the photoelectrons is shown in Fig. 10. The design is nearly identical to that described by Riach. The collector, along with the electronic system used for the dc differentiation, are discussed in considerable detail in ref. 14. Briefly, the energy distribution curves (EDC's) were obtained by measuring the derivative of the retarding potential characteristic between the sample and the cylindrical collector. This was accomplished by applying a retarding ramp voltage to the collector (.02 volts/sec) and simultaneously time-differentiating the sample current. Spherical collector geometry (for radial electron trajectories) was not necessary because of the enclosed collector. The photoelectrons could traverse the inner region a number of times until they approached the collector surface along field lines.

The effect of the nonideal collector geometry was probably only to skew the energy distributions toward slightly lower energies. The skewing was considered negligible in the present experiment (or at least the same for similar retarding voltages) so that EDC's for the various low work function surfaces were compared with confidence. The resolution of the collector was found to be better than .15 eV by comparing the width of an EDC from a cesiated tantalum sample with the value $h\nu-\varphi$, where the photon energy $h\nu$ was chosen near the photothreshold energy and the work function φ was determined from a Fowler-Nordheim plot of the photoelectric yield.

The photoelectric yield curves in the present experiment were used chiefly to determine photoelectric thresholds. The thresholds, in turn, were compared with work functions to determine surface potentials. This aided in the formulation of the Ge/Cs/0 electronic model. The photoelectric yield curves were also used to calculate white light sensitivity (sec. III. 3. e). The resulting number was used to indicate cathode performance, although more often the yield at a particular photon energy was used for that purpose.

The photoelectron energy distribution curves (EDC's) were used to identify the various emission processes contributing to the yield. They were particularly useful in separating surface state from

16

valence band emission and for determining relative charges in band-bending as a function of cathode formation. The EDC's were virtually noise-free because of the high signal levels typically encountered. They were also extremely reproducible for a given surface.

III. RESULTS

1. Sample Preparation

An intrinsic sample (40 Ω-cm n-type undoped) was chosen for the Ge/Cs/0 study so that the electron energy bands would be essentially "flat" over the region of photoelectron escape. This ensured that the photoelectric data would reflect unambiguously the position of the energy bands at the sample surface. It also ensured that emission from occupied surface states lying in the band-gap could be distinguished from valence band emission.

The germanium samples used in the experiment were oriented by the optical reflectogram technique[24] and were cut to within 1° of the (100) surface. The working faces were made 0.707 X 0.707 cm and were mechanically polished to an optically flat mirror finish, ending with .05μ alumina abrasive. The polished samples were degreased either by ultrasonic cleaning in methanol or by boiling in trichloroethylene and then rinsing in acetone and deionized water. The latter process left a considerable amount of carbon on the surface as determined by AES. Prior to insertion into vacuum the samles were dipped several times into concentrated hydrofluoric acid to remove the surface oxide and the accompanying damaged layer due to mechanical polishing. Each HF dip was followed by a rinse in deionized water.

Vacuum processing consisted of a series of sputter-anneal treatments sufficient to remove surface contamination and structural damage. The main processing objective was the elimination of surface contamination as determined by AES. In addition to the sputter-anneal treatments, a long term outgassing of the sample and holder was also performed early in the cleaning process. The outgassing temperature was 950°C (the sample reached only 550°C) and the time approximately 30 hours.

A typical sputter treatment consisted of removing several hundred atom layers of germanium using 100-200 eV argon ions, while an anneal treatment consisted of raising the sample temperature to at least 550°C for approximately 15 minutes. Two or three such cycles were usually sufficient to reduce the level of surface contamination to near the limit of detectability by AES. This amounted to less than 5% of a monolayer of foreign atoms (<2%m C, <1%m Ta, <2%m other), and was sufficient to make all of the electrical and structural measurements reproducible to within experimental error.

Once the germanium sample was sufficiently free of surface contamination, this condition was rather easily maintained. The chemical composition of the surface, the work function, the LEED pattern, and the ESER data remained unchanged for periods of several days in vacuum. Occasionally the sample had to be resputtered and annealed to rid the surface of minute quantities of carbon. The carbon would build up over a period of time due to cracking of adsorbed background gases by the high energy electron beam used for AES. To ensure the removal of the carbon, 50 to 100 atom layers of germanium was typically removed.

During the course of the experiment the sample was checked routinely with ESER to detect chemical and structural variations occurring on the clean surface. The magnitude of the diffraction peaks in the clean surface ESER data proved to be a reliable means of determining the effectiveness of the anneal treatment and also of detecting the presence of minute quantities of contamination. The use of ESER rather than AES for routine examination avoided frequent exposure of the sample to high energy electron bombardment and the attendant buildup of surface contamination.

Repeated Cs-0 activation cycles did not have a detrimental effect upon the clean germanium surface. The cesium oxide layer was quite easily removed by heating, and the resulting surface showed no evidence of any remaining cesium or oxygen. The work function and ESER data obtained after heating were identical within experimental error to the data obtained after heating followed by a single sputter-anneal treatment. Both measurements were capable of detecting less than 0.5% of a monolayer of cesium on the surface.

2. Clean Surface Characterization

The principal contaminant observed on the germanium sample prior to sputtering was carbon. There was typically a sufficient quantity to completely obliterate the germanium peaks in the Auger spectrum. From the size of the carbon Auger peak (C:KLL, 270 eV) on this surface, the limit of detectability of carbon on germanium was estimated to be about 1% of a monolayer. The carbon level was never allowed to increase above 3% of a monolayer, a level which did not seriously affect the ultimate Ge/Cs/0 photoresponse.

A typical Auger spectrum from the clean Ge(100) surface is shown in Fig. 11. In addition to the residual carbon, a slight amount of tantalum contamination (less than 2% of a monolayer) also remained. The tantalum was a byproduct of the sputtering process as described in Sec. II. 2. The surface also contained an undetermined but presumably small amount of argon (the sensitivity of AES to argon is not known precisely). This small quantity of argon, also a product of the sputtering operation, could not be driven from the surface upon heating, even if the sample was heated to near the melting point (~950°C). The presence of tantalum and argon slightly in excess of the minimum amounts did not markedly affect any of the clean surface parameters. It was presumed that carbon, tantalum, and argon in the normal amounts did not seriously affect the ultimate Ge/Cs/0 photoresponse.

The LEED pattern from the clean Ge(100) surface was exceptionally sharp and clear, and exhibited the strong 1/2-order reflections typical of this surface[25,26]. Additional streaked 1/4-order features were also present but these features were weak relative to the other reflections except at low energies. Photographs of the LEED pattern at 21 eV and 4 eV incident electron energy are shown in Fig. 12.[26] The pattern is identical to that observed by Lander and Morrison[26], except, perhaps, for more sharply resolved 1/2 1/2 spots. As with Lander and Morrison, the 1/4-order streaks could not be resolved into spots with careful annealing.

The accompanying ESER data for the clean surface is shown in Fig. 13. The data compares favorably with that of Chen[27] taken with the same instrument on Ge(100). The diffraction peaks in the present experiment, however, were about 75% larger because of the ability to adjust for precise normal electron incidence. The most obvious feature in the clean surface curve is the large peak at 8.5 eV. This peak was used to gauge the effectiveness of the anneal treatment. Its magnitude relative to the background was reproducible to within 5% from run to run.

Not quite so reproducible was the reflectivity background itself, which increased somewhat, especially in the 0 to 5 eV range, whenever the surface was contaminated or improperly annealed. At one point in the experiment the background was quite high and variable because of a leak which had developed in the vacuum system. "Clean" surfaces produced under these conditions gave inferior results when activated with cesium and oxygen. Surfaces with ESER data having low backgrounds and large diffraction peaks yielded the best photoelectric sensitivities upon activation.

The clean surface work function was measured using the retarding potential technique described in Sec. II. 8 and was found to be constant to within $\pm$ .02 eV from run to run. An absolute value was determined by comparing the retarding potential curve with that from a surface of known work function. The reference surface was Ta-Cs, prepared by depositing cesium to saturation (for uniformity) on a freshly cleaned tantalum sample. Oxygen was also present on the surface, further reducing the surface barrier. A yield curve was taken and the threshold region fit to Fowler's[28] theory of photo-emission for metals. The fit between the experimental data and the theoretical curve is shown in Fig. 14. A work function of 1.78 $\pm$ .05 eV was determined which corresponded to a clean surface work function of 4.69 $\pm$ .08 eV. This result is within experimental error of the value 4.75 eV obtained by Jeanes and Mularie[18] on an identical sample (cut from the same boule and prepared in an identical manner).

No photoelectric data was taken on the clean surface because of the window limitation described in Sec. II. 9. Instead, the photoelectric data of Jeanes and Mularie was used, which indicated that the Ge(100) surface was degenerately p-type, with little or no deviation from degeneracy throughout cesiation. Their measurements extended to the minimum work function coverage near .7m.

3. Cathode Formation Process

The Ge/Cs/O photosurface was prepared by the same two-step process used to activate silicon to NEA. Cesium was deposited on the clean germanium surface until the coverage saturated, whereupon oxygen was admitted until the photosensitivity maximized. Typically 1.2m of cesium was deposited during the initial cesiation in order to ensure coverage saturation. Any degree of cesiation short of saturation gave inferior results upon oxidation. The monochromator system was usually used for the light source during optimization (tuned to 0.826μ or 1.50 eV photon energy), but occasionally a tung-

sten lamp or the fluorescent room lights were used. The end results in each case were the same.

Other methods of activation were examined besides the simple two-step process. One was a multi-step process in which the cesium depositions totaled one monolayer and the oxygen exposures following the cesium depositions were quantities consistent with unity sticking probability. The results of this process, described in Sec. III. 4, were essentially the same as for the two-step process. Other methods of activation were tried which usually involved heavy oxygen exposures or were attempts to build up thick layers of cesium oxide. These experiments are described in Sec. III. 6. None of the latter methods proved to be superior to the two-step process and for that reason were not examined in detail. The results given here are for the two-step process unless otherwise indicated.

a. Surface Chemical Composition

Cesiated Surface

The sources used for cesium deposition have been discussed in Sec. II. 4. The cesium ion gun was used in favor of the molecular source because of the ability to measure and control the amount of cesium deposited. One of the problems associated with this technique was the evolution of oxygen by the ion source during deposition. The oxygen problem, however, was not serious, and was minimized by operating the gun as outlined in Sec. II. 4.

The presence of oxygen on the sample was detected by means of AES using the $O:KL_2L_2$ transition (520 eV). The magnitude of the oxygen Auger peak was usually compared to that of the nearby cesium peak ($Cs:M_5N_{4,5}N_{4,5}$ transition, 565 eV) to estimate the amount present. The O/Cs ratio was typically kept below .07, a factor of 10 smaller than the value characteristic of the Ge/Cs/O surface. This amount of oxygen was slight enough that the individual stages of cesiation and oxidation were clearly differentiated in all of the measurements. Furthermore, oxygen contamination in the quantities evolved from the source had no effect on the performance of the final surface. Only cesiated surfaces were noticeably affected. This matter is discussed further in Sec. III. 4.

A typical Auger spectrum from a fully cesiated surface (~1m cesium) is shown in Fig. 15. Besides the germanium, cesium, and oxygen peaks, carbon, tantalum and argon peaks are also visible. The latter are the same peaks that were observed on the clean surface (Fig. 11) but attenuated somewhat due to the presence of the cesium overlayer. The germanium Auger peaks are also noticeably attenuated from their clean surface values (40% attenuation for the 85 eV peak).

A special attempt was made to examine ion-deposited surfaces for sodium, since the cesium ion source was made from sodium zeolite by an ion exchange process (Sec. II. 4). The $Na:Kl_2L_2$ transition (~990 eV) was used for this purpose. From an earlier experiment in which a full monolayer of sodium was deposited on the sample,

the sensitivity of the LEED-Auger analyzer to sodium was estimated to be ~5% of a monolayer. No sodium was ever observed in the Auger spectrum.

Cesiated surfaces prepared by molecular adsorption, unlike those prepared by ion deposition, showed absolutely no evidence of oxygen contamination. However, molecularly-deposited surfaces which had undergone considerable electron bombardment (as a result of AES, for example) exhibited a noticeable amount of carbon contamination (5 to 10% of a monolayer) after a period of time. The carbon was localized to those areas of the surface where the electron beam was incident and was believed to be due to the cracking of methane on the sample surface. The methane emanated from the molecular source during deposition (Sec. II. 4). The carbon-contaminated areas were also deficient in cesium following cesium saturation, indicating that the carbon probably affected cesium adsorption. Carbon contamination was not a problem on molecularly-deposited surfaces that had not undergone electron bombardment.

An attempt was made to determine whether the electron bombardment during AES was in any way damaging to the cesiated surface other than via the hydrocarbon dissociation already discussed. A thorough examination was made of the AES, LEED, ESER, and work function data from both freshly-cesiated (ion-deposited) and electron-bombarded surfaces for evidence of desorption or rearrangement of the cesium layer. No changes were observed, indicating that AES could be performed without fear of disturbing the cesium layer.

The ability to determine the actual cesium coverage on the sample was essential for understanding the physical structure of the adsorbed layer. The coverage measurement is discussed in detail in Secs. II. 4 and IV. 3. b. The relationship between actual and measured cesium coverage is examined, along with the possible errors in the coverage measurement itself. In the interest of making as few assumptions as possible before all of the data is presented, the results in this section are given in terms of measured coverage with the understanding that the actual coverage does not differ significantly from the measured coverage.

As part of the effort to understand the cesium adsorption process, coverage saturation was investigated by means of AES. The implication of earlier work by Weber and Peria[29] on the Ge(100)-Cs system was that saturation occurred at the work function minimum near .7m coverage. The present Auger data also demonstrated the existence of a coverage saturation, but at a point at least .2m beyond the work function minimum coverage. The saturation coverage was found to be stable in vacuum, even to the electron bombardment of the Auger beam (2000 eV, 50 μa, 1 to 2 mm diameter).

The Auger data indicating cesium saturation is shown in Fig. 16. The magnitudes of the Ge:$M_{2,3}M_4V$ (85 eV) and Cs:$M_5N_{4,5}N_{4,5}$ (565 eV) peaks are plotted as a function of cesium coverage. The other germanium and cesium peaks behaved similarly. The large peaks between 45 and 50 eV were not chosen because of the coincidence of the germanium and cesium peaks there. The curves in Fig. 16 exhibit a

linear or nearly linear relationship between Auger peak height and cesium coverage in the region below .8m, and a constant magnitude beyond. These results clearly indicate a coverage saturation. Since Auger electrons typically originate from several atom layers deep, the peaks would certainly have continued to change with cesiation had the coverage not saturated.

In order to ensure good coverage uniformity in the saturation experiment, the cesium was deposited using the molecular source. Surfaces deposited in this manner were found to be uniform to within the limit of detectability by AES, independent of the degree of cesiation. The only exception was the areas of the sample that had undergone previous electron bombardment, which were carbon-contaminated and deficient in cesium (Sec. III. 3. a). This is the reason that the cesium Auger peak heights at 1.16 and 1.31m in Fig. 16 are smaller than at .95 and 1.45 m. The latter two points were also slightly affected causing saturation to occur at a lower measured coverage than usual.

The coverage scale in Fig. 16 was deduced with the aid of the work function data which was taken concurrently with the Auger data. Coverage values were determined first in a relative sense from the exposure time to the source, assuming a constant deposition rate. Then a point near the low coverage side of the work function minimum was identified as to coverage using the work function vs. coverage data obtained with the ion source. This point, near .55m, was the highest of the coverages still easily identified by work function. Because the coverage was deduced in this fashion, the data of Fig. 16 is subject to the same errors as the ion source data.

It is important to note that the 565 eV cesium Auger peak (Fig. 16) is 20% larger at saturation than at the coverage corresponding to the work function minimum. This result clearly refutes earlier evidence[29] that coverage saturation for Ge(100)-Cs occurs at the work function minimum. This conclusion is substantiated by measurements of work function, ESER, and photosensitivity (Secs. III. 3. c, III. 3. d, III. 3. e, and III. 3. 4).

Optimized Surface

The oxidized (or optimized) surface was also examined with AES. A typical spectrum is shown in Fig. 17. Again the initial carbon, tantalum, and argon peaks are attenuated by the overlying surface layer. Comparison with Fig. 15 indicates that no additional carbon accumulated during oxidation even though small amounts of CO, CO_2, and CH_4 were observed along with the oxygen with the mass spectrometer. This was taken as adequate proof that the oxidation procedure was satisfactory.

The presence of oxygen on the surface was detected by means of the O:KLL Auger peak at 520 eV. For 2000 eV exciting electrons, the magnitude of the oxygen peak was $0.7 \pm .1$ when compared to the neighboring $Cs:M_5N_{4,5}N_{4,5}$ peak. The amount of oxygen corresponding to the ratio was not known precisely, but the LEED data (Sec. III. 3.b)

suggested some multiple of one-half monolayer in the optimized layer. An oxygen exposure of approximately .02 Langmuir was calculated from the pressure indicated by the ion pump, but the latter was probably low (perhaps by a factor of 100) because of the relative positions of the pumps, gas inlet, and sample. The O/Cs ratio was roughly half that observed on a surface that had been deliberately exposed to an excess of oxygen (factor of 1000 greater than that needed for optimization).

It is interesting to note that the $Cs:M_{4,5}N_{4,5}N_{4,5}$ (565, 580 eV) Auger peaks underwent about a 15% increase in size upon oxidation. This can be seen from a comparison of the Auger spectra of Figs. 15 and 17, which were recorded at identical sensitivities. The increase probably represents an increase in the backscattering of the cesium Auger electrons due to the presence of the oxygen. A similar increase was observed by Goldstein[7] for Si/Cs/0 which Levine[6] used to support his contention that the oxygen atoms occupied sites physically beneath the cesium layer. A similar conclusion may be applicable to germanium.

AES also indicated that the optimized surface was extremely uniform in cesium and oxygen content. No variation was observed over the surface to within the limits of reproducibility of the measurement.

Unlike the Ge/Cs surface (ion-deposited), the Ge/Cs/0 surface was somewhat affected by the electron beam used for AES (2000 eV, 50 μa). The changes that took place were slight, however, since the photoelectric properties of the cathode were hardly affected during the course of a normal measurement. Work function, AES, and ESER indicated some slight desorption of the oxygen without any accompanying disruption of the cesium layer. The ability of the surface to readsorb oxygen at the appropriate sites was not impaired.

b. Low Energy Electron Diffraction

LEED was used to examine the two-dimensional structural periodicity of the cathode surface. Both the cesium and the oxygen were observed to adsorb in an ordered fashion onto specific sites on the germanium surface. This is demonstrated by the LEED photographs in Fig. 18 taken at 19 eV incident electron energy. The upper photograph is from a typical fully cesiated surface and the lower photograph is from the corresponding optimized surface. Both patterns exhibit strong 2x1 diffraction, indicating that the adsorption occurs with the same periodicity as the clean germanium surface. There are no obvious "extra" features in the patterns which would suggest a partial filling of sites or the existence of some other type of structural imperfection. These LEED results are identical to those observed by Goldstein[7] for Si/Cs and Si/Cs/0.

LEED was also used to examine the adsorption processes which occurred during cathode formation. The technique proved to be especially sensitive in the low coverage region during cesiation, and for that reason yielded the most information there. Changes

24

which occurred in the LEED pattern at higher cesium coverages and during oxidation were less dramatic.

The LEED results in the low coverage region are summarized in Fig. 19. The LEED pattern is shown there as a function of cesium coverage with the incident energy adjusted in each case to accentuate the "extra" features. In the 0 to .15m range the clean surface 1/4-order features become increasingly diffuse while enlarged 4x3 features begin to appear. The 4x3 pattern is quite complex because there are two possible mutually perpendicular orientations of 4x3 domains on the surface. Between .15 and .3m the 4x3 features gradually give way to sharp 2x3 reflections. The latter disappear between .3 and .5m as the final 2x1 features become dominant. Some weak intervening 1/4-order features are visible in the .33m photograph.

At coverages beyond .5m the LEED technique was relatively insensitive to cesium adsorption. The 2x1 reflections persisted in this region, and no distinct changes occurred other than slight variations in the intensities of the 1/2-order spots and the background. In some of the later LEED data (second sample), extremely weak 1/2 1/2 spots were visible on the fully-cesiated surface indicating possible vacancies in the 2x1 net.

The only change which occurred in the LEED pattern during oxidation was the strengthening of the 1/2-order reflections relative to the integer-order spots. The diffraction pattern from the optimized surface was always noticeably more intense and sharp.

c. Elastic Specular Electron Reflectivity

The existence of strong diffraction peaks in the ESER data throughout cathode formation provided additional proof that the cesium and oxygen adsorbed in an ordered fashion. The curves obtained from the fully cesiated and optimized surfaces are shown in Fig. 13 along with the data from the clean surface. The peaks there represent only the 00 beam intensity variation since the other diffraction beams are excluded by the planar suppressor geometry. There is also a possibility that some of the low energy peaks may be due to surface state resonances[30]. The smoothly-varying background present in all of the curves is most likely due to the inability of the suppressor grid to eliminate completely the inelastically scattered portion of the electron beam.

The reproducibility of the ESER data from run to run for a given surface was generally quite good. This was especially true for the clean surface, the fully-cesiated surface, and the optimized surface since these surfaces were uniform and well-defined. The reproducibility from sample to sample was somewhat less satisfactory. The peak magnitudes were much the same but the backgrounds differed slightly, especially in the low energy region. The conditions causing the differing backgrounds did not show up in any of the other clean surface measurements, and no definite connection could be established between the magnitude of the background and success of the activation. Since these factors seemed to point to an apparatus effect rather than to an actual surface condition, the operation of the ESER instrument was examined closely. No obvious difficulties

were found, but the possibility of an apparatus effect was not entirely discounted. In any case, the differing backgrounds were not considered a serious problem because successful activation appeared to depend upon the magnitude of the diffraction peaks relative to the background rather than on the background magnitude itself.

It was evident throughout the course of the experiment that the ESER data was sensitive to even very minute structural changes on the cathode surface. The same sensitivity has been observed by Chen[27] for several other germanium-alkali systems. An example of this sensitivity is shown in Fig. 20. The clean surface curve is plotted in that figure along with the data from the same surface covered with only .003m of cesium. The effect of this slight amount of cesium on the electron reflectivity is easily discernible. The same type of data was used to illustrate the ability of simple heating to restore the clean germanium surface following Cs-O activation. The electron reflectivity curves were identical whether the surface was only heated or whether the surface was heated and then sputtered and annealed.

Other examples of the structural sensitivity of the ESER data are discussed in future sections. In the paragraphs immediately following, ESER is examined as a function of cathode formation. The cesiation process is examined first, followed by the oxidation process. The data serves mainly as a basis for identifying and comparing surfaces, and is especially helpful in later experiments involving abnormalities in cathode formation (Sec. III. 5). The development of the diffraction peaks during cathode formation is also helpful in understanding the adsorption processes.

The ESER data is shown first as a function of cesium coverage (Fig. 21). The numbers near the curves refer to the measured cesium coverage (in monolayers). On the left are those curves in the interval $0 > \theta > .5m$, while on the right are the curves for $\theta > .5m$. Only the 0-25 eV range is shown because most of the interesting structure appeared there.

The ESER data in the 0 to .5m range is characterized by the gradual disappearance of the clean surface peak A at 8.5 eV and the appearance and steady growth of the peak B between 15 and 20 eV. The various ordered structures observed with LEED in this coverage range are not differentiated in the curves, suggesting that ESER was generally not sensitive to the lateral cesium-cesium spacings. The region beyond .5m is characterized by the rather sudden appearance of the peak C at 16 eV and the double peak D near 3 eV. These abrupt changes occur at a coverage definitely less than the work function minimum and coincide with a major change in the effect of oxygen adsorption on the work function (Sec. III. 4). The ESER features continue to grow with cesium coverage until they stabilize near .9m. The stabilization is thought to indicate coverage saturation since the .9m value agrees within experimental error with the saturation coverage determined by AES (Sec. III. 3. a). Additional cesiation results only in a slight deterioration in D, probably because of oxygen contamination from the ion source.

In spite of the oxygen and uniformity problems associated with the ion source, the curves of Fig. 21 are felt to accurately represent the electron reflectivity variation as a function of cesium coverage. Fully cesiated surfaces deposited with the molecular source exhibited only slightly more pronounced diffraction features (less than 5% difference) and identical work functions. The coverage scale of Fig. 21 was checked by depositing with the molecular source just beyond minimum work function on one sample and then measuring the electron reflectivity. The uniformity of the molecular source was good enough that there was no question that minimum work function had been achieved at all points on the surface. The electron reflectivity curve was nearly identical to the .7m ion source curve of Fig. 21.

The ESER data of Fig. 21 was compared to that obtained for Ge(100)-Cs by Chen[27]. The data matched favorably in the low coverage region but peak B was considerably larger in Chen's data and continued to grow as cesium was deposited beyond 1 monolayer. The differences were attributed to oxygen-contaminated cesium deposition in Chen's case. The work function results substantiated this conclusion.

Fig. 22 shows the changes that occur in the ESER data during oxidation. The numbers above the curves refer to arbitrary stages of oxidation. The number "1" is the data from the freshly cesiated surface, and the number "7" the data from the optimized surface. The dominant feature is the appearance and growth of the large peak F above B. This is accompanied by the disappearance of the double peak D and the growth of the peak E out of the shoulder at 5.5 eV. Experiments on partially-cesiated surfaces (Sec. III. 4) show that the magnitude of F is largely dependent upon the amount of oxygen on the surface, and that F is indeed a separate peak rather than just an extension of B. If an excess amount of oxygen was admitted to the surface immediately following optimization, the magnitude of F continued to increase, even though the photoelectric yield had begun to decrease. The peak typically increased by about 20% before it began to deteriorate with excess oxygen (steps 8-13).

There was also an aging phenomenon (not fully understood) associated with the oxidation process. Whenever a slightly over-oxidized surface was allowed to sit for several hours, the photosensitivity would gradually increase (<10%) beyond the initial optimum value. Even surfaces that had not been deliberately over-dosed usually showed some increase in yield with time, perhaps due to loosely bound oxygen which was slowly incorporated into the surface layer. Optimized surfaces, in fact, were never observed to decrease in photosensitivity in vacuum. In one case the observation time was several weeks.

d. Work Function

The work functions of the various cathode surfaces were derived by subtracting accurate measurements of work function changes from the 4.7 eV clean surface work function. The changes or "shifts" were measured with the apparatus described in Sec. II. 8. The work function change was consistently $3.18 \pm .05$ eV for the fully-cesiated surface ($\varphi = 1.52$ eV) and as high as $3.76 \pm .05$ eV for the

27

optimized surface (φ = .94 eV). The latter value, which depended
upon a number of factors including aging of the surface following
oxidation, agreed quite well with the photoelectric threshold of
.96 eV observed by Caldwell, Kalweit, and Kennedy[31] for a heavily
doped p-type sample.

Both the Ge/Cs and Ge/Cs/0 work functions were uniform to
within .03 eV across the sample surface. The uniformity was the
same regardless of whether the ion source or the molecular source
was used for cesium deposition. In each case the uniformity was
achieved simply by depositing enough cesium to ensure coverage
saturation over the entire sample.

The 3.18 eV shift obtained for Ge/Cs was reproducible to with
$\pm$ .02 eV from run to run, and stable within the same limits for
periods exceeding 30 hours. Occasionally, when cesium was deposited
beyond the saturation coverage, the shift was several hundredths
of an electron volt smaller than usual, presumably because of the
excess cesium. The shift, however, returned within minutes to the
3.18 eV value as the cesium was allowed to desorb.

The Ge/Cs work function was not particularly sensitive to the
arrangement of cesium on the surface. For example, in one experiment
(Sec. III. 5. c) where the freshly cesiated surface was heated to ~100°C
and then recesiated to replace the small amount of cesium desorbed,
the work function remained unchanged even though LEED and ESER
indicated there was some surface disorder.

The work function was somewhat more sensitive to surface con-
tamination, especially to oxygen. Oxygen-contaminated surfaces had
work functions as much as 0.55 eV lower than non-contaminated sur-
faces, depending upon the quantity of oxygen present. The 3.18 eV
Ge/Cs shift was for a molecularly-deposited surface which was free
of oxygen contamination. The same value, however, was achieved on
ion-deposited surfaces, providing the source was operated in the
manner described in Sec. II. 4 in order to minimize the evolution
of oxygen.

The Ge/Cs/0 surface was not quite as reproducible as the Ge/Cs
surface and generally required an aging process before the work
function stabilized. The work function shift was usually in the
neighborhood of 3.68 eV immediately following oxidation and then
typically increased another .05 eV during the next several hours.
There was a corresponding increase in the photoelectric yield and
in the ESER peak F. The aging phenomenon has been discussed in
Sec. III. 3. c.

Unlike the Ge/Cs work function, the Ge/Cs/0 work function was
extremely sensitive to the ordering of the cesium layer. In the
same experiment described earlier in this section (also Sec. III. 5. c.)
during which the Ge/Cs surface was heated slightly and then re-
cesiated, the final work function after optimization was several
tenths of an electron volt higher than normal. LEED and ESER in-
dicated a disruption of the normal surface order. AES revealed a

deficiency in oxygen, suggesting that the chemical reactivity of the surface to oxygen had been altered.

All forms of contamination on the initial germanium surface were detrimental to the Ge/Cs/0 work function. The contamination generally caused a larger variation in the Ge/Cs/0 work function than in the corresponding Ge/Cs work function. Initial C, Ta, and 0 contamination were examined in particular.

The change in the Ge(100)-Cs work function ($\Delta\varphi$) vs. cesium coverage (θ) was checked against the published data of Weber and Peria[29]. The results are plotted in Fig. 23. Only the coverage region beyond .5m is shown because this was the only region where there were significant variations between the two sets of results. The measured coverages corresponding to the work function minima agree to within experimental error, but the actual work function shifts at these minima differ by approximately 0.2 eV. The present studies indicate that the surface described by Weber and Peria was probably slightly oxygen-contaminated from the cesium ion source. Their results, in fact, were reproduced on the present sample by depositing the cesium at a slower rate, thereby allowing more oxygen to adsorb on the sample. The shift of 3.28 obtained at the minimum work function point in the present experiment agrees well with the value 3.3 measured by Jeanes and Mularie[18], who took similar precautions to avoid oxygen contamination.

Another important difference between the two sets of data (Fig. 23) involves the observation of coverage saturation. Although not specifically stated, the implication of the work of Weber and Peria is that the cesium coverage saturates at the work function minimum. Additional cesium increases the work function for a short period of time but the value eventually returns to the minimum as the cesium desorbs. This is indicated by the dashed line in the figure. No such behavior was observed in the present experiment. Work functions for surfaces covered beyond the minimum point were found to be stable in time and did not return to the minimum value. Surfaces covered beyond saturation occasionally exhibited work functions which decayed in time, but the decay was to a level corresponding to the 3.18 eV shift rather than to the work function minimum. This data fit well with the observations of saturation discussed in other parts of Sec. III. 3.

e. Photoelectric Emission

The Ge/Cs and Ge/Cs/0 spectral yields are shown in Fig. 24. The curves are corrected for the reflectivity of germanium using the published data of Philipp and Taft[32]. The yields are thus expressed in terms of electrons/absorbed photon rather than electrons/incident photon. The two curves in the figure were typical of the surfaces studied and were reproducible within experimental error from run to run.

Photoelectron energy distributions (EDC's) taken on the same two surfaces are shown in Figs. 25 and 26. In each figure the curves are shown at intervals of .25 eV in photon energy and the abscissa

is plotted as $E-E_f-h\nu$ to reveal the energies of the initial states. All of the curves were virtually noise-free because of the high signal levels encountered. Consequently, successive traces for a given surface and photon energy were identical. The reproducibility from run to run was also excellent.

Spectral yields and energy distributions were generally not measured on cathode surfaces which were at intermediate stages of activation. The partially-cesiated surfaces, for example, were not studied partly because of the window limitation discussed in Sec. II. 9 and partly because of the availability of photoelectric data in this region (Jeanes and Mularie[18]). Photoelectric measurements were taken between minimum work function and saturation, however, because data on the position of the valence band with respect to the Fermi level (surface potential) in this range was not available. The results are described later in this section.

In preparing the EDC's for display, the low energy tails in all of the distributions were cut off arbitrarily by extrapolating the linear portions of the low energy edges to zero. The tails or broadened edges were due to emitter nonuniformities, magnetic fields, nonideal geometry, and collector reflectivity changes. These factors actually broadened the entire distribution but the greatest effect was in the low energy region. Even with the edge extrapolation the energy distributions were generally .1 to .2 eV wider than $h\nu-\varphi_s$ (φ_s = sample work function), the maximum theoretical width assuming no broadening.

Normalization of the EDC's was straightforward because all of the distributions used in the figures were taken at the same sensitivity. The curves were corrected only for the magnitudes of the photon flux. The normalization factors derived in this manner were typically within several percent of those obtained by making the enclosed areas proportional to the respective yields. The only exceptions were those curves taken near the threshold ($h\nu-\varphi_s \leq .5$ eV) where broadening was significant because of the narrowness of the distributions. The "area" factors for some of the curves taken in this region varied by as much as 20% from the "sensitivity" factors. Such errors were not expected to affect the interpretation of the data.

Ge/Cs photoemission

The Ge/Cs yield curve of Fig. 24 was very similar to that observed by Jeanes and Mularie[18] on the minimum work function surface ($\theta\sim .7m$) in that very little structure was evident that could be attributed to bulk band features. An experimental photo-electric threshold (ξ) was determined by fitting the emission in the threshold region to a 5/2 power law (i.e. $Y\propto(h\nu-\xi)^{5/2}$). Such a power law dependence is well-based in theory and experiment[33,34]. The exponent 5/2 was chosen because bulk indirect processes were observed to dominate the Ge/Cs photoemission in the threshold region (discussed later in this section). A value for ξ of $1.52 \pm .05$ was found graphically by extrapolating to zero yield a plot of $Y^{2/5}$ vs. photon energy. The extrapolation is shown in Fig. 27. Since

the Ge/Cs work function was also near 1.5 eV (Sec. III. 3. d), the surface appeared to be strongly p-type. This hypothesis is reasonable in view of the conclusion of Jeanes and Mularie[18] that the minimum work function surface is degenerately p-type.

A series of EDC's was taken at 3.25 eV photon energy as a function of cesium coverage to detect any movement of the high energy edges between minimum work function and saturation. The curves, shown in Fig. 28, exhibit little or no shift (<0.1 eV) in the high energy edges in the range $0 > .5m$. The Fermi level was placed in the diagram in accordance with the data of Jeanes and Mularie. The placement was within experimental error of the value determined from the final work function after correcting for the increased width of the distribution due to the lack of collector resolution.

The Ge/Cs EDC's corresponding to the spectral yield of Fig. 24 are shown in Fig. 25. The curves are displayed at various photon energies between 1.75 and 3.50 eV, and the Fermi level has been placed to correspond with Fig. 28. The behavior of the distributions as a function of photon energy is similar to that observed by Jeanes and Mularie for the .5m surface. The high energy edges are coincident except for the curves near 3 eV. The behavior of the latter has been attributed to the onset of direct transitions at a feature of the Brillouin zone structure, viz., the $\Gamma_{25'} \rightarrow \Gamma_{15}$ direct energy gap at $k = 0$ (Fig. 29)[18]. The observed photon energy range of 3.0 to 3.3 eV for such structure is in good agreement with band structure calculations[35]. The same behavior has been observed by Riach[14] for the Ge(111)-Cs system. A somewhat different interpretation is offered here involving transitions from filled surface states in the bandgap region. This is discussed in detail in Sec. IV. 2.

Ge/Cs/0 photoemission

The spectral yield after optimization with oxygen (Fig. 24) shows considerably more structure than the corresponding Ge/Cs data. The most prominent feature is the sharp rise near 2 eV. The same rise was observed by Riach[14] for Ge(111)-Cs-0 but could not be correlated with any of the bulk band structure. Another feature is the shoulder below 1.5 eV. This appears to be due to surface state emission (Sec. IV. 2). Again a photoelectric threshold ξ was determined by extrapolating a plot of $Y^{2/5}$ to zero yield (Fig. 27). A value of 1.14 + .05 eV was obtained. This represented a shift ($\delta\xi$) of .38 eV from the Ge/Cs value. The corresponding work function change between the two surfaces ($\delta\varphi$) was .54 eV.

The Ge/Cs/0 EDC's ($h\nu = 1.50$ to 3.50 eV) are shown in Fig. 26. The curves have once again been shifted by the differences in the photon energies to reveal the initial states. The Fermi level has been placed at a position consistent with that of Fig. 28, assuming that the collector work function did not change during the oxidation process. This assumption was later verified by retaking the Ge/Cs photoelectric data.

The behavior of the Ge/Cs/0 distributions as a function of photon energy appears to be quite complex, at least in the limited range of photon energies used in the experiment. The high energy

31

edges of the distributions vary considerably with photon energy, especially in the 2.5 to 3.5 eV region. This behavior is characteristic of direct excitations, and is believed to arise from transitions involving surface states (Sec. IV. 2). The low energy edges of the curves coincide as expected and are shifted by approximately .6 eV from the position of the Ge/Cs low energy edges. This is consistent with the observed work function decrease of .54 eV if the greater widening of the Ge/Cs/0 curves due to the collector resolution is taken into account.

The 2870°K "white light" sensitivity of the Ge/Cs/0 surface of Fig. 24 was 45 µa/lumen. This was a factor of 13 larger than that of the corresponding Ge/Cs surface. Both sensitivities were calculated from the uncorrected yield data using a tabular procedure.[36] The Ge/Cs/0 value was somewhat lower immediately following oxidation, consistent with the aging phenomenon mentioned earlier (Sec. III. 3. d). The 45 µa/lumen value compares favorably with the 50 µa/lumen value reported by Caldwell, Kalweit, and Kennedy[31] for p^+ Ge(100)/Cs/0, which had a 0.2 eV lower photoelectric threshold. The dark current from the activated surface in the present experiment was typically $\sim 1 \times 10^{-10}$ amps/cm^2.

4. Experiments Involving Oxidation of Partially Cesiated Surfaces

Several additional experiments were carried out involving the addition of oxygen to partially-cesiated surfaces. These experiments were designed to obtain more information about the structure of the cesium oxide layer. Surfaces formed in this manner fell into one of two catagories, depending upon the behavior of the photosensitivity with oxidation. Surfaces covered initially with greater than .5m of cesium exhibited an increase upon oxidation, while surfaces covered initially with less than .5m showed a decrease. Each initial coverage range required a different method of oxygen exposure. The two cases are discussed separately below.

$\theta > .5m$

The first set of experiments was undertaken on surfaces covered initially with .5m of cesium or more. Since the photosensitivity of these surfaces increased with oxidation, the procedure was to expose until maximum photosensitivity was reached and slightly passed. The sensitivity typically returned to the maximum shortly after the oxygen was shut off. This process was repeated for a variety of initial cesium coverages between .45 and 2.0m. The results of these experiments are summarized in Figs. 30 and 31. Fig. 30 shows the work function data for both the cesiated and oxidized surfaces, while Fig. 31 shows the corresponding photosensitivities. The work function curves indicate saturation near .9m cesium coverage, while the photoelectric curve indicates saturation near 1.05m. The former value was expected to be low because the measurement was taken at the center of the sample where the coverage was high. The latter value was expected to be high because the measurement was an average over the entire sample area.

The photosensitivity plot merits further consideration because the data is more complete in the .5m region. It is significant,

for example, that no increase in photosensitivity was observed for
an initial cesium coverage of .5m, and that an increase less than
one-tenth of that at saturation was observed at the work function
minimum. A nearly identical increase was observed on a uniform
molecularly-deposited minimum work function surface (Sec. III. 3. c),
all parts of which had been covered to a point definitely beyond
the work function minimum. These observations clearly refute earlier
evidence that coverage saturation occurs for Ge(100)-Cs at the work
function minimum.

The fluorescent room lights were used to obtain the data of
Fig. 31. The photosensitivity increase observed at saturation with
this source was 7-fold, even though the "white light" value discussed
earlier (Sec. III. 3. e) was nearly 13-fold. The reason for the
difference was the smaller infrared component of the fluorescent
source. It is apparent from the yield curves of Fig. 24 that the
largest sensitivity increase resulting from oxidation occurs in
the infrared region of the spectrum.

$\theta < .5m$

The second set of experiments was conducted on surfaces covered
initially with .5m of cesium or less. Since the photosensitivity
decreased with oxidation for such surfaces, it was not clear to what
extent oxygen should be admitted. Using AES, however, it was dis-
covered that the oxidation of such surfaces was somewhat self-
limiting. The amount of oxygen readily adsorbed was roughly pro-
portional to the amount of initial cesium, and was not particularly
sensitive to the extent of the oxygen exposure. The sticking
probability appeared to be near unity until the point at which the
O/Cs Auger peak ratio was comparable to that for the normal optimiz-
ed surface. Some deviation from proportionality was observed at
low cesium coverages, where the O/Cs ratio was lower than normal
following oxygen exposure. The sticking probability for oxygen
appeared to be small beyond the point of proportionality since the
O/Cs ratio remained nearly constant with additional exposure.
The relationship between oxygen exposure and Auger peak height
on cesiated surfaces was not examined in detail.

A similar saturation was observed in the ESER data. The magni-
tudes of the diffraction features, which were quite dependent upon
the amount of oxygen on the surface, stabilized at the point of
rapid decrease in oxygen sticking probability. They continued to
increase slightly with additional oxygen, as was previously ob-
served on the fully cesiated surface. The magnitude of peak F
was largely dependent upon the total amount of oxygen on the surface,
and was nearly independent of the amount of cesium, except as the
cesium affected amount of oxygen readily absorbed. The addition
of oxygen to a cesium-only surface, for example, caused a large
increase in F, while the addition of cesium to a partially-cesiated
and partially-oxidized surface caused little or no change. The
insensitivity of F to additional cesium was evident even though AES
indicated a substantial increase in the amount of cesium present
and the work function decreased by several tenths of an electron
volt.

The foregoing results are demonstrated in Fig. 32 where ESER, AES, and work function results are shown at several stages of activation from a cathode formed by a four-step process. The procedure in the experiment was to partially cesiate the clean germanium surface (ESER curve 1), oxidize to saturation (curve 2), complete the cesiation (curve 3), and then oxidize to maximum photosensitivity (curve 4). The results shown in the figure are not the best that were obtained because the oxygen dose prior to curve 2 was excessive. The data is, however, fairly illustrative of the general behavior described earlier. If the oxygen exposure had been normal, peak F in ESER curves 2 and 3 would have been more nearly alike, and the final work function would have been lower.

The same behavior described in the previous paragraphs has also been observed for cathodes formed by multi-step processes. If the oxygen exposures at intermediate stages of activation were of normal length, the final work functions were identical within experimental error to those for samples prepared by the normal two-step process. The oxygen and cesium Auger peak magnitudes (and therefore the coverages) were also identical to those from normal surfaces.

Several other observations are worthy of note. First, it was clear that cesium had to be present on Ge(100) in order for oxygen to adsorb readily. Exposure of the clean surface to the amounts of oxygen normally needed for activation resulted in no buildup of oxygen that could be detected by AES, ESER, or work function. This undoubtedly reflects the low sticking probability for oxygen on clean germanium (2.4×10^{-3} for Ge(100)[25]). It was also evident that the O/Cs Auger peak ratio observed on partially cesiated and oxidized surfaces did not deviate significantly from the value observed for fully activated surfaces. Finally, the extent of the work function shift beyond the 3.18 eV value for a fully-cesiated surface appeared to be solely dependent upon the total amount of oxygen on the surface, independent of when the cesium was adsorbed. All of these observations demonstrate the dependency of the oxygen coverage on the cesium coverage.

5. Studies of Abnormalities in Cathode Formation

a. Initial Contamination

The initial germanium surface was kept as free as possible of contamination during most of the experiment so that optimum photoemission could be achieved. This allowed the surface characterization to be meaningful. It was informative, however, to deliberately introduce surface contamination prior to cathode formation to examine the effect upon the activation process. Only initial oxygen contamination was examined in detail, since oxygen was a vital constituent of the final photosurface. Other forms of contamination (e.g. carbon) produced similar results.

Plotted in Fig. 33 is ESER data from clean, cesium-saturated, and optimized surfaces following initial oxygen exposures of 0, 1, and 5 on a relative scale. The exposure corresponding to "1" was

roughly 100 times that normally used for optimization and the resultant oxygen Auger peak was approximately 1/10 that observed on the normal optimized surface. The deteriorative effect of the initial oxygen on the diffraction features at all stages of cathode formation is apparent. The two sets of curves for the cesium-saturated and optimized surfaces are not unlike those obtained from partially cesiated surfaces (Fig. 21). If specific cesium sites can be associated with the reflectivity peaks B and C, the former set of curves suggests incomplete cesium adsorption onto sites associated with C. The net effect of the oxygen contamination was to decrease the photosensitivity of the final surface.

The work function and AES data corresponding to Fig. 33 is summarized in Fig. 34. Also included in the figure is data from an experiment where the relative oxygen exposure was "20". The work function results in all cases demonstrate that initial oxygen contamination is detrimental to cathode performance and that the final surface after such treatment contains less cesium than normal. The implication of this data when coupled with the corresponding ESER data is that the initial heavy oxygen exposure promotes adsorption which blocks potential sites for cesium adsorption which are necessary for proper optimization.

b. Contaminated Cesium Deposition

The contamination associated with each of the cesium sources has been discussed at length in earlier sections (Secs. II. 4 and III. 3. a). The molecular source emitted slight amounts of hydrocarbons (especially methane) during deposition, while the ion source, when operated improperly, evolved small quantities of oxygen. The methane contamination, as discussed earlier, did not present any particular problems unless the cesiated surface was bombarded for a period of time with high energy electrons, as, for example, during AES. Such surfaces exhibited a gradual buildup of carbon due to cracking of the methane. The oxygen contamination associated with the ion source was also of little or no consequence to the final photosurface. The presence of oxygen simply made it difficult to separate the effects of cesiation and oxidation at intermediate stages of cathode formation. When the ion source was operated as outlined in Sec. II. 4, the two processes were easily distinguished.

Figure 35 shows ESER data from a fully cesiated surface deposited using improper ion gun potentials. The gun was defocused such that cesium was deposited at 1/10 the normal rate, thereby increasing the arrival rate of oxygen at the surface relative to that of cesium. The 0/Cs ratio corresponding to the dashed curve was .5, indicating considerable oxygen contamination. The reflectivity features are identical to those of partially-oxidized fully-cesiated surfaces (Fig. 22) where the oxygen was introduced following cesiation rather than continuously throughout deposition. This fits with the earlier observation (Sec. III. 4) that the Cs-0 structure is the same whether the oxygen and cesium adsorption occurs in single or in multiple steps.

c. Ordering Imperfections

The role of structural perfection in determining the ultimate Ge/Cs/0 photoresponse has been discussed somewhat in earlier sections.

35

It has been demonstrated, for example, that the cesium and oxygen adsorb onto the germanium surface in an ordered fashion, and that any disruption of the regular arrangement by the initial surface contamination limits the ultimate cesium coverage and degrades the photosensitivity. It has also been shown that surfaces having the sharpest LEED patterns and strongest electron reflectivity features typically exhibit the best photoresponse.

Similar observations have been reported by Goldstein[7] for Si/Cs/0. Surfaces successfully activated to NEA exhibit LEED patterns with sharply defined spots and low backgrounds, while surfaces activated unsuccessfully exhibit LEED patterns with blurred or streaky spots. The Auger spectra from both surfaces are identical, indicating the problem is structural in nature.

None of the LEED patterns observed in the present experiment exhibited such gross variations. Slight deviations were sometimes observed but these were usually also accompanied by slight changes in the Auger spectra. Improperly annealed surfaces, for example, exhibited some excess argon and did not activate to normal photo-sensitivity. Similar behavior was observed for carbon, tantalum, and oxygen contamination. Structural and chemical changes were usually much more evident in the ESER data than in the LEED patterns.

An examination was made of the importance of proper surface or-dering in the activation process. Disordering was accomplished by heating the freshly cesiated surface to ~100°C to a point where the work function had increased by several tenths of an electron volt. The surface was then recesiated to replace the small amount of desorbed cesium. After such treatment, LEED and ESER data indicated that at least some of the surface atoms had undergone irreversible structural rearrangement. The only surface parameter not affected was the Ge/Cs work function.

The ESER data for this study is summarized in Fig. 36. Struc-tural changes are clearly indicated by the changes in peaks B and C relative to the normal curve. The LEED patterns from both surfaces were also weak when compared to the normal Ge/Cs pattern, and all of the beams were streaked (including the 1/2 1/2 areas). The streak-ing was thought to indicate some sort of lateral distortion such as broken Ge-Ge surface pairs, cesium vacancies, irregular cesium spacings along surface rows, or some other rearrangement involving the Ge-Cs bonding (Sec. IV).

The 565 eV cesium Auger signal on the recesiated surface was 8% smaller than on the freshly cesiated surface, and after oxidation to maximum photosensitivy the 0/Cs ratio was only 0.37 (approxi-mately half the normal oxygen signal). The photoelectric yield was also poor. The implication was that some sort of irreversible structurable rearrangement had taken place which inhibited oxygen adsorption.

6. Other Methods of Cs-0 Activation

Several attempts were made to grow thick cesium oxide layers on the germanium sample in order to achieve a better photoelectric yield than that obtained via the normal "two-step" activation pro-

cess. Cesium oxide growth on III-V semiconductors is usually ac-
complished by alternating cesium and oxygen exposures, each time
optimizing the photoelectric yield with either the cesium or the
oxygen[37]. The cesium oxide growth process in the present experi-
ment was complicated by the inability to monitor photoemission dur-
ing cesiation, since only the ion source was available for cesium
deposition at the time of the measurements. This made it necessary
always to terminate the procedure with an "optimizing" oxidation
before taking measurements. Two methods of growth were utilized,
neither of which yielded cathodes more sensitive than those produced
by the normal "two-step" process.

The first method consisted of treating the Ge/Cs/0 surface with
a heavy dose of oxygen and then exposing the surface alternately
to cesium (1 monolayer) and oxygen, each time optimizing the photo-
electric yield with oxygen. Cs-0 treatments beyond the first did
not increase the photosensitivity (2870°K white light) by more
than 20% or decrease the work function by more than .05 eV. The
LEED pattern remained unaltered after four such treatments, probably
indicating that succeeding layers were not sticking.

The second method was identical to the first, except that the
succeeding oxygen exposures were heavy (several Langmuir) rather
than just sufficient to optimize the photoelectric yield. Whenever
work function or photoelectric data was desired, the final cesiation
was followed by an "optimizing" oxidation. Cesium and oxygen ex-
posures equivalent to 18 monolayers of cesium were applied, but it
was impossible to determine the thickness of the cesium oxide layer
because of the uncertainty in the extent of cesium desorption.
Evidence that some buildup occurred was obtained from the observa-
tion of exoelectronic emission during oxidation. Efficiencies in
excess of 10^{-4} electrons per incident molecule were observed, in-
dicative (for cesium oxide) of thick, low work function layers[37].
The photosensitivities observed, however, were considerably poorer
than for the normal Ge/Cs/0 surface.

IV. DISCUSSION

1. Clean Surface Structural Model

In order to determine the appropriate Ge/Cs/0 structural model, it is first necessary to understand the clean Ge(100) structure. The literature is somewhat inconclusive on this matter because of differing LEED observations and differing interpretations of these observations[25,26,38,39]. No definitive study has been reported to date linking specific LEED features with the chemical and structural quality of the surface. The LEED observations of the present experiment, along with the corresponding Auger and ESER data, were therefore quite helpful in selecting a clean surface model. These results, presented in Secs. III. 2, and III. 3, are summarized briefly below.

First, it is clear from the strength of the half-order and integer-order spots in the LEED patterns from both clean and cesiated surfaces, that the clean Ge(100) structure is predominantly 2x1 in character. It is also evident that the extra 1/4-order features in the LEED pattern are real and probably not linked to surface contamination. While it is true that the initial surface could not be entirely rid of contamination, it is also true that the presence of these contaminants, in excess of the normal amounts, weakened or blurred the 1/4-order LEED features, degraded the ESER peaks, and adversely affected subsequent activation. Finally, the 1/4-order LEED features disappeared completely with cesium adsorption and were not present on the final Ge/Cs/0 surface. The disappearance of the 1/4-order features has also been reported by Chen[27] for Ge(100)-Cs, as well as for Ge(100)-Na and Ge(100)-K.

The structural model which best fits these experimental observations is that of Schlier and Farnsworth shown in Fig. 37. The uppermost atomic layer in this model consists of rows of paired atoms which give the LEED pattern its 2x1 character. The 4-fold rotational symmetry of the pattern is due to mutually perpendicular domains which exist on the surface (See Appendix). The streaked 1/4-order features can be explained by a slight periodic distortion along the paired rows. This distortion must then be postulated to relax during cesium adsorption. Earlier surface models proposed by Lander and Morrison[26] and by Seiwatz[39] were not used in the present interpretation because the reconstruction proposed in each case was too severe to explain the weakness of the 1/4-order LEED features and their disappearance with cesium adsorption. The reasoning behind the present choice is discussed in the Appendix.

2. Ge/Cs/0 Electronic Model

A complete characterization of the Ge/Cs/0 photoelectric behavior would require treatment of each of the separate processes involved in photoemission: photoexcitation (or optical absorption), transport to the surface, and escape through the potential barrier at the surface. All of these processes are quite complex and defy exact theoretical treatment. The situation is made even more com-

plex by the presence of intrinsic surface states, and by states resulting from the cesium and oxygen adsorption. Despite this complexity, it was possible to derive some basic information about the Ge/Cs/0 emission processes from the measured yield and photoelectron energy distribution curves. While there was an admitted lack of photoemission data at high photon energies and as a function of cathode formation, such omissions were not expected to seriously affect the interpretation.

The Ge/Cs/0 photoemission is treated here independently of the surface structural model. This is because the conditions at the immediate crystalline surface (structure and chemical composition) were expected to affect significantly only the escape portion of the photoemission process, which can be characterized largely in terms of electron affinity and work function. Both of these parameters are experimentally measurable quantities. Surface structure and surface chemistry could also affect photoelectron transport somewhat via band-bending, but this was not a major factor in the present experiment because of the near-flat-band conditions which prevailed at the photon energies of interest.

The aim of the photoemission study was to understand the emission from the intrinsic sample well enough to be able to predict the photoelectric behavior of a cathode formed from p-type material. The threshold emission was of particular interest because of its use in determining photoelectric threshold and ultimate photosensitivity, and also because of the possibility of observing surface state emission. The interest in the threshold region explains why the photoelectric measurements were not extended to higher photon energies by installing a special window.

The consistency of the measured work function (4.7 $\pm$ .1 eV) with other published data was pointed out in Sec. III. 2. It was also assumed there, on the basis of the work of Jeanes and Mularie[18], that the clean surface was degenerately p-type due to filled acceptor-like surface states below the valence band maximum. This assumption was necessary because, as mentioned above, the present apparatus was not suited for clean surface photoelectric studies. The existence of p-type degeneracy is supported by other published work[40,41].

If Poisson's equation is solved for germanium in the bent-band region, it can be shown that an electric field of at least 2.5×10^5 volts/cm is required to bend the energy bands strongly p-type[42]. This result is for an intrinsic sample without surface states. For Ge(100), the field is supplied by filled acceptor-like surface states situated at or below the valence band maximum. By Gauss' law the surface electron density required to produce this field is 2×10^{12} cm^{-2}. Since the intrinsic carrier concentration (n_i) at room temperature is 2.4×10^{13} cm^{-2} for germanium, there are sufficient electrons in the conduction band to supply the necessary charge.

The space charge produced by the electric field extends roughly a Debye length into the sample (6800 $\overset{\circ}{A}$ for Ge). This distance is much greater than the mean escape depth for photoelectrons, even at

the low photon energies used in the experiment (1.5 to 3.5 eV).
While there is no published data available on the photoelectric
escape depth for germanium at low photon energies, the results of
Allen and Gobeli[43] suggest that the value is probably very small
($\ell < 50\text{Å}$) for all photon energies at which electron-electron scatter-
ing (pair production) can occur. All of the photon energies used
in the present experiment fell above this threshold, so that band-
bending was not expected to affect the photoelectron energy dis-
tributions. Even if the distributions were altered slightly, this
would not affect the positions of the high energy edges, which were
the only features actually used to identify emission mechanisms.

In order to understand the changes that occur as cesium is
deposited onto the clean surface, it is important to note that the
cesium adsorbs, at least initially, as an ion. The ionization occurs
because the germanium work function (4.7 eV) is greater than the
first cesium ionization potential (3.98 eV). Adding cesium to the
surface can also be thought of as adding donor-like states to the
surface somewhat above the Fermi level, from which electrons empty
into the unoccupied intrinsic surface states and somewhat into the
space charge region. The filling of the surface states causes the
energy bands to bend downward, leaving the surface increasingly n-
type. In many alkali-semiconductor systems this process continues
until the Fermi level encounters the adsorption-created states
higher in the bandgap. The density of those states is equal to the
surface density of alkali. In no case is the interpretation of the
observed band-bending straightforward or unambiguous. This is
because the energy distribution and/or density of surface states
changes during adsorption as does the occupation of these states.

The Ge(100) band-bending as a function of cesium coverage has
been studied quite extensively by Jeanes and Mularie[18]. Their re-
sults, while extending only to the minimum work function coverage,
show that the Ge(100) surface remains degenerately p-type through-
out cesiation. The series of EDC's vs. cesium coverage (hν = 3.25 eV)
observed in the present experiment (Fig. 28) indicates that there
is probably little or no additional deviation from p-type degeneracy
between minimum work function and saturation. The stabilization of
the Fermi level at the valence band maximum is also supported by
the agreement of the $Y^{2/5}$ threshold (1.52 $\pm$ .05 eV) with the measur-
ed work function (1.52 $\pm$ .10 eV). The Ge/Cs EDC's (Fig. 25),
plotted vs. hν in a manner that reveals the energy of the initial
states, verify that the threshold emission is largely valence band
emission. (The interpretation of the Ge/Cs EDC's is discussed later.)

One of the important results of the band-bending investigation
is that, unlike several other alkali-semiconductor systems, the
Fermi level for Ge(100) remains very near the valence band maximum
at all cesium coverages. Consequently, the photoemission from the
filled surface states is largely masked by the valence band contribu-
tion, making it impossible to conclude much about the surface state
density or distribution. All that can really be said is that the
charge contributed by the cesium to the surface states combined
with the changing surface state density is insufficient to shift

40

the energy bands by more than .1 eV. In view of the behavior of
the surface potential for other alkali-semiconductor systems as a
function of cesium coverage, these observations may indicate that
the adsorption-created states, which are plentiful at the latter
stages of deposition, may lie very near or even below the valence
band maximum.

An examination of the Ge/Cs EDC's as a function of photon
energy (Fig. 25) helps to clarify the threshold emission. The high
energy edges of the distributions are of particular interest be-
cause they represent emission from the highest lying filled states.
Surface state emission would appear in this region, if present.

It is evident from Fig. 25 that the high energy edges of the
Ge/Cs EDC's are nearly coincident for all photon energies measured,
indicating that indirect transitions dominate the threshold emission.
It is also evident from the slight motion of the high energy edge
with photon energy near 3 eV that there is some accompanying direct
behavior at that energy. These observations are in substantial
agreement with the results of Jeanes and Mularie, which are valid
for the minimum work function surface but are expected to carry
over to the saturated surface as well.

A closer examination of the Ge/Cs EDC's near 3 eV photon energy
reveals an unexpected characteristic of the high energy edges.
Rather than appearing as a shoulder on the indirect background as
observed by Jeanes and Mularie, the direct emission appears more
as a separate peak at higher energy. The difference in the two
observations stems most likely from the better energy resolution
experienced in the present experiment. The existence of a direct
peak higher in energy than the corresponding indirect peak implies
that the electrons contributing to the two peaks originate from
different initial states. If the two peaks had originated from
the same initial state, the direct peak would appear lower in
energy than it actually does.

In view of this observation, a logical interpretation of the
Ge/Cs EDC's is that the larger indirect contribution originates
from the $\Gamma_{25'}$ valence band maximum, while the smaller direct con-
tribution originates from surface state levels. While it is pos-
sible that the observed spin-orbit splitting of the valence band
at the $\Gamma_{25'}$ point could also account for this behavior, it is un-
likely that the emission from the higher-lying 4-fold degenerate
level could be so small. Also, the splitting of .29eV is much
greater than the width of the observed structure in the high energy
edges. The surface state interpretation is therefore favored.
The surface potential appears to fall between .05 and .1 eV for
this surface.

The Ge/Cs/0 EDC's (Fig. 26) exhibit a behavior similar to
the Ge/Cs EDC's but greatly accentuated. Evidently, some band-
bending toward n-type occurs during oxidation. The existence of a
separate direct peak in these curves is obvious, especially when
comparing the 2.75 and 3.00 eV curves. It is also clear from a

41

comparison of the two curves that the high energy edges of the two contributions are separated by ~.25 eV. This value should be very nearly equal to the surface potential. Again the larger indirect component is due to valence band emission, while the smaller direct component is due to surface state emission. This conclusion is consistent with the observed position of the Fermi level.

The direct emission evident in both the Ge/Cs and Ge/Cs/0 EDC's can be better understood with the aid of the E vs. $\vec{K}$ diagram of Fig. 29. There is some question as to whether such a diagram (which applies to the bulk lattice) can provide any useful information at all concerning direct transitions out of surface states, since $\vec{K}$-conservation requires that the transitions be parallel to the surface in real space. Such a restriction appears to limit the transitions to higher lying surface levels, although transitions could also occur to bulk states providing that their wave functions extended to the surface. The latter appears to be true in the present experiment since the emission seems to be characteristic of transitions to bulk levels. The onset of direct emission near 3 eV corresponds closely to the $\Gamma_{25} \rightarrow \Gamma_{25}$ separation, while the behavior below 2 eV is characteristic of direct transitions to lower lying conduction band levels from relatively flat regions of $\vec{K}$-space.

The two sets of distributions can be used to check the relative amount of band-bending between the two surfaces. They must, however, be normalized to each other before any comparison can be made. This has been done in Fig. 38, where the Ge/Cs and Ge/Cs/0 3.00 eV distributions are shown. For both surfaces this was the photon energy that caused the greatest excursion of the high energy edge. Extrapolation of the two indirect edges representing valence band emission shows that the bands bend ~.2 eV toward n-type upon oxidation. This result agrees within experimental error with the value calculated from the work function and photoelectric threshold data (Secs. III. 3. d and III. 3. e), and also with the difference in estimated surface potentials. The band-bending and work function results are summarized in Fig. 24.

3. Ge/Cs/0 Structural Model

a. Value of the ESER Data

The potential use of the ESER data for determining actual surface atomic positions has been discussed in Sec. II. 7. The extreme sensitivity of the measurement to the arrangement of the uppermost atomic layer has been noted, as was the difficulty of data interpretation. The same sensitivity that was observed by Chen[27] was also observed in the present experiment. This is demonstrated by the considerable changes that occur in the ESER data upon cesium adsorption (Fig. 21), at the same time that only slight changes, if any, occur in the underlying germanium structure.

Some attempt has been made to reconcile the clean surface ESER data with the Ge(100) diffraction data of Erickson[44]. A comparison indicates that the 61 eV peak is likely a second order Bragg maximum resulting from the 1.4 Å spacing between successive (100)

42

planes. The 8.5 eV peak could well be the first order maximum, but this is purely speculative because of the uncertainty in the inner potential correction. It is not likely that multiple scattering theory will soon be applied with success to Ge(100). The large lattice spacing and the covalent nature of the bonding presently make it difficult to obtain a reliable potential for carrying out the required calculations[44].

Because of these difficulties, the ESER data was used primarily for identification and comparison of surfaces. These efforts were largely successful because of the high reproducibility of the data for a given surface. There was also an attempt to draw some conclusions about the cesium oxide structure from the development of the ESER peaks during cathode formation. This usually required associating the development of a particular reflectivity peak with adsorption onto a particular surface site. The possibility that such an assumption might not be valid was always kept in mind.

b. Cesium Coverage Determination

The possible sources of error in the cesium coverage measurement are listed in Sec. II. 4. Of the various factors mentioned there, three have a significant bearing on the present results. These are deposition uniformity, deposition area, and sticking probability. The latter has been neglected so far in the discussion and will be treated following a summary of the effect of deposition uniformity and area. Briefly, the coverage error deriving from uncertainty in the deposition uniformity or area was $^{+23\%}_{-3\%}$. These error limits represent $^{+10\%}_{-0\%}$ for uniformity, $^{+10\%}_{-0\%}$ for area, and + 3% for instrument error. The one-sided error limits reflect the fact that the cesium coverage was always greatest at the center of the sample where all of the experimental data was taken, and that the coverage calculations were carried out using the maximum sample area. These conditions assured that the measured cesium coverage represented a lower bound for the actual coverage, providing the sticking probability was unity.

While the absolute coverage measurements were affected by both uniformity and area, relative measurements were affected only by uniformity. This fact made it possible to isolate a number of important features in the work function and reflectivity data with respect to cesium coverage. The ability to determine relative coverages was enhanced in some instances by using the molecular source for uniform deposition and identifying the surfaces by work function. A number of these experiments have been described in Secs. III. 3 and III. 4.

By using the molecular and ion sources in this complementary fashion, it was possible to establish that coverage saturation occurs at least .2m beyond the work function minimum, and that the work function minimum occurs approximately .15m beyond the point at which the abrupt changes take place in the ESER data. The latter coverage also signals the point at which addition of oxygen to the surface decreases rather than increases the work function. From the error limits that apply, it is safe to say that all three points

occur at measured coverages at or beyond .5m and that saturation
occurs at a coverage $\geq$.85m. The major departure from earlier inter-
pretation is that cesium saturation occurs beyond rather than at
the work function minimum.

The matter of sticking probability complicates the coverage
interpretation somewhat. It has been assumed so far in the dis-
cussion that the sticking probability of cesium on germanium is
unity throughout the range of cesium coverage and drops rapidly to
zero at saturation. While unity sticking probability is clearly
an attractive assumption in view of the chemical reactivity of
germanium to cesium, such a relationship is not certain. It is
reasonable to say, however, that the value lies near unity in the
low coverage range (θ < .5m) on the basis of the LEED structures
observed there (Sec. III. 3. b). The AES results of Fig. 16 imply
further that the sticking probability remains constant throughout
the range of cesium coverage, providing the relationship between
Auger peak height and actual cesium coverage can correctly be
assumed to be linear. Ion energy was not expected to be a factor,
since earlier studies[46] indicate that the zero coverage sticking
probability (Cs and Ge(100)) does not vary by more than a few per-
cent in the 2-50 eV range. Ion energies in the present experiment
were ~2 eV.

Perhaps the most convincing support for unity sticking prob-
ability comes from the work function data of Weber and Peria[29]
for various semiconductor-alkali systems. In these studies the
authors were able to correlate break points in work function vs.
measured coverage curves with the filling of particular sites
on semiconductor surfaces. The Ge(111) - Na, K, Cs and Si(111) -
Na, K, Cs data quite clearly indicate unity sticking probability,
since the break points are consistent with the expected site oc-
cupation. The Ge(100) and Si(100) results are less convincing
because the break points are not as pronounced. The work function
minima, however, occur at coverages consistent with unity or near-
unity sticking probability.

On the basis of these arguments, it is assumed that the stick-
ing probability of cesium on Ge(100) is unity throughout the range
of measured coverage. The actual cesium coverage therefore differs
from the measured coverage by at most $^{+20\%}_{-0\%}$ with an added $\pm$ 3%
instrument error. Any disagreement with the unity sticking prob-
ability assumption would probably require a major reinterpretation
of the structural data.

c. Cesium Adsorption

It is evident from both the ordered structures observed in the
LEED patterns and the sharp diffraction features observed in the
ESER data throughout cesiation that the cesium adsorbs in an ordered
fashion onto the germanium surface. This is certainly true in the
low coverage region (θ < .5m) where LEED indicates the existence
of several distinct surface phases with at least partial ordering
(Fig. 19). The apparent insensitivity of LEED to adsorption in

the region beyond .5m raises some question as to the long-range
order for those coverages, especially since the ESER data is not
necessarily sensitive to lateral surface spacings and therefore
cannot be used to detect lateral surface order. It is probably
safe to assume, however, that the final Ge/Cs/O surface has excel-
lent long-range order solely on the basis of the sharp, intense,
low-background LEED pattern.

The LEED observations also rule out any adsorption process
involving reconstruction of the underlying germanium structure,
since the 2x1 features present on the clean surface predominate
throughout the entire range of cesium coverage. The occurrence of
both 4x3 and 2x3 features in the .1 to .3m region further demon-
strates the strength and influence of the underlying paired row
structure. The existence of such features suggests that the cesium
adsorbs randomly at distinct positions along the paired rows but
that nearest and next-nearest neighbors are excluded. The exclu-
sion undoubtedly breaks down as the adsorption proceeds, since the
1/3-order features disappear with increasing cesium coverage.

Random adsorption with exclusion in the low coverage region
almost certainly requires the formation of antiphase domains[47]
on the surface. The effect of such ordering upon the LEED pattern
can be demonstrated with the aid of Fig. 39. Several types of do-
main relationships are possible, depending upon the cesium cover-
age. These are illustrated in the figure along with the resultant
LEED patterns determined using the formulation of Park and Madden[47].
The beams affected by the presence of antiphase domains are indicat-
ed by lines, which denote streaks. For the domains shown, only the
1/4 1/3 beams should be affected and only in the .055 to .125m
range. This observation fits well with the actual features which
occur in the LEED photographs. The same reasoning can be applied
to show why antiphase domains should have no effect on the 1/2 1/2
beams in the coverage range where they appear.

The sharpness of the 1/2-order LEED beams in the low coverage
region (0 < .5m) implies that only one type of site is being filled
initially. If such were not the case, the development of antiphase
domains would cause the 1/2-order beams to streak or blur. The
periodicity of the LEED pattern indicates that the site has a 2x1
distribution over the surface, with perpendicular domains having
dimensions comparable to or larger than the coherence width of the
electron beam (~1000 Å). The sites might well be the "cave" sites
between the paired rows as suggested by Levine[6], or alternatively
the "pedestal" sites atop the rows.

The development of only a single new peak in the electron reflec-
tivity data (at B) in the low coverage region also supports "one-
site" initial adsorption. This evidence, of course, is dependent
upon the validity of associating B with a particular adsorption
site. The steady growth of B in spite of the changing surface
periodicity suggests that B arises from a Cs-Ge spacing rather than
from a lateral Cs-Cs spacing.

The sudden appearance of new peaks in the reflectivity data
at .5m suggests that a new cesium site is beginning to be filled,

presumably following the completion of the filling of the first site. The new site, like the first, has 2x1 periodicity but is undoubtedly energetically less favorable for adsorption, at least in the low coverage region. One possible configuration consistent with a fairly even distribution of cesium over the surface is one in which the second half-monolayer of atoms occupies sites along rows midway between the 2x1 rows formed during the first half-monolayer adsorption. Whether or not the "second" sites are completely filled at saturation is not clear from LEED, since LEED was not particularly sensitive to cesium adsorption in that region. The AES results indicate at least a partial filling of these sites. These observations depend somewhat upon the ability to determine the actual cesium coverage, a topic which has been discussed in Secs. II. 4 and IV. 3. b.

The difference between the two cesium sites is further demonstrated by the action of oxygen on the work function of the sample in the two coverage ranges. For initial coverages less than .5m, the effect of oxygen adsorption is to increase the work function, while for coverages greater than .5m, the effect is to decrease the work function. This behavior implies that a noticeable vertical separation exists between the two cesium layers and that the oxygen layer lies midway between. This arrangement would allow the oxygen atoms, which act as acceptors and receive net charge during adsorption, to cause the observed work function shifts in the two regions of cesium coverage.

The initial cesium layer ($\theta \leq$ .5m) most likely lies in the "trough" regions between the germanium double rows, and perhaps in the "cave" sites so labeled by Levine. The second cesium layer ($\theta >$ .5m) most likely occupies the "pedestal" areas consistent with an even distribution of cesium over the surface. In this configuration each layer would have a 2x1 periodicity with respect to the bulk net. The oxygen layer, in turn, would almost be required to occupy the regions between the "pedestals" in order to be physically beneath the uppermost cesium layer.

d. Oxygen Adsorption

The experimental LEED data is somewhat less helpful for understanding the oxygen adsorption than it was for understanding the cesium adsorption. The most significant LEED observation was the sharp, low-background pattern which showed no evidence of extra features other than the normal 1/2-order spots. Such quality usually implies excellent long-range surface order and in this case suggests that the oxygen adsorption is complete, the coverage being some multiple of one-half monolayer.

The strength of the 1/2-order LEED beams shows that the 2x1 character of the underlying germanium layer is duplicated or even enhanced in the cesium oxide layer. The strong diffraction peaks in the Ge/Cs/0 electron reflectivity data also imply that the uppermost layer is well-ordered. The latter conclusion is based in part on Chen's observation[27] that the diffraction peaks in the electron reflectivity curves arise principally from top layer scattering.

46

As in the case of cesium adsorption, much information concerning the role of oxygen was gathered from experiments involving oxidation of partially-cesiated surfaces (Sec. III. 4). The significant results of these experiments can be summarized as follows:

1) Oxygen does not adsorb readily (i. e., with unity sticking probability) onto Ge(100) without prior cesium adsorption.

2) The amount of oxygen readily adsorbed onto a cesiated surface is proportional, to a first approximation, to the cesium coverage. There was some evidence that proportionality does not hold for low cesium coverages ($\theta < .2m$).

3) Early adsorption of oxygen onto a partially-cesiated surface does not adversely affect future cesium or oxygen adsorption. The optimized surface, in fact, may actually be formed by a number of cesium and oxygen exposures.

4) The work function of a fully-cesiated partially-oxidized surface depends solely upon the amount of adsorbed oxygen, independently of when or in how many steps the cesium is adsorbed.

5) The magnitude of the diffraction peaks in the ESER data from a fully-cesiated partially-oxidized surface depends largely upon the amount of adsorbed oxygen, independently of when or in how many steps the cesium is adsorbed.

The dependence of the oxygen adsorption on cesium coverage shows that the cesium participates actively in the oxygen-surface bond. Either the oxygen bonds directly to the adsorbed cesium or the cesium promotes oxygen-germanium bonding. At any rate, the sticking probability of oxygen on Ge(100) increases from 2.4×10^{-3} for the clean surface[25] to near unity after cesium is adsorbed. In this respect the oxygen and cesium do not compete for sites on Ge(100).

The position of the oxygen layer with respect to the two cesium layers has been discussed in Sec. IV. 3. c. The comments there are based upon the behavior of the work function upon oxidation of surfaces at various stages of cesiation. The results indicate that the oxygen layer lies midway between the two cesium layers in the direction of the surface normal, and space limitations suggest further that the oxygen lies in the "trough" regions between the double rows.

The amount of oxygen in the optimized layer was not readily measured. The excellent quality of the Ge/Cs/O LEED pattern, however, and the existence of strong 2x1 features implied that the oxygen coverage was some multiple of one-half monolayer. No attempt was made to determine the precise amount of oxygen from exposure time and pressure because of the problems inherent in measuring oxygen pressure. It is doubtful, in fact, that an estimate of the actual exposure could even be made to within a factor of two. A value of one monolayer is favored because of the absence of 1/4-order LEED features after oxidation of a .5m Ge-Cs

47

surface. Such features might be expected if one-half monolayer
were assumed because the proportionality or near-proportionality
of oxygen coverage to cesium coverage would require one-quarter of
a monolayer of oxygen on the intermediate surface.

The observation of a smaller O/Cs Auger peak ratio for surfaces
covered initially with less than .2m of cesium implies that each
oxygen atom on the final Ge/Cs/0 surface may actually bridge two
neighboring cesium atoms. The smaller O/Cs ratio would be expected
at low coverages because of the smaller number of neighboring ce-
sium atoms. This point requires further investigation.

e. Comments Regarding the Possible Application of the Levine
    Structural Model to Ge/Cs/0

The Levine structural model for Si/Cs/0[6], based on the experi-
mental results of Martinelli[5] and Goldstein[7], is shown in Fig. 40.
The clean silicon surface, like germanium, is assumed to have the
Schlier and Farnsworth paired row structure. The adsorbed cesium
resides in 4-fold coordination with the silicon on "pedestal" sites
atop the double rows, while the oxygen occupies the "cave" sites
between the rows. Both constituents are present in quantities of
one-half monolayer, each residing in a 2x1 configuration on the sur-
face. The reduced work function of the surface is due in part to
the dipole layer formed by the oxygen and cesium ions. Details of
the model are discussed in ref. 6.

There are a number of experimental similarities between Ge/Cs/0
and Si/Cs/0. Many of these have been discussed or at least men-
tioned during the course of the paper. Because of the similarities,
the application of the Levine structural model to Ge/Cs/0 must be
considered.

Briefly, the experimental similarities are:

1) Similar activation procedures. Both cathodes are formed
    by first saturating the clean surface with cesium, then
    optimizing the photoelectric response with oxygen.
2) Similar clean surface LEED observations. Patterns from
    both surfaces exhibit 2x1 diffraction. The only difference
    is the absence of the additional 1/4-order features for
    silicon. Such features were observed by Lander and Morrison[26]
    but not by Goldstein[7].
3) Identical LEED patterns for fully-cesiated and fully-
    activated surfaces. Both patterns exhibit strong 2x1
    diffraction.
4) Marked sensitivity to deviations from structural and
    chemical perfection.

In spite of these similarities, a number of experimental ob-
servations for Ge/Cs/0 have been discussed which are not compatible
with the Levine structural model. The basic inconsistency between
the present observations and the Levine model is that there is
considerable support for a double rather than a single 2x1 cesium
layer. While evidence may be lacking that the second 2x1 layer is

complete, it is apparent that a single 2x1 layer is not sufficient for photo-optimization. The measurements clearly indicate that the point of cesium saturation (which must be reached for optimization) is distinct from either the minimum work function point or the .5m point, both of which occur at lower coverages and can be uniquely identified with particular features in the experimental data.

It would be premature at this point to propose a structural model for Ge/Cs/0 which would pinpoint the exact positions of the cesium and oxygen atoms within the 2x1 surface net. The ability to do so would certainly be enhanced if the ESER data could be interpreted. A more thorough examination of the 0/Cs ratio for partially-cesiated partially-oxidized surfaces would also be helpful. The available data, however, implies that two ordered cesium layers do exist, one likely associated with the surface "pedestals" and the other with the surface "troughs". The oxygen layer is also ordered and most likely occupies a position between the two cesium layers. The function of the oxygen layer is not entirely clear, but the charge configuration in the surface region must be redistributed during adsorption in a manner that enhances the surface dipole. The oxygen may accept charge from the cesium or it may actually alter the position of the cesium with respect to the germanium.

V. CONCLUSIONS AND RECOMMENDATIONS

In summary, a work function of .95 $\pm$ .10 eV and a white
light sensitivity of 45 μa/lumen was achieved on an intrinsic Ge(100)
sample via the application of cesium and oxygen. The activation
procedure was the same as the two-step process used to achieve NEA
on Si(100), that of saturating the clean surface with cesium and
then maximizing the photoelectric yield with oxygen. While the
work function value is not low enough to be able to achieve NEA
on a strongly p-type sample, the photoelectric results indicate
that the white light sensitivity would be improved somewhat. Even
if it were possible to achieve NEA with germanium, the dark current
would undoubtedly be too large for many applications.

The principal value of the present study was the insight added
to the semiconductor-Cs-O activation process which at the present
time is not well understood. While an exact structural model was
not deduced from the experimental results, the evidence was clear
that the Levine structural model did not apply to Ge/Cs/O, contrary
to expectation. It would be informative to carry out the same in-
vestigation with Si/Cs/O, since preliminary results for that system
indicate that one-half monolayer of cesium may not be sufficient to
achieve NEA[46,48]. Cesium saturation was found to occur at a cover-
age beyond the work function minimum, contrary to one of the basic
assumptions of the model. A modification might be required allowing
a basis of two rather than one cesium atom per site on the 2x1 sur-
face net.

Another important result of the experiment was the observation
of surface state emission in the photoemission. The Ge/Cs and Ge/
Cs/O EDC's near 3.0 eV photon energy were particularly interesting
because the behavior there, previously attributed to bulk emission,
was very likely due to transitions involving surface states. The
direct behavior of the surface state emission was also interesting.
The photoelectric measurements should be extended to higher photon
energies and measured with better resolution in order to increase
confidence in the observations.

Finally, the usefulness of the ESER technique in structural
determination was also demonstrated. It was possible, for example,
even without identifying the exact origin of the diffraction peaks,
to extract useful information concerning adsorption processes. The
curves were also helpful in identifying and comparing surfaces.
Because of the wealth of potentially valuable structural information
contained in the ESER data, more effort should be expended in the
future in the theoretical interpretation.

APPENDIX

Ge(100) Structural Model

At the present time, there is little agreement in the litera-
ture on a structural model for Ge(100). To date, at least four
different structures have been proposed[25,26,38,39], none of which
is fully consistent with the LEED observations of the present ex-
periment. Two are based on the LEED observations of Farnsworth,
Schlier, and co-workers[25], and two on the observations of Lander
and Morrison[26]. Schlier and Farnsworth report patterns exhibiting
1/2-order spots, while Lander and Morrison report 1/4-order features
in addition to the 1/2-order spots. The four structural models are
shown in Fig. 41 for comparison with each other. All of the models
postulate the existence of mutually perpendicular surface domains
to account for the 4-fold rotational symmetry observed in the LEED
pattern. Such domains exist quite naturally on nonsmooth surfaces
of diamond structured crystals because of the alternating bonding
directions between successive (100) layers.

The Schlier and Farnsworth model[25] was the earliest proposed
for the Ge(100) surface. This model accounts for the 1/2-order
LEED features by assuming that adjacent rows of surface atoms pair
together into double rows, halving the number of free bonds and
leaving the surface in a lower energy state. The Haneman[38] model
explains the 2x1 periodicity by assuming that atoms in every second
row are raised with respect to atoms in neighboring rows. Both
models were deduced on the basis of the Schlier and Farnsworth
observations.

Lander and Morrison[26], who first observed the 1/4-order fea-
tures, propose a partial layer of atoms above a normal Schlier and
Farnsworth surface. The partial layer consists of pairs in a 4x2
arrangement. Siewatz[39] proposes a similar model, but the top
layer instead is complete and consists of "conjugated chains" parallel
to the underlying rows. Both models require that the interaction
between (11) top layer rows be weak in order that short range order
or streaking of the 1/4-order LEED features might occur. The top
layer rows are rows of pairs in the Lander and Morrison model and
chains in the Seiwatz model.

The difficulty in selecting a clean surface model in the pres-
ent experiment is that the latter two models, while seemingly able
to account for all of the LEED features observed, are not consistent
with the present LEED observations from cesiated surfaces. While
both models correctly predict the existence of streaked 1/4-order
features on the clean surface, they do not favor the disappearance
of these features as cesium is adsorbed. In neither model would one
expect the surface atomic arrangement or Ge-Ge bonding to be easily
altered with alkali deposition. Rather, one might expect the 1/4-
order features in the LEED pattern to persist or to be enhanced,
contrary to observation. In addition, both models predict 1/4-order
features from the clean surface which are much stronger than those
observed. Both models were rejected for these reasons.

In determining the appropriate clean surface model, both the weakness of the 1/4-order LEED features and their disappearance with cesiation were taken as evidence that the surface is basically 2x1 in nature. The additional features were viewed as resulting from a slight perturbation of the 2x1 net. The model of Schlier and Farnsworth was favored as a first approximation because of energy considerations. Green and Seiwatz[49] have demonstrated that the paired configuration of top layer atoms in that model is energetically favorable to the unpaired state because the energy released by bond formation is greater than the resultant distortional energy. The calculation also shows that the pairs tend to form rows rather than joining together randomly on the surface. Staggered pairs or unpaired rows would cause streaking of the 1/2-order beams in the LEED pattern, contrary to the observations.

The severity and also the stability of the top layer reconstruction associated with the Schlier and Farnsworth model imposes a rather rigid constraint upon the arrangement of the underlying layers. It is obvious that there must be a region of transition between the paired surface rows and the deeper bulk configuration. The greatest amount of bond distortion will likely occur between first and second layer atoms, with successively diminishing amounts between deeper layers. The lattice strains could quite conceivably result in a slight readjustment of the uppermost layer without destroying the 2x1 periodicity. Because of the periodic nature of the lattice, additional features might well appear in the LEED pattern.

It is significant that neighboring surface pairs within a row share common underlying atoms, while neighboring rows are coupled only indirectly through third layer atoms. This fact requires that a distortion be propagated in a periodic fashion within a row, but places no strong requirement on the periodicity of the distortion between rows. This is consistent with the streaking of the secondary features in the LEED pattern, indicating long range order in one direction only. It is evident from inspection that the distortion must have a periodicity of two (in terms of substrate unit mesh lengths) along a row and a periodicity of two or four in the perpendicular direction. The latter periodicity depends upon the orientation of neighboring rows relative to each other. With respect to the distortion associated with a particular row, a neighboring row may be identical or may be shifted by one substrate unit meshlength. This allows both 2x2 and 4x2 meshes on the surface.

Fig. 42 shows two examples of possible distortions of the Schlier and Farnsworth model which are consistent with the secondary diffraction features observed. The surface of Fig. 42a consists of alternately raised and lowered pairs, while the surface of Fig. 42b has alternately displaced pairs, requiring also that one atom in each pair be raised above the other. In both models the absence of strong coupling between the double rows allows both 2x2 and 4x2 surface meshes (as shown), and makes possible the short range order observed in the LEED pattern in the direction of the repeating distance of four. Arrows in both drawings indicate roughly the directions of displacement of the second layer atoms.

52

In order to discuss the resultant LEED pattern, it is useful to think of the surface as made up of a number of large domains in the two perpendicular surface orientations, each of which is further divided into a succession of long narrow subdomains. The subdomains are all of the same structure (either 2x2 or 4x2) but may be shifted relative to each other by a unit mesh length along a direction parallel to the surface rows. In the terminology of Park and Madden[47], the subdomains are termed antiphase domains and the intervening boundaries antiphase boundaries. The connecting vector across the boundary determines whether the subdomains are in or out of phase with each other and consequently whether or not disorder effects will be evident in the LEED pattern.

Fig. 43 illustrates the application of this formulation to both 2x2 and 4x2 surface nets. At the left are the real surface nets and at the right the resultant reciprocal nets. The effect of the presence of several antiphase domains within an area smaller than the coherence zone (the crystal surface region over which the primary wave field is effectively coherent) is indicated by elongated spots or streaks. The spots are elongated in one direction only because all of the antiphase boundaries are parallel to each other. The streaks indicate irregularly spaced boundaries. If the boundaries were regularly spaced instead, the elongated areas would appear as double spots (split beams) rather than as streaks. Using the formulation of Park and Madden, splitting is predicted for beams with indices [h,k] such that $h = \pm 1/2, \pm 3/2, \pm 5/2,...$ for the 2x2 net and such that $k = \pm 1/4, \pm \overline{3}/4, \pm \overline{5}/4,...$ for the 4x2 net.

If the foregoing interpretation is correct, comparison with the clean surface LEED pattern (Fig. 12) indicates that while both 2x2 and 4x2 nets exist on the surface, the 2x2 net probably has the longer range order. This is evident from the better resolution of the 1/2 1/2 spots relative to the 1/4-order streaks. The nature of the 1/4-order streaking indicates that the antiphase boundaries are both irregularly spaced and parallel. Whatever the details of the perturbed structure, however, it is clear from the experimental data that the distortion does not persist as cesium is adsorbed.

REFERENCES

1. J. van Laar and J. J. Scheer, Philips Tech. Rev. $\underline{29}$, 54 (1968).

2. J. J. Scheer and J. van Laar, Solid State Commun. $\underline{3}$, 189 (1965).

3. A. A. Turnbull and G. B. Evans, Brit. J. Appl. Phys. (J. Phys. D) $\underline{1}$, 155 (1968).

4. D. G. Fisher, R. E. Enstrom, J. S. Escher, and B. F. Williams, J. Appl. Phys. $\underline{43}$, 3815 (1972).

5. R. U. Martinelli, Appl. Phys. Lett. $\underline{16}$, 261 (1970).

6. J. D. Levine, Surface Sci. $\underline{34}$, 90 (1973).

7. B. Goldstein, Surface Sci. $\underline{35}$, 227 (1973).

8. R. U. Martinelli, J. Appl. Phys. $\underline{44}$, 2566 (1973).

9. R. U. Martinelli, J. Appl. Phys. $\underline{45}$, 1183 (1974).

10. J. R. Howorth, R. Holtom, A. L. Harmer, and E. W. Trawny, Appl. Phys. Lett. $\underline{21}$, 316 (1972).

11. R. L. Erickson in: Physics of Electron-Electron and Electron-Photon Interaction, Ed. W. T. Peria, Technical Report AFAL-TR-69-177, April 1969

12. B. Goldstein, Bull. Am. Phys. Soc. $\underline{17}$, 254 (1972).

13. H. E. Farnsworth, R. E. Schlier, T. H. George, and R. M. Burger, J. Appl. Phys. $\underline{29}$, 1150 (1958).

14. G. E. Riach, Technical Report AFAL-TR-71-235, March 1971. Portions are contained in Surface Sci. $\underline{40}$, 479 (1973).

15. R. Riesz and G. H. Dieke, J. Appl. Phys. $\underline{25}$, 196 (1954).

16. C. C. Chang, Surface Sci. $\underline{25}$, 53 (1971).

17. R. E. Weber and L. F. Cordes, Rev. Sci. Instr. $\underline{37}$, 112 (1966).

18. M. R. Jeanes and W. M. Mularie, Technical Report AFAL-TR-72-242, August 1972.

19. L. F. Cordes, Ph. D. Thesis, University of Minnesota, 1966.

20. H. D. Hagstrum, Phys. Rev. 119, 940 (1960).

21. W. Klein, Rev. Sci. Instr. 42, 1082 (1971).

22. P. J. Estrup and E. G. McRae, Surface Sci. 25, 1 (1971).

23. R. J. Zollweg, J. Appl. Phys. 34, 2590 (1963).

24. G. H. Schwuttke, J. Electrochem. Soc. 106, 315 (1959).

25. R. E. Schlier and H. E. Farnsworth, J. Chem. Phys. 30, 917 (1959).

26. J. J. Lander and J. Morrison, J. Appl. Phys. 34, 1403 (1963).

27. J. M. Chen, Ph. D. Thesis, University of Minnesota, 1968. Portions are contained in: Proc. 4th Intern. Materials Symp., Structure and Chemistry of Solid Surfaces, Ed. G. Somorjai (Wiley, New York, 1969).

28. R. H. Fowler, Phys. Rev. 38, 45 (1931).

29. R. E. Weber and W. T. Peria, Surface Sci. 14, 13 (1969).

30. E. G. McRae, Surface Sci. 25, 491 (1971).

31. L. V. Caldwell, H. W. Kalweit, and A. J. Kennedy, Conference on Photoelectric and Secondary Electron Emission, Minnesota, 1973.

32. H. R. Philipp and E. Q. Taft, Phys. Rev. 113, 1002 (1959).

33. E. O. Kane, Phys. Rev. 127, 131 (1962).

34. T. E. Fischer, Surface Sci. 13, 30 (1969).

35. M. L. Cohen and T. K. Bergstresser, Phys. Rev. 141, 789 (1966).

36. E. H. Eberhardt, Appl. Optics 7, 2037 (1968).

37. J. J. Uebbing and L. W. James, J. Appl. Phys. 41, 4505 (1970).

38. D. Haneman, Phys. Rev. 121, 1093 (1961).

39. R. Seiwatz, Surface Sci. 2, 473 (1964).

40. Y. Margoninski, Phys. Rev. 132, 1910 (1963).

41. P. Handler and W. M. Portnoy, Phys. Rev. 116, 516 (1959).

42. R. Weiwatz and M. Green, J. Appl. Phys. 29, 1034 (1958).

43. F. G. Allen and G. W. Gobeli, Phys. Rev. $\underline{144}$, 558 (1966).

44. R. L. Erickson, Ph. D. Thesis, University of Minnesota, 1972; AFAL-TR-76-36.

45. J. Pendrey, private communication.

46. W. T. Peria, Physics of Electron-Photon Interaction, Technical Report AFAL-TR-73-43, January 1973.

47. R. L. Park and H. H. Madden, Surface Sci. $\underline{11}$, 188 (1968).

48. F. Kub, private communication.

49. M. Green and R. Seiwatz, J. Chem. Phys. $\underline{37}$, 458 (1962).

CONVENTIONAL "HOT ELECTRON" PHOTOCATHODE
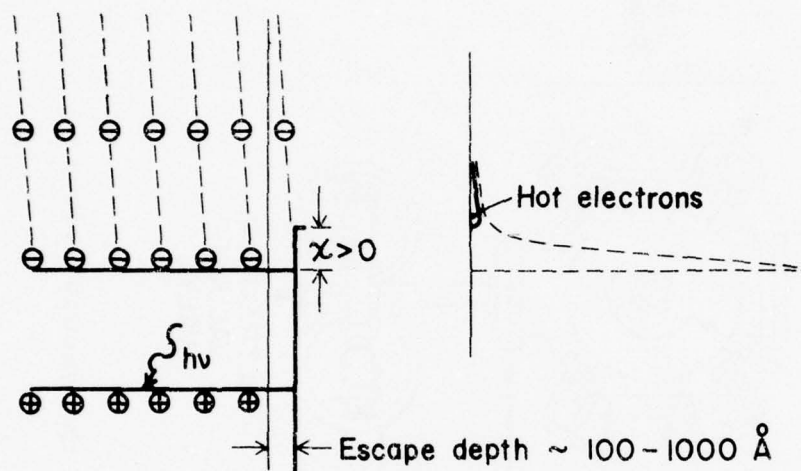
NEGATIVE ELECTRON AFFINITY (NEA) PHOTOCATHODE
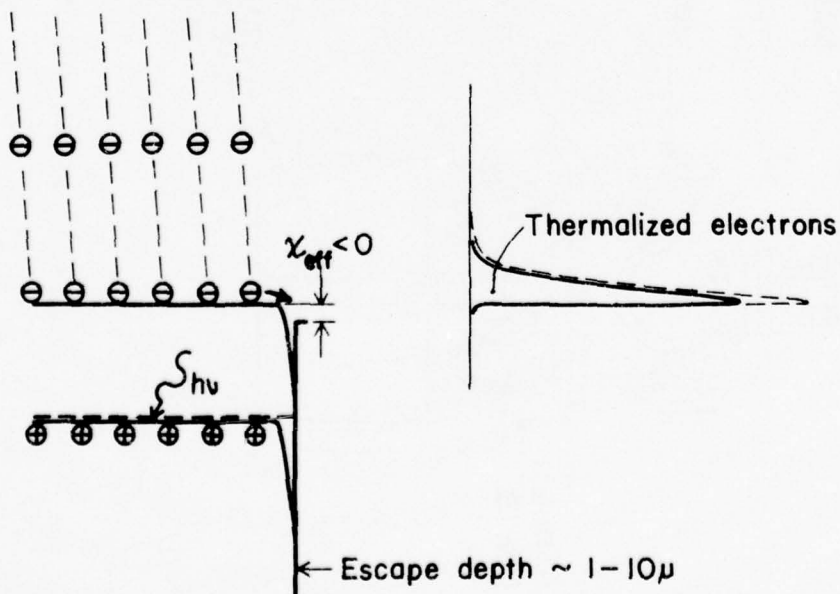
Figure 1   Comparison of a hot electron
emitter and an NEA emitter

57
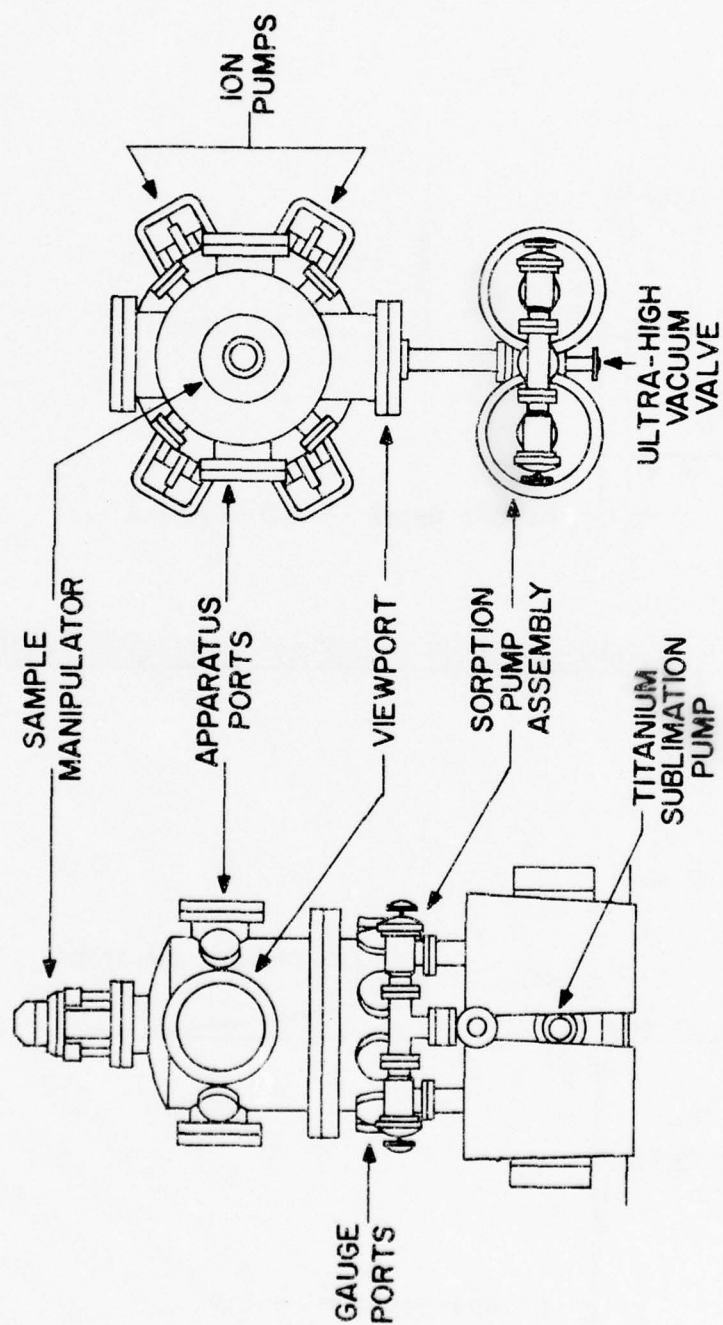
Figure 2   Front and Top views of the vacuum system

MASS SPECTRUM

TOTAL PRESSURE
<1×10⁻¹⁰ TORR

H_2^+

He^+

C^+, CH^+, CH_2^+

CH_3^+, CH_4^+, CH_5^+

H_2O^+

Ne^+

C^+

CO^+

Ar^+

CO_2^+

2 4   12   18   28   40 44
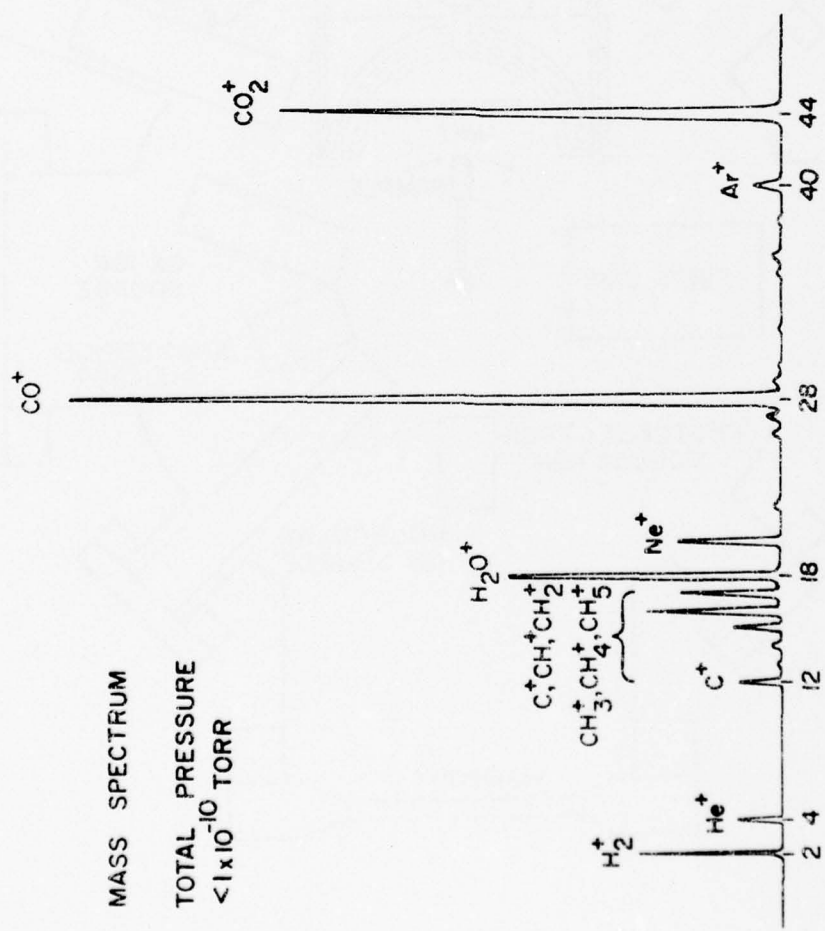
Figure 3   Mass spectrum of the residual gas
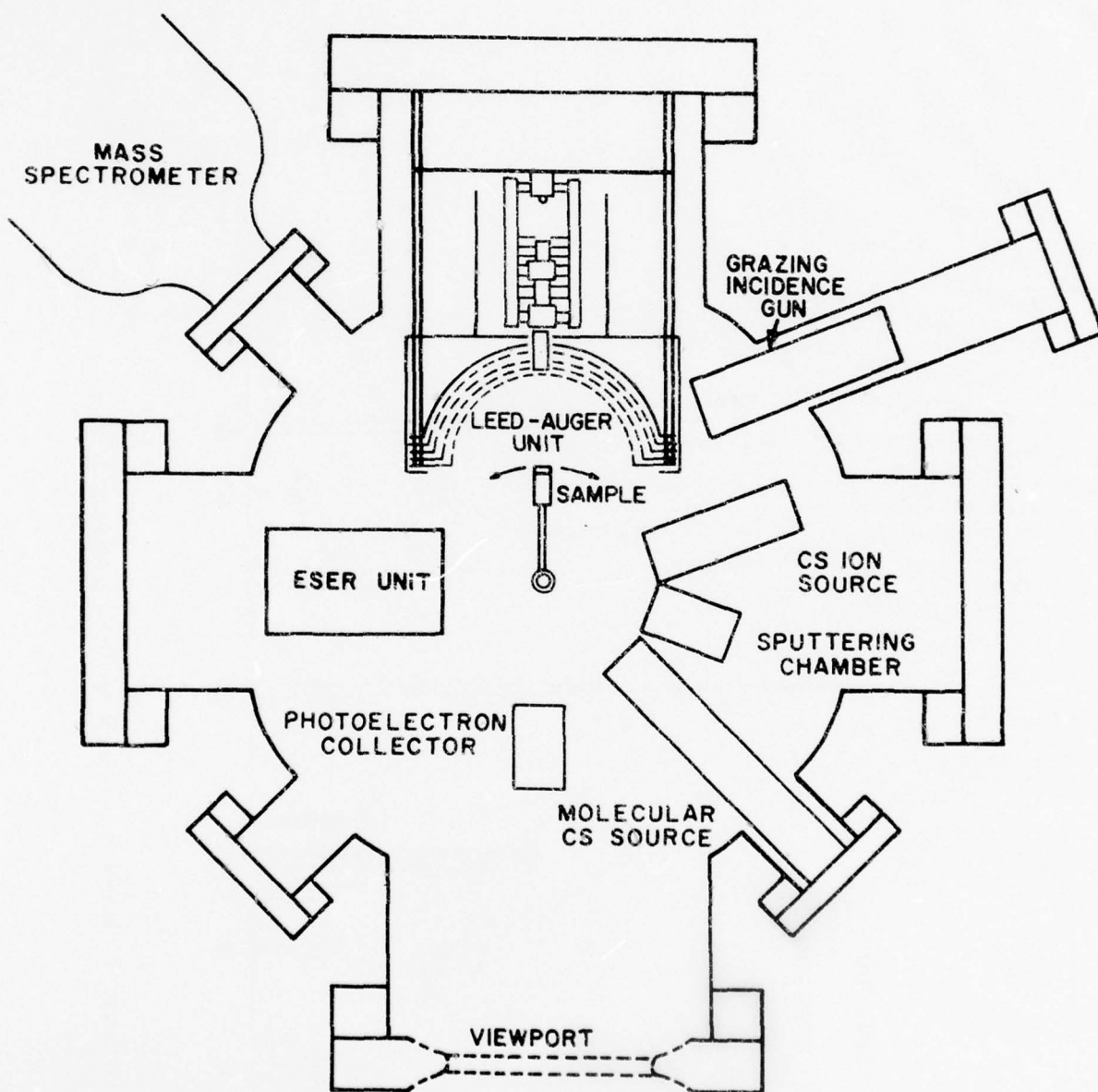
Figure 4   Cross-section of the vacuum system

60
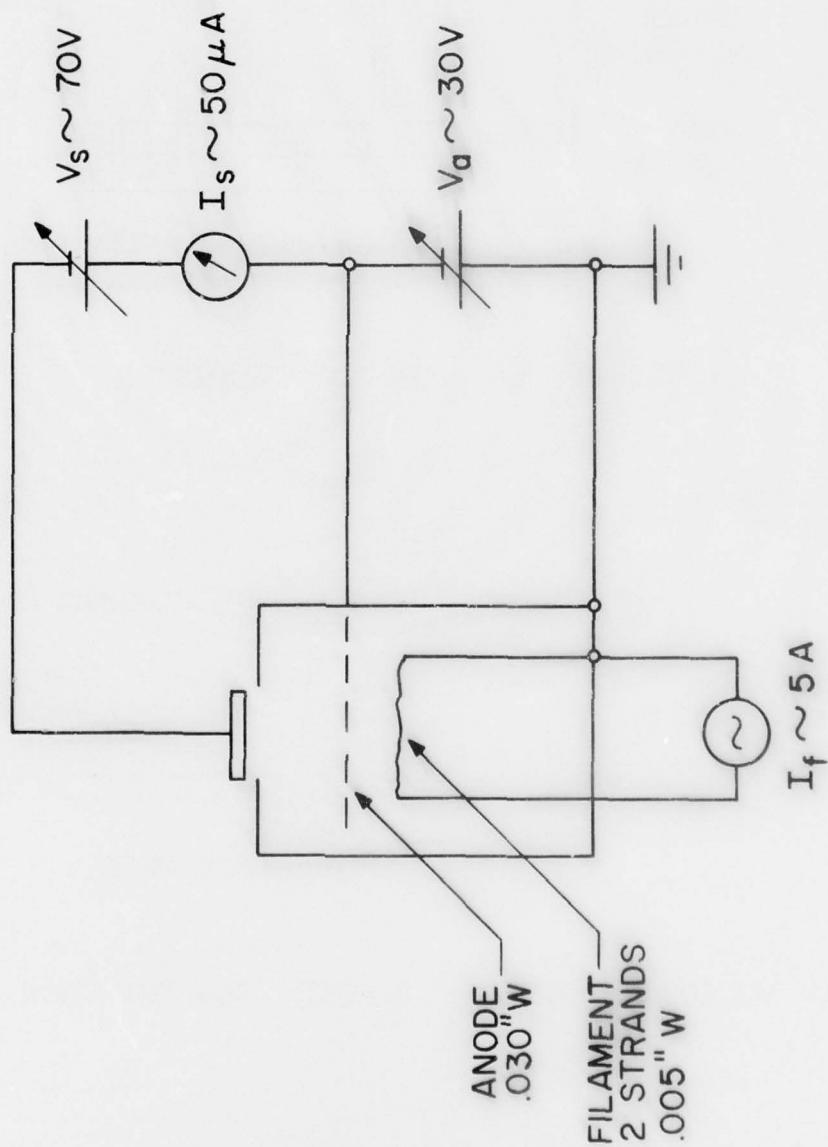
Figure 5 Sputtering chamber and circuit diagram

61

MASK

100 X 100 LINES PER INCH
304 STAINLESS STEEL GRIDS
80 % TRANSMISSION

GRID

SOFT GLASS ROD

GRID
$V_G = -10V$

TARGET
$V_T = -6V$

SOURCE
$V = 0V$

HEAT SHIELD
$V_S = 0V$

MASK
$V_M = -4V$

DRIFT TUBE
$V_3 = -14.8V$ $V_2 = -260V$ $V_1 = -11.3V$

1cm
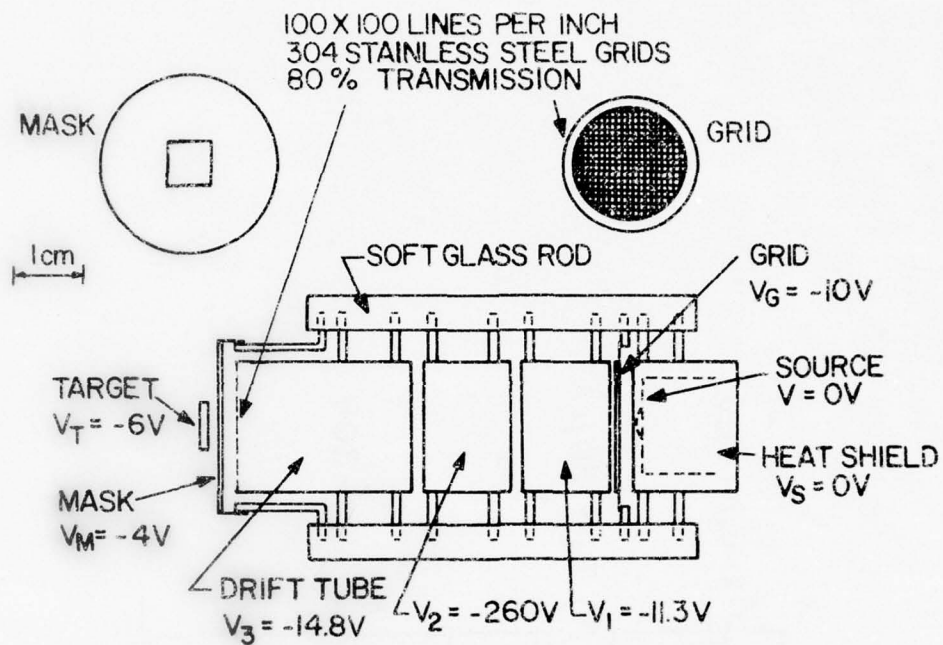
a.) CESIUM ION GUN CONFIGURATION

2cm

VALVE

DRIFT
TUBE

COPPER TUBING

REMOVABLE
MASK

CESIUM
AMPULE

THERMOCOUPLES
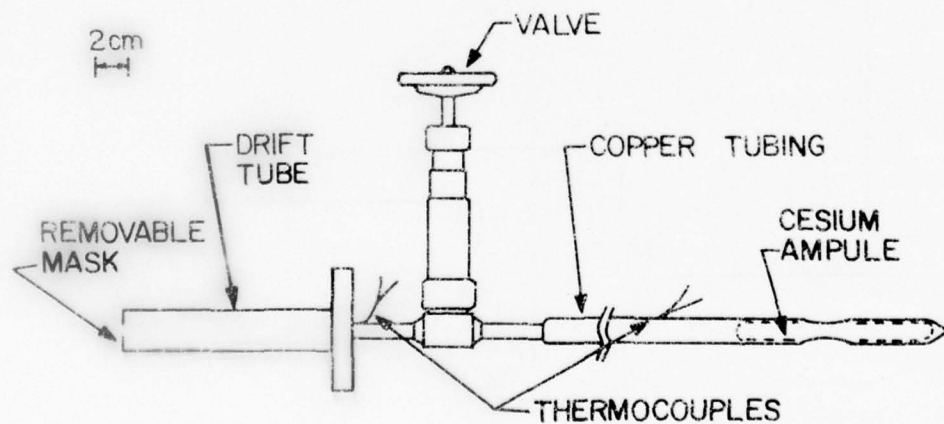
b.) MOLECULAR CESIUM SOURCE CONFIGURATION

Figure 6   Sources used for cesium deposition

62
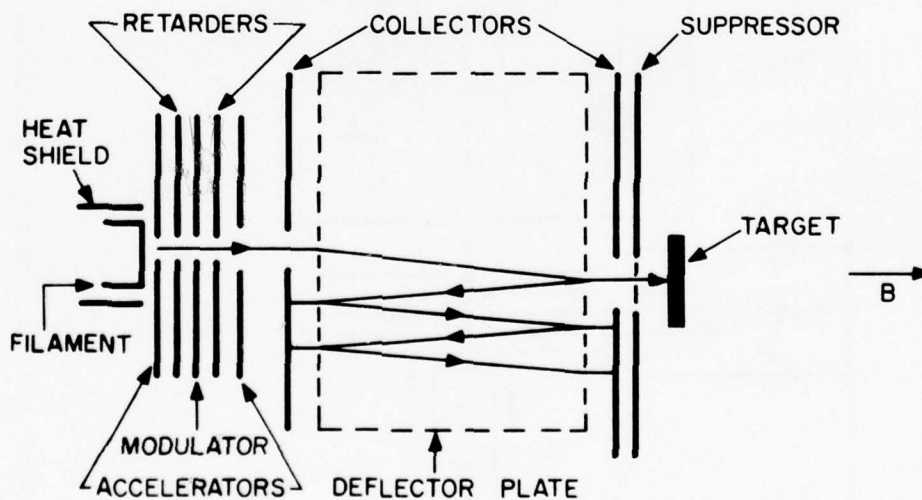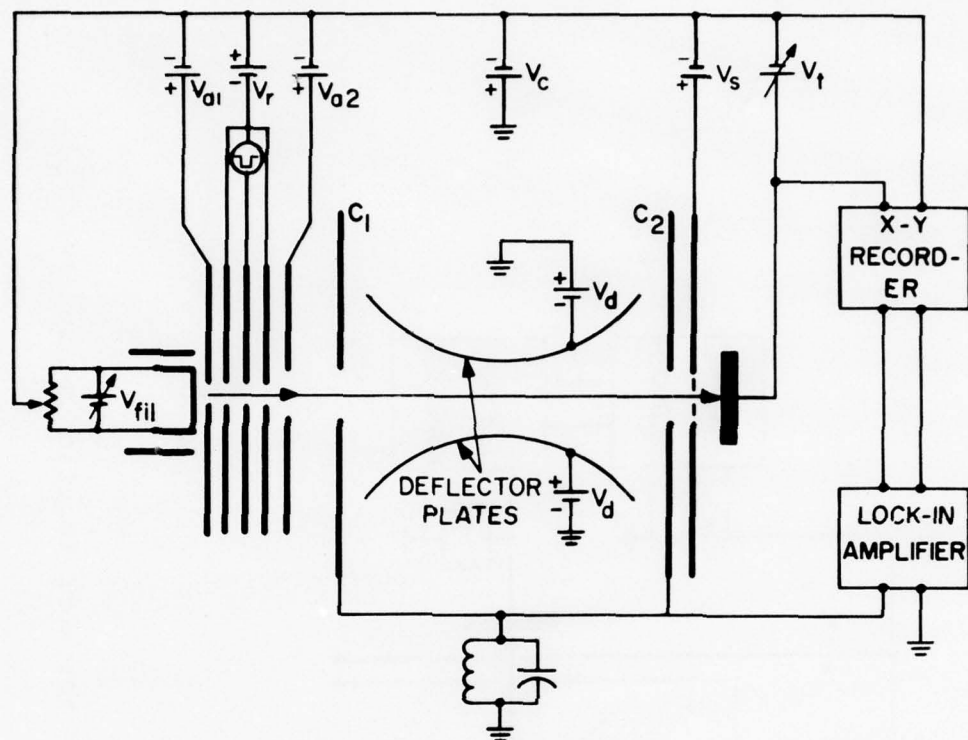
Figure 7   Low energy electron gun and associated circuitry
used to measure elastic specular electron reflectivity.
Side and top views showing electron trajectories.
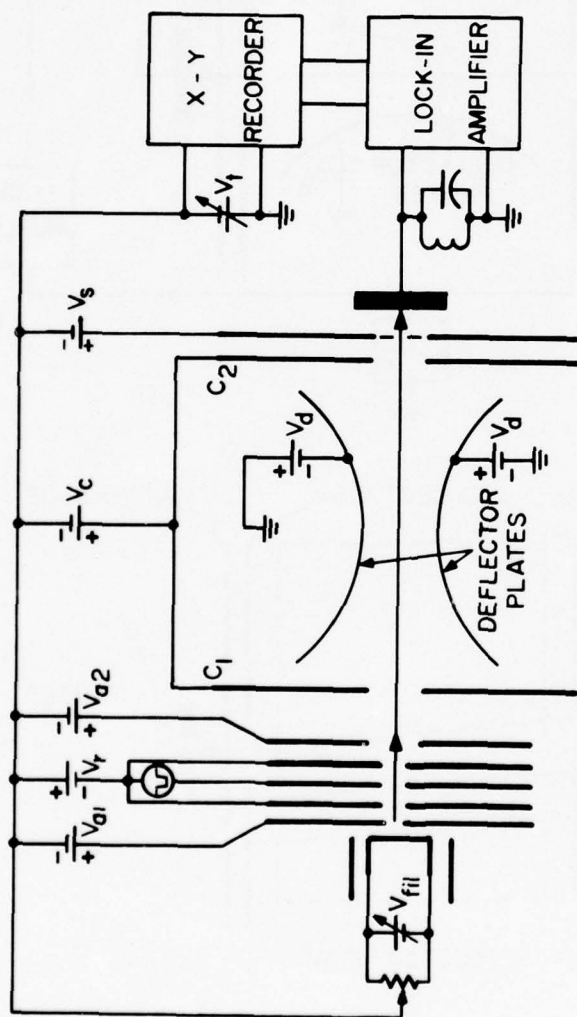
Figure 8 Use of the low energy electron gun for work function measurements

SAMPLE

935 PHOTOCELL

ACHROMATIC LENS

ACHROMATIC
CONDENSER

917 PHOTOCELL

FILTERS

MONOCHROMATOR

LIGHT SOURCE

MONOCHROMATOR

CONDENSER

CONDENSER
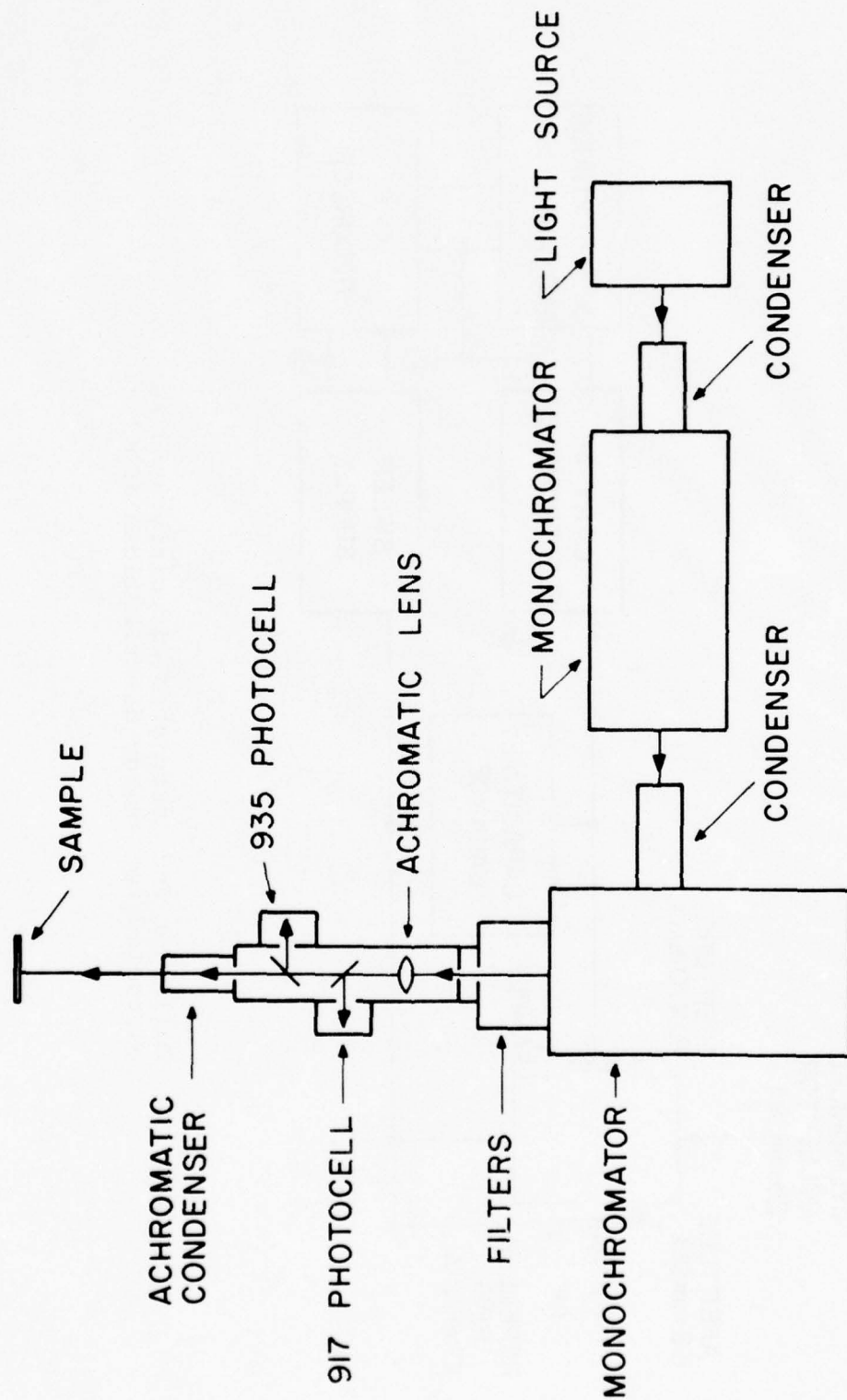
Figure 9 Block diagram of the optical system
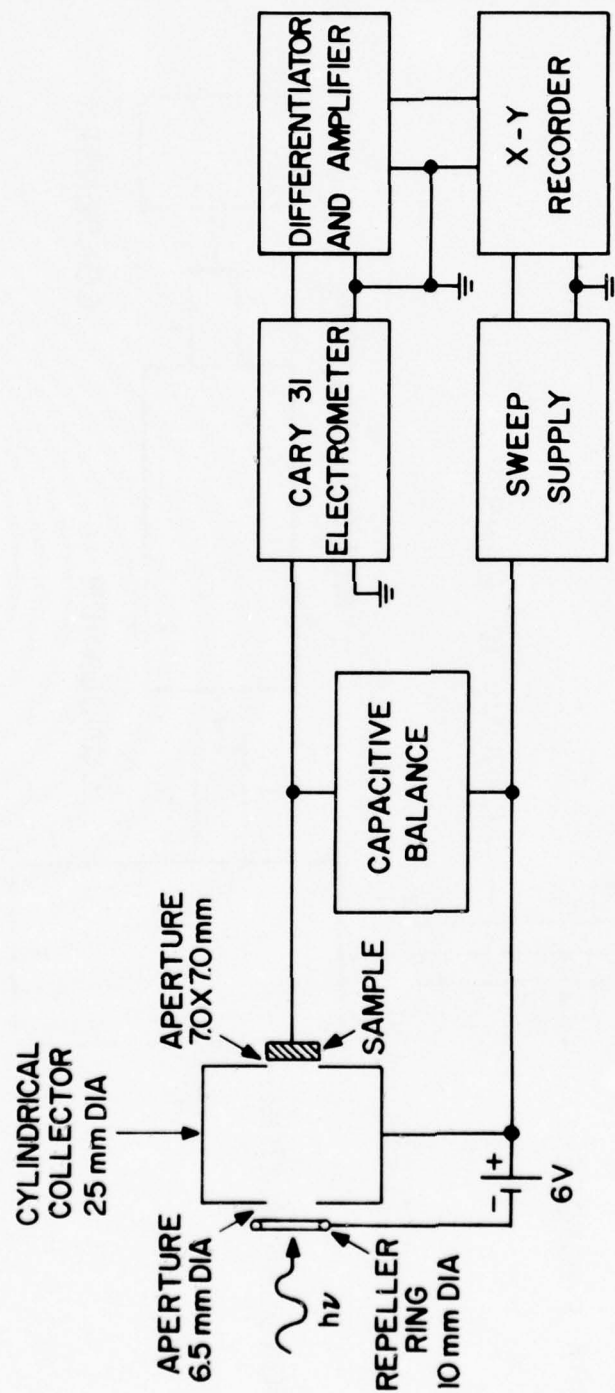
Figure 10 Collector and associated circuitry used to measure photoelectron energy distributions (EDC's)

278028

Ge (100)
2000 eV, 50μA

C

Ar

Ta

Ge

Ge

Ge

Ge

Ge

X2000

X500

X100

X10

$\dfrac{dN}{dE}$

ELECTRON ENERGY (eV)

0   100   200   300   400   500   600   700
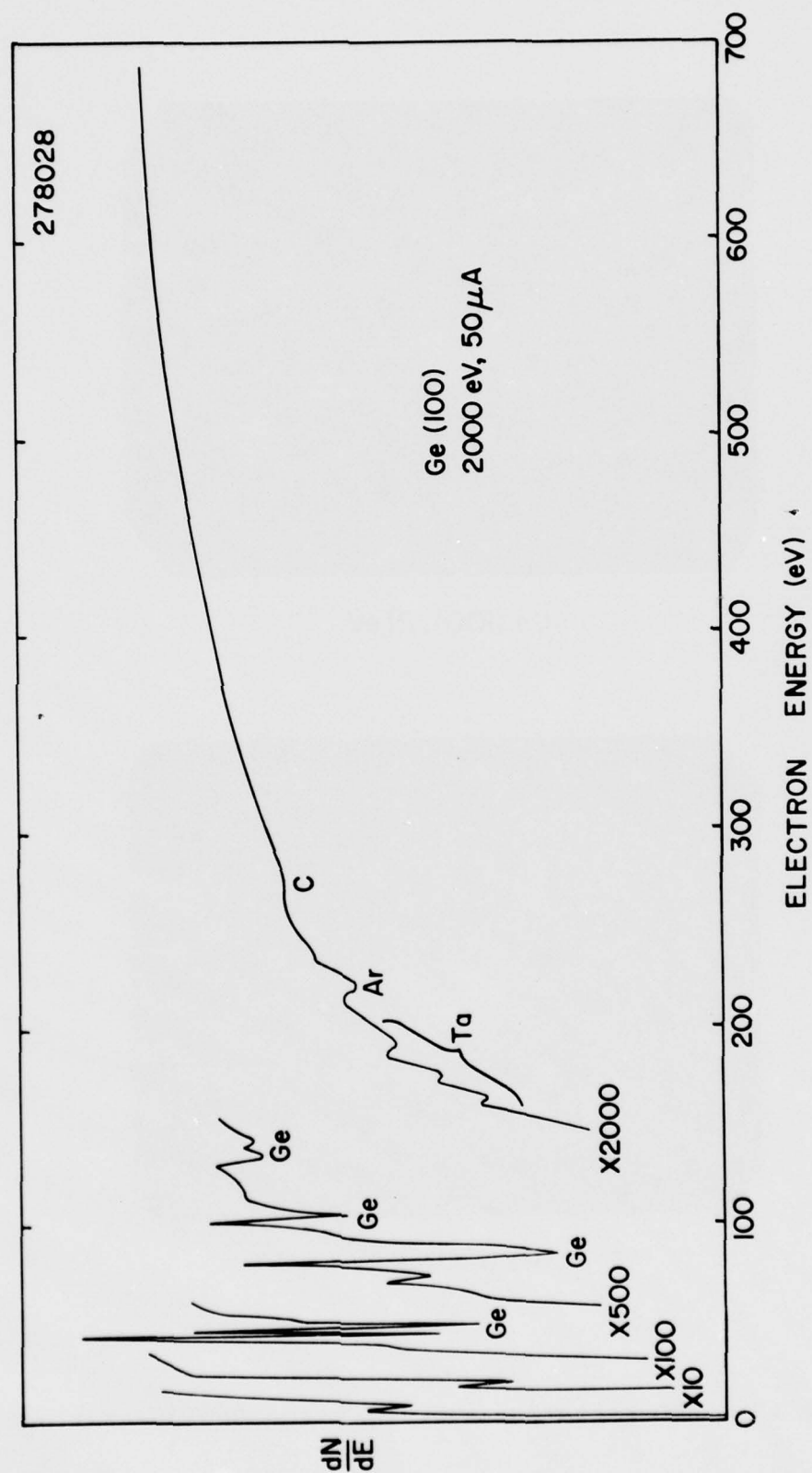
Figure 11 Auger spectrum from the clean Ge(100) surface

67
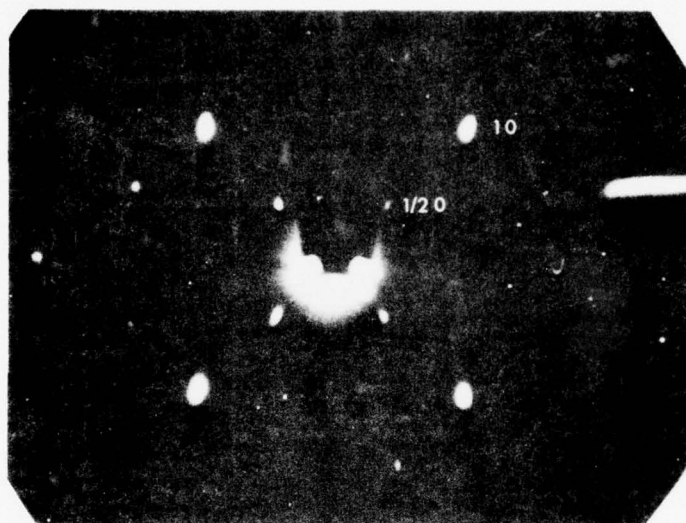
Ge (100), 21 eV
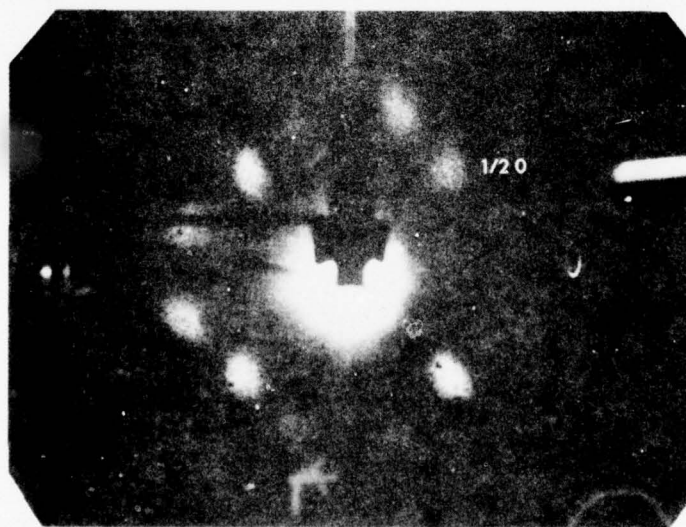
Ge (100), 4 eV

FIGURE 12   LEED patterns from the clean Ge(100) surface
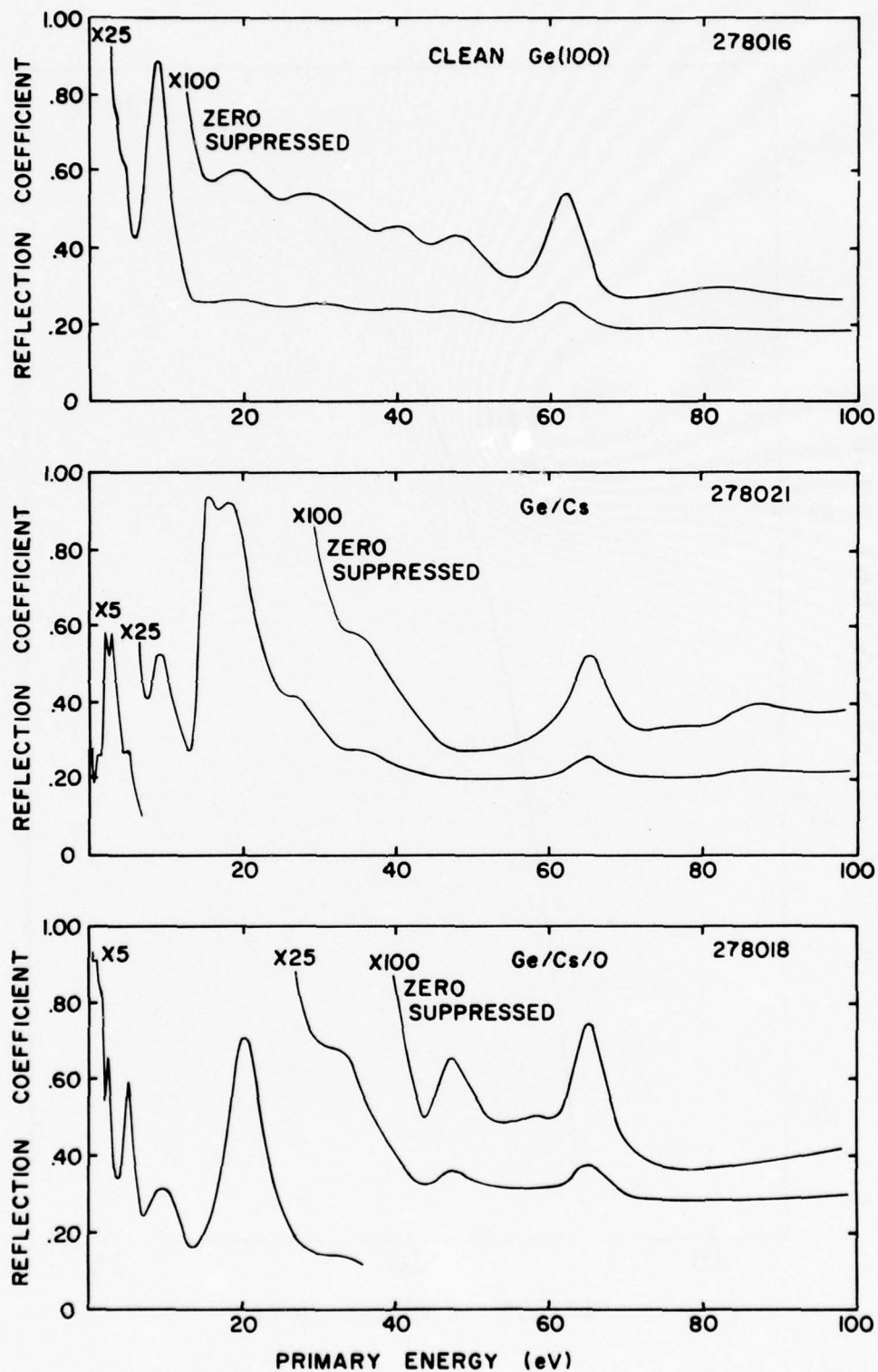
Figure 13   ESER data for the clean Ge(100) surface,
the Ge/Cs surface, and the Ge/Cs/0 surface

69

272042

YIELD (ELECTRONS/INCIDENT PHOTON)

10^{-4}

10^{-5}

10^{-6}

10^{-7}

$\phi = 1.78\ eV$

1.5   2.0   2.5

PHOTON ENERGY (eV)
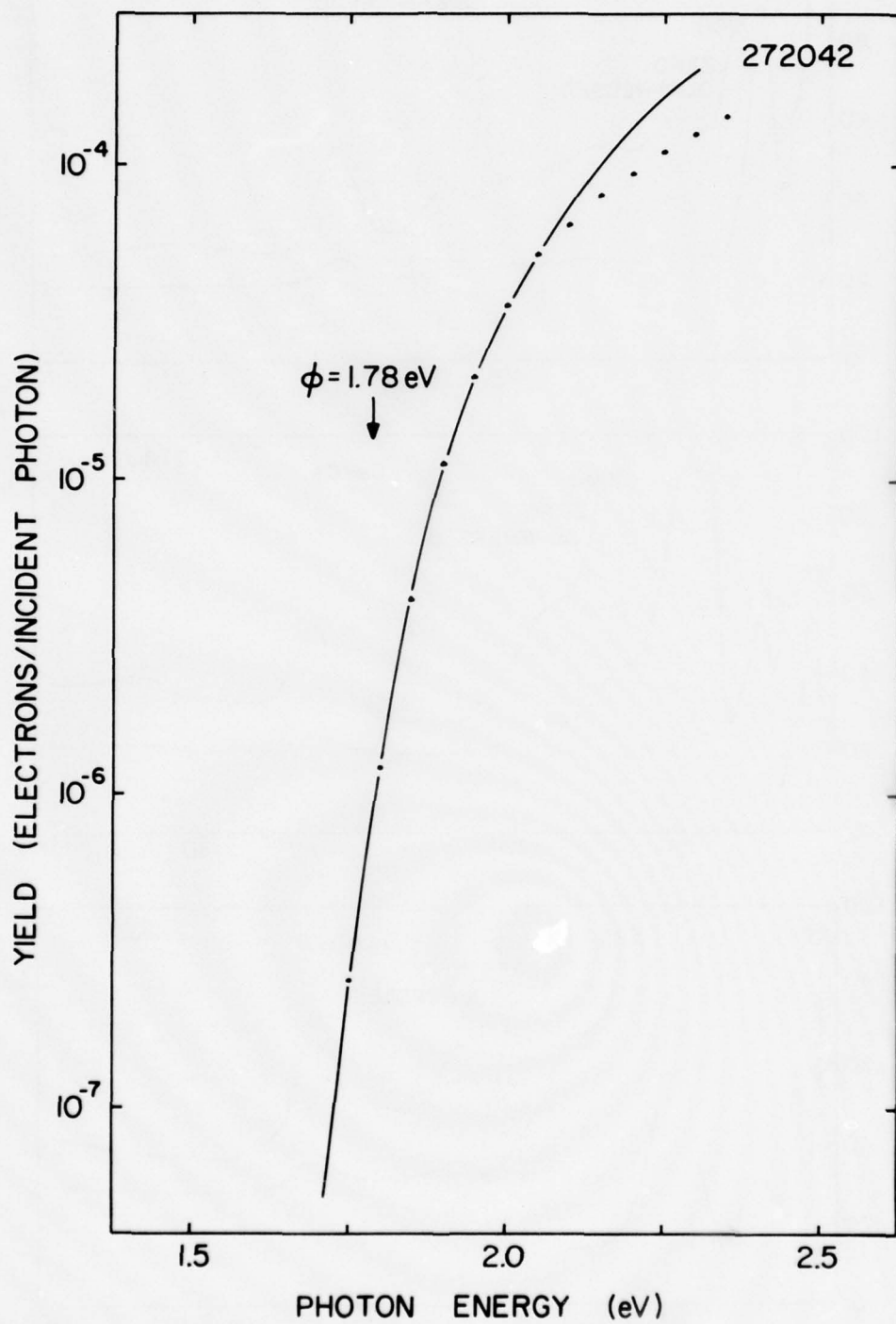
Figure 14   Yield curve for Ta-Cs fit to a Fowler curve
            with $\varphi = 1.78$ eV

70
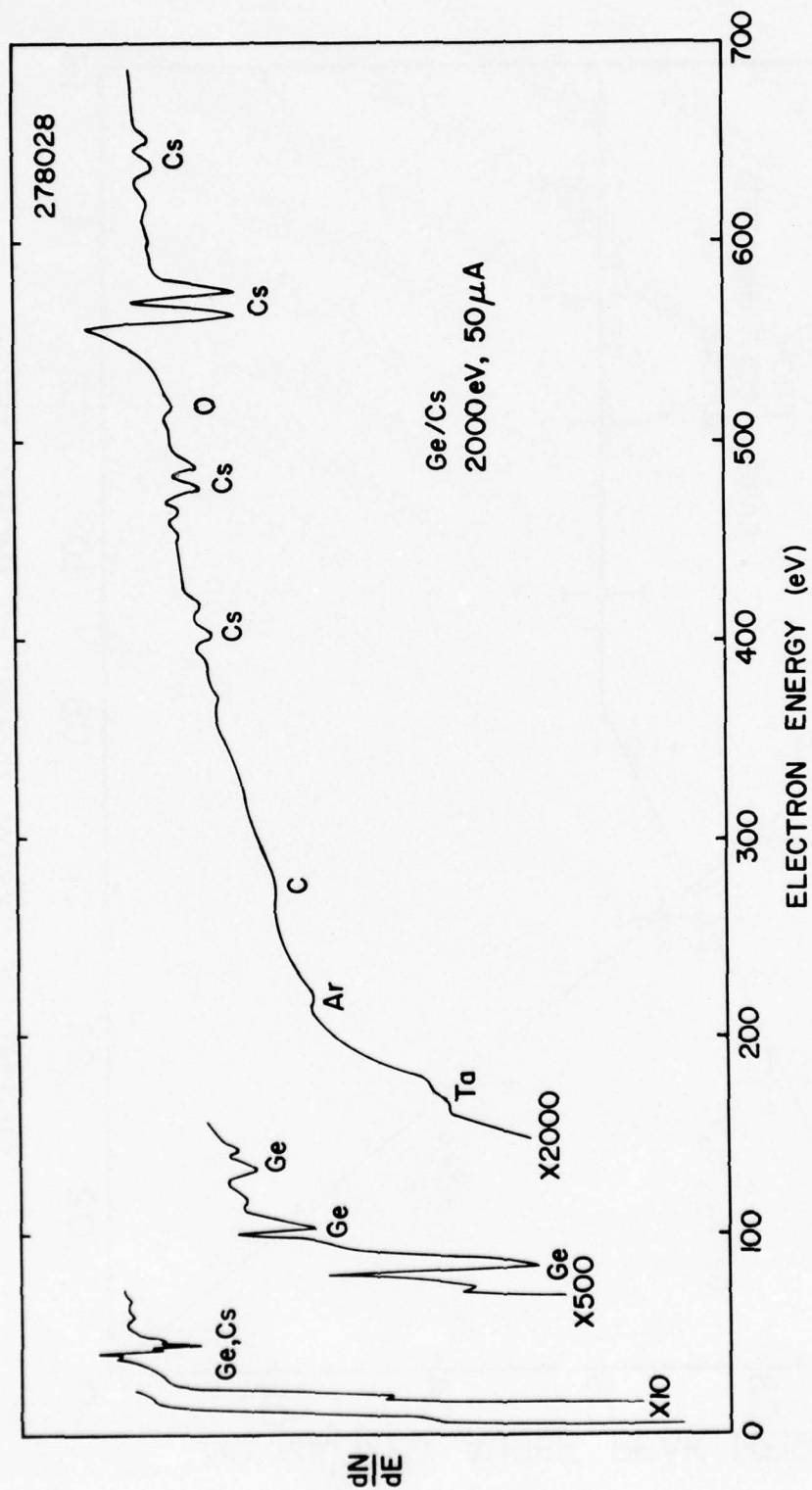
Figure 15 Auger spectrum from the Ge/Cs surface

71
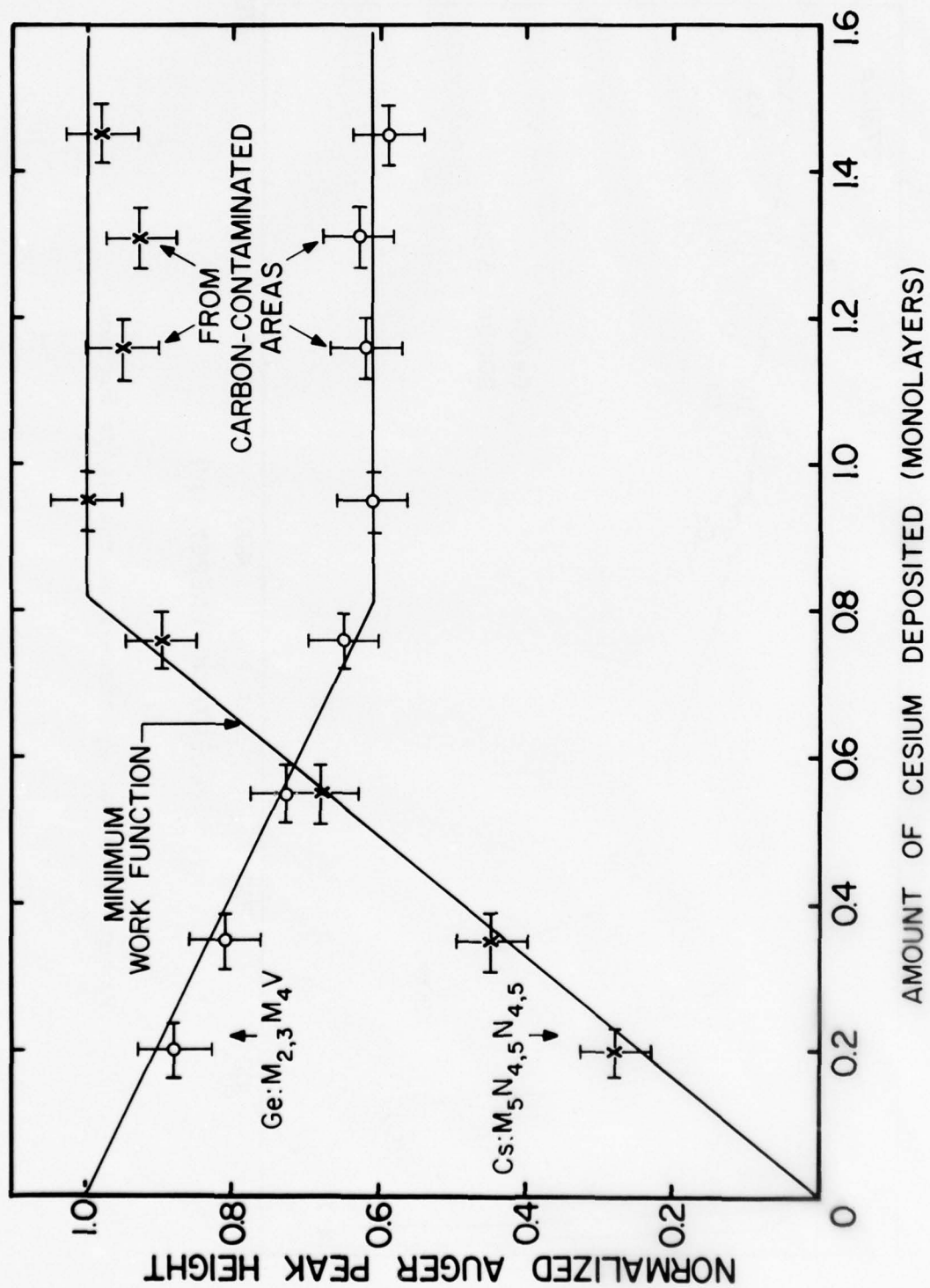
Figure 16 Auger magnitudes vs. amount of cesium deposited
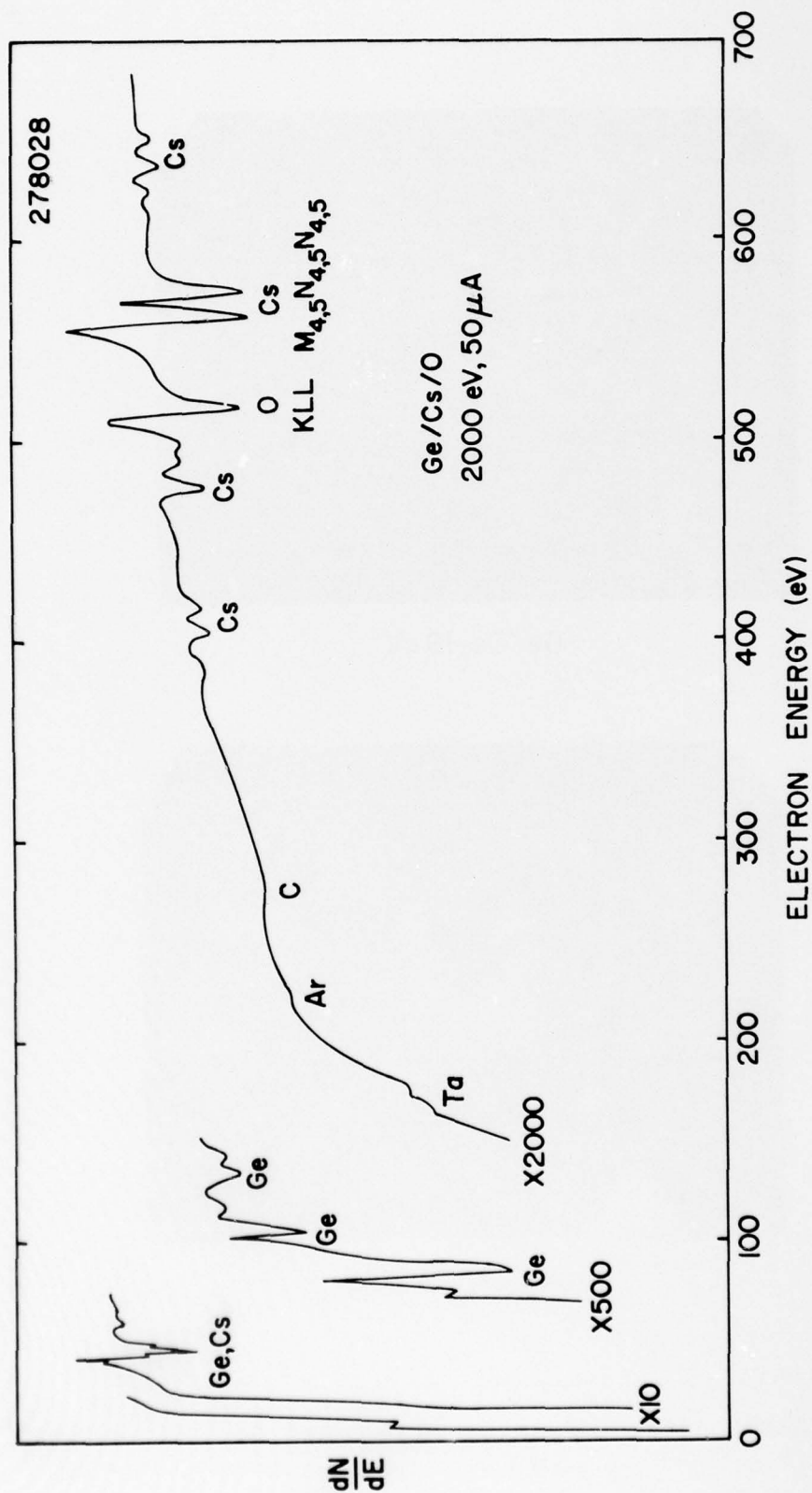
Figure 17 Auger spectrum from the Ge/Cs/0 surface

73
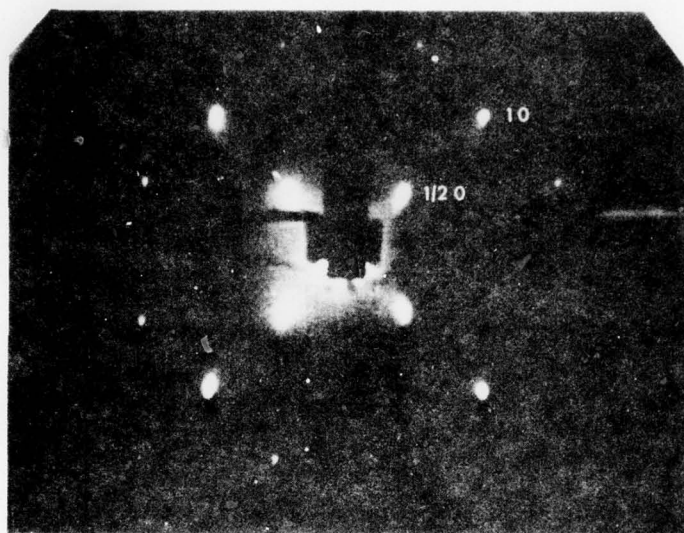
Ge/Cs, 19 eV
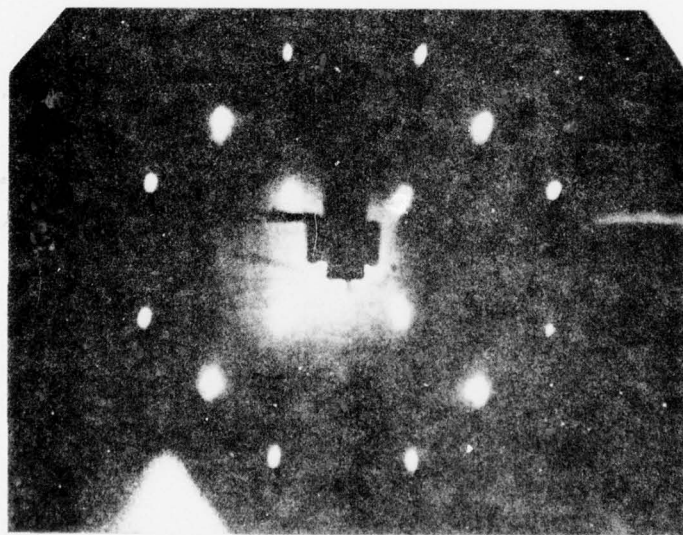
Ge/Cs/O, 19 eV

FIGURE 18   LEED patterns from the Ge/Cs and Ge/Cs/O surfaces

74

$\theta = .15$ $\theta = .10$ $\theta = .05$ $\theta = 0m$

$\theta = .50$ $\theta = .33$ $\theta = .25$
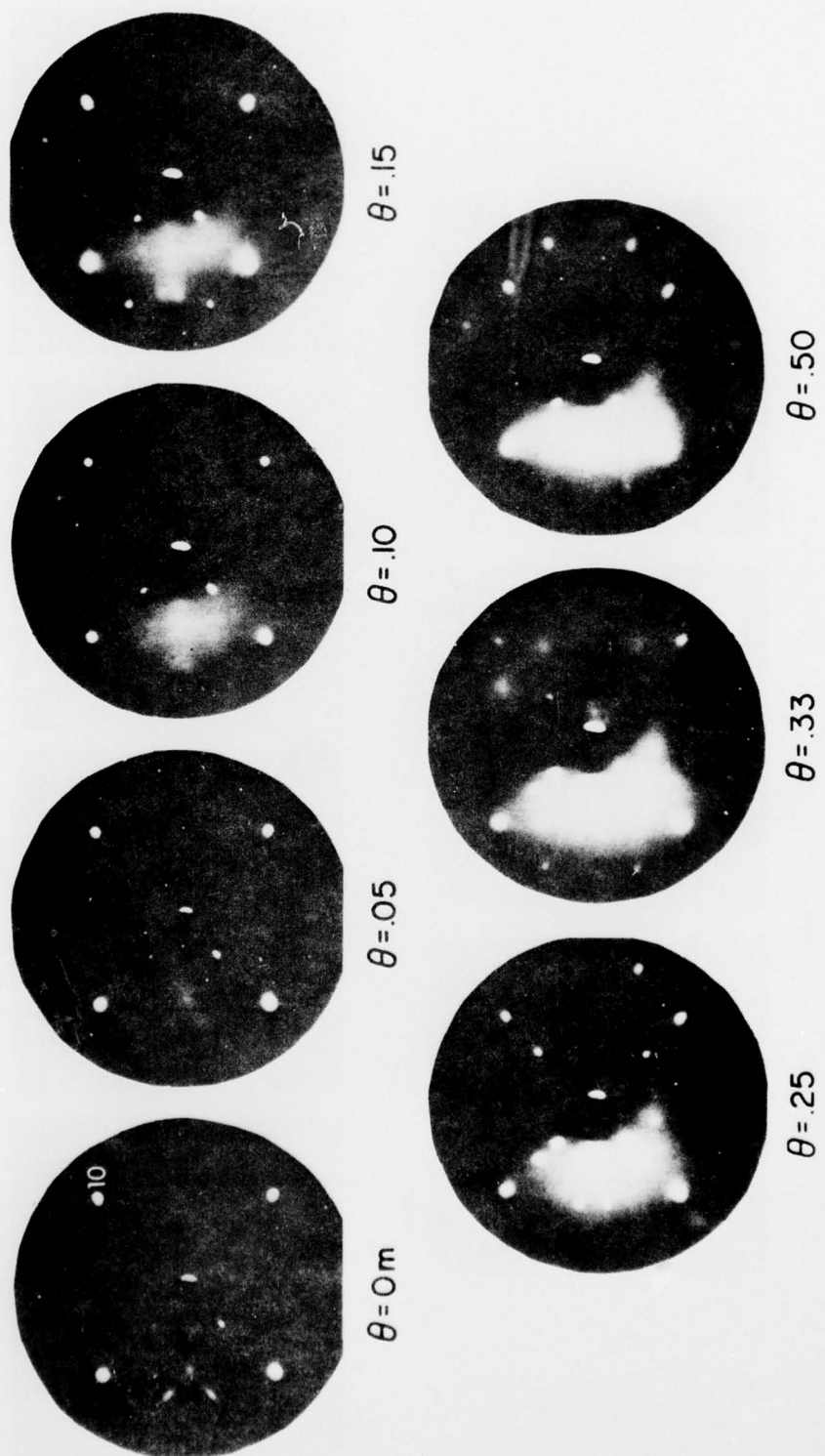
FIGURE 19   The Ge-Cs LEED pattern vs. cesium coverage

75
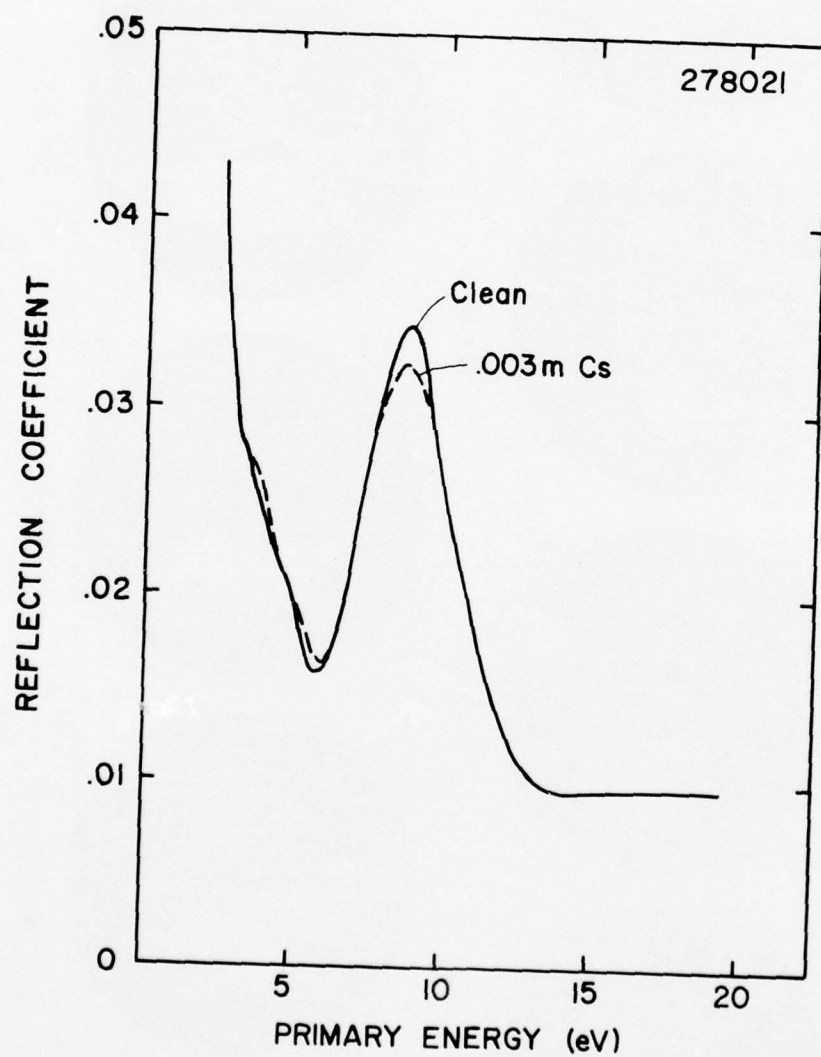
Figure 20   The effect of a small amount of cesium
on the Ge(100) ESER

76
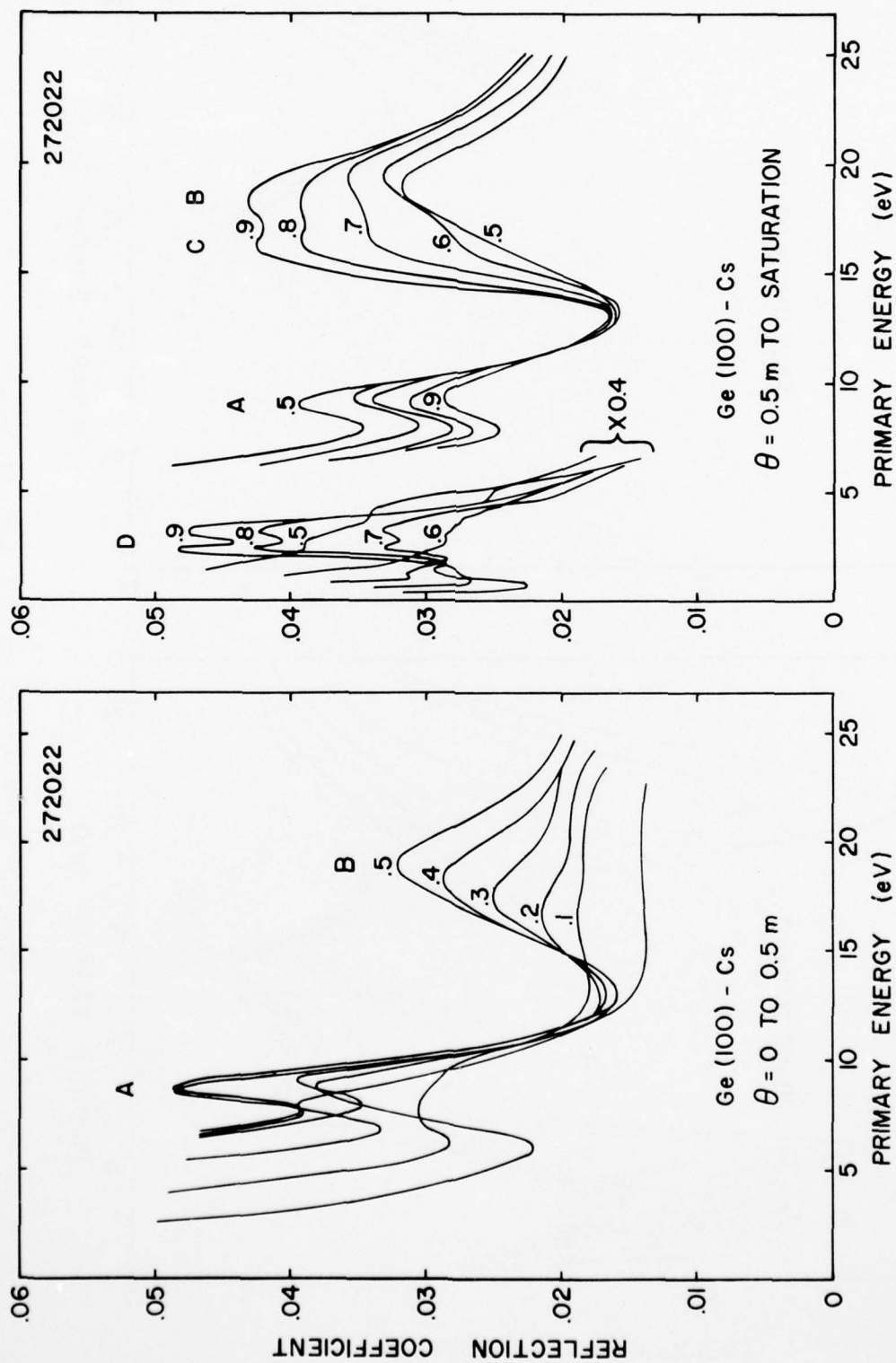
Figure 21 ESER vs. cesium coverage for Ge(100)
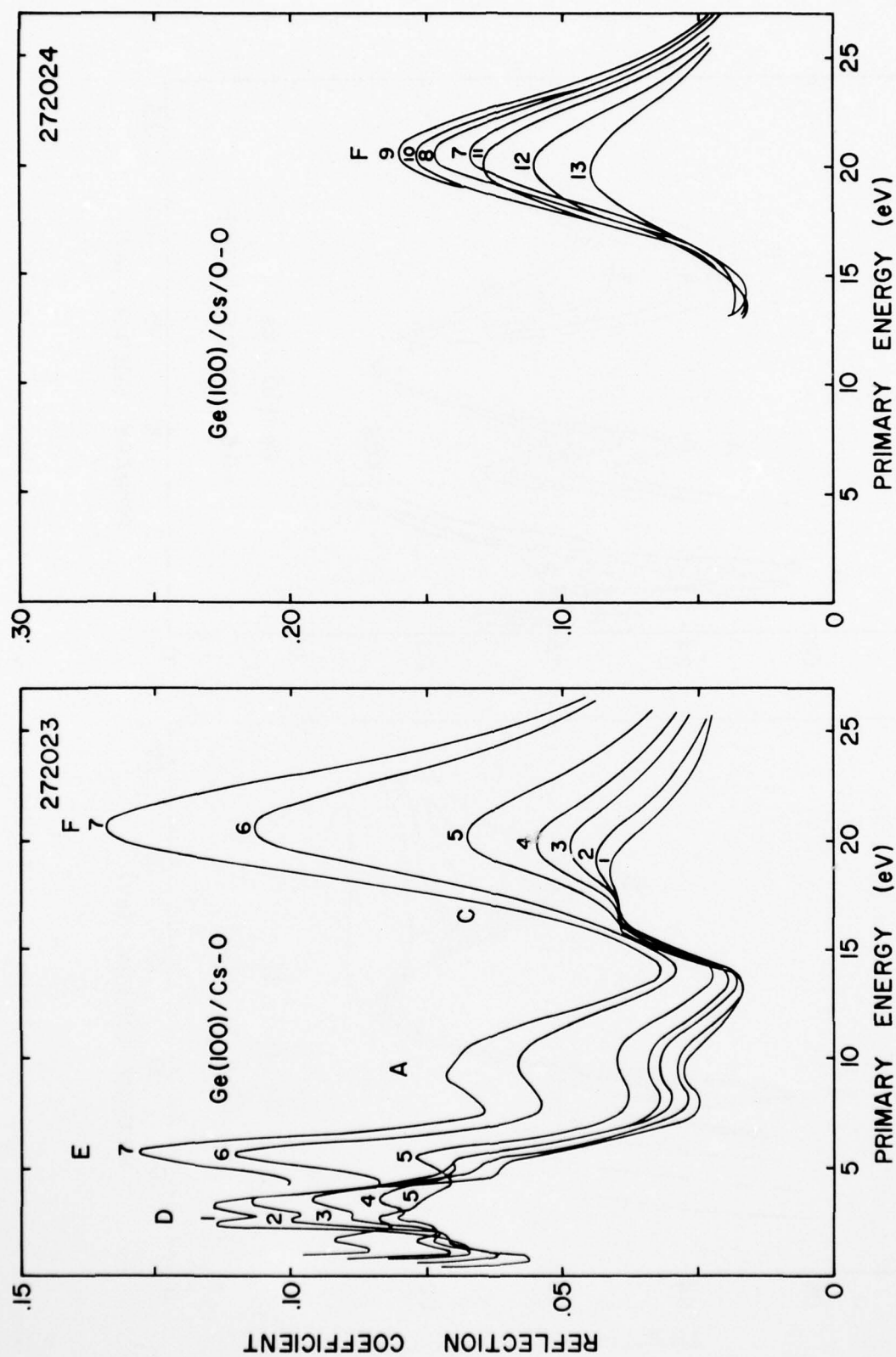
Figure 22 ESER vs. oxidation for Ge(100)/Cs

78

AMOUNT OF CESIUM DEPOSITED (θ, MONOLAYERS)
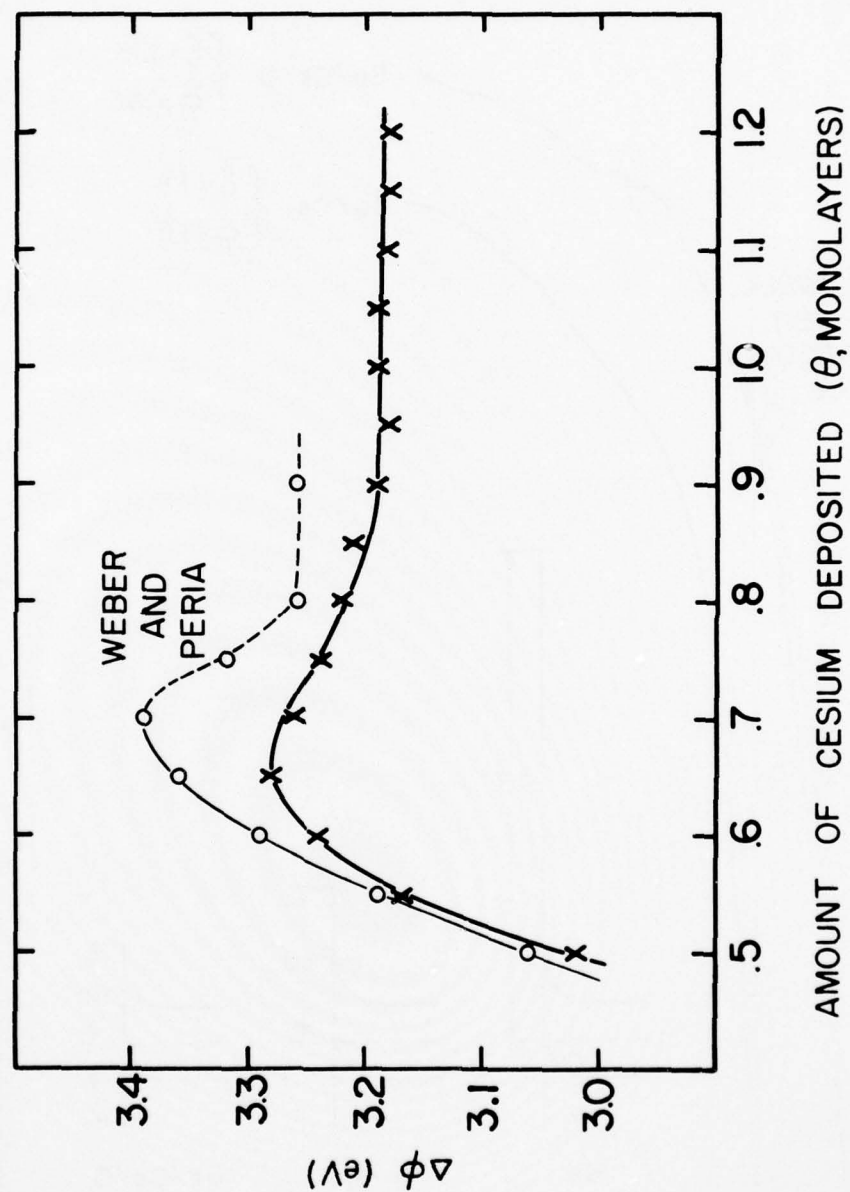
Figure 23 $\Delta \phi$ vs. θ for Ge(100)-Cs
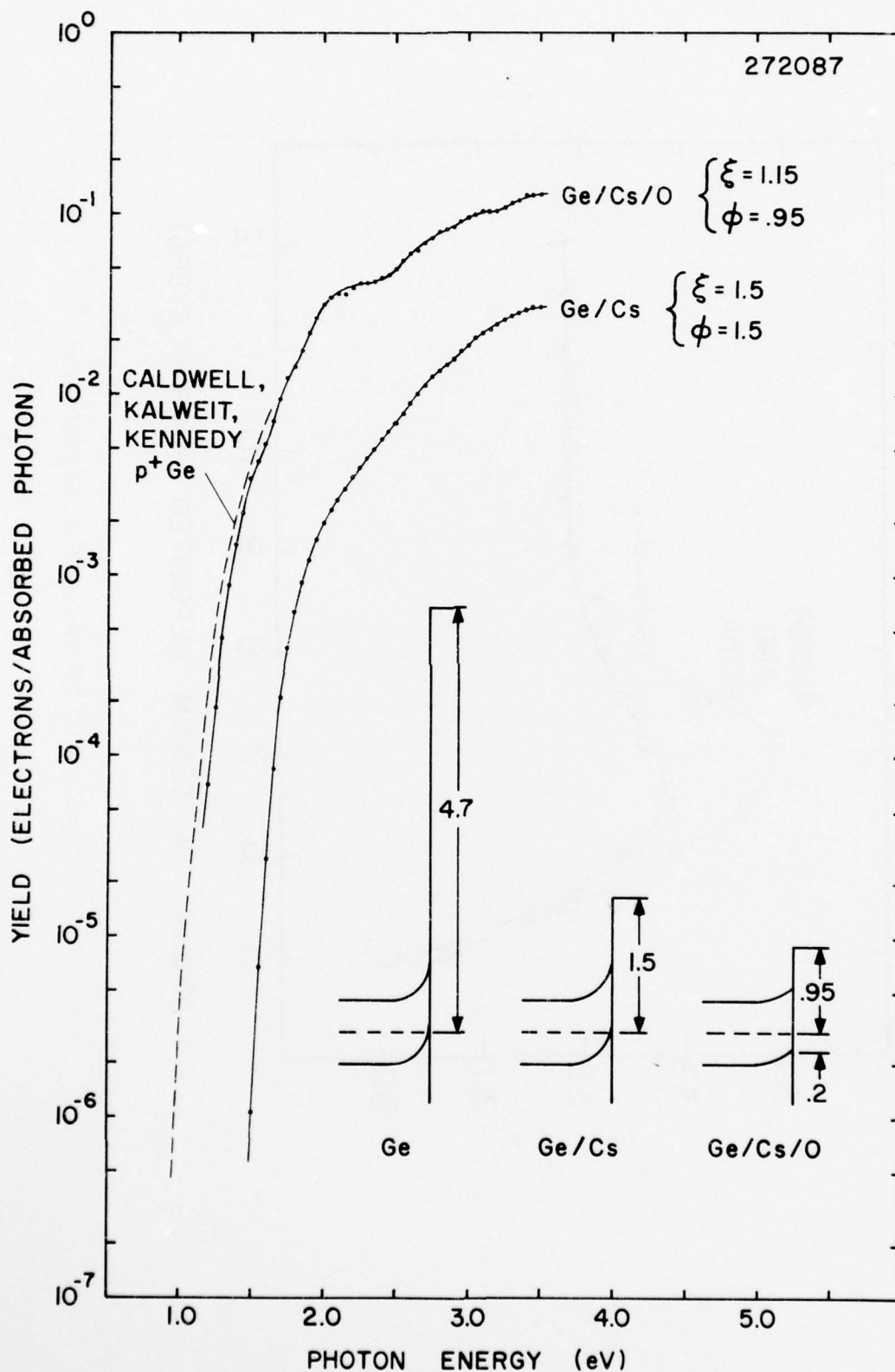
Figure 24   Spectral yields for Ge/Cs and Ge/Cs/0

80
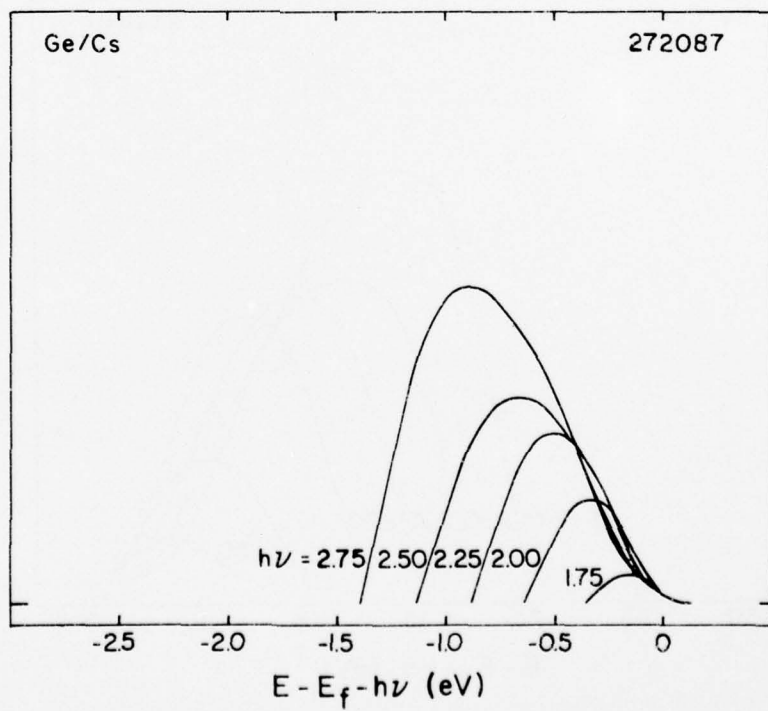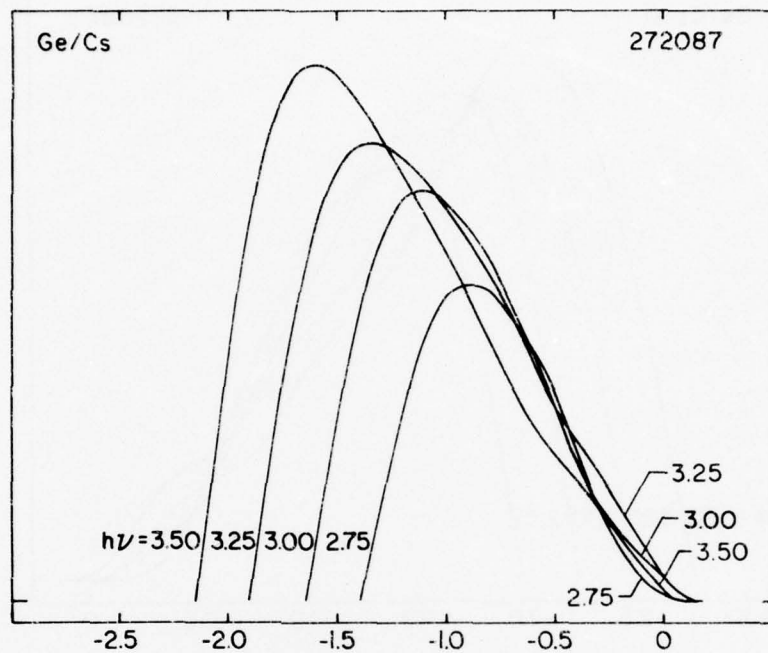
Figure 25   EDC's for Ge/Cs

81
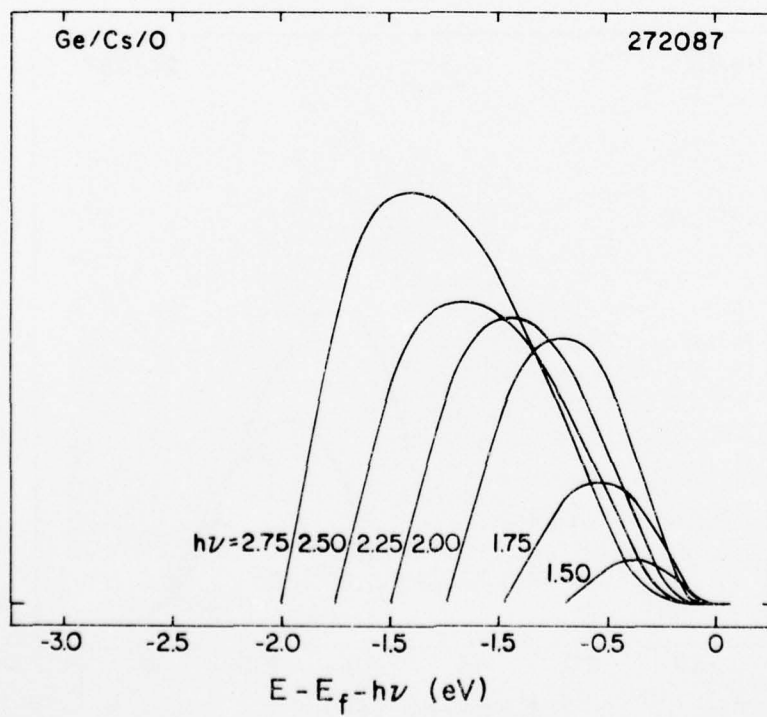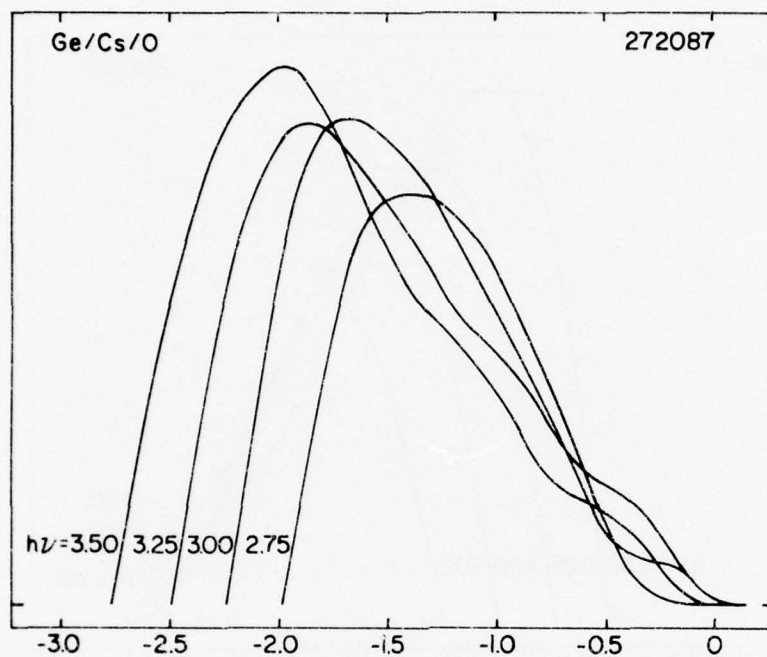
Figure 26   EDC's for Ge/Cs/0

82
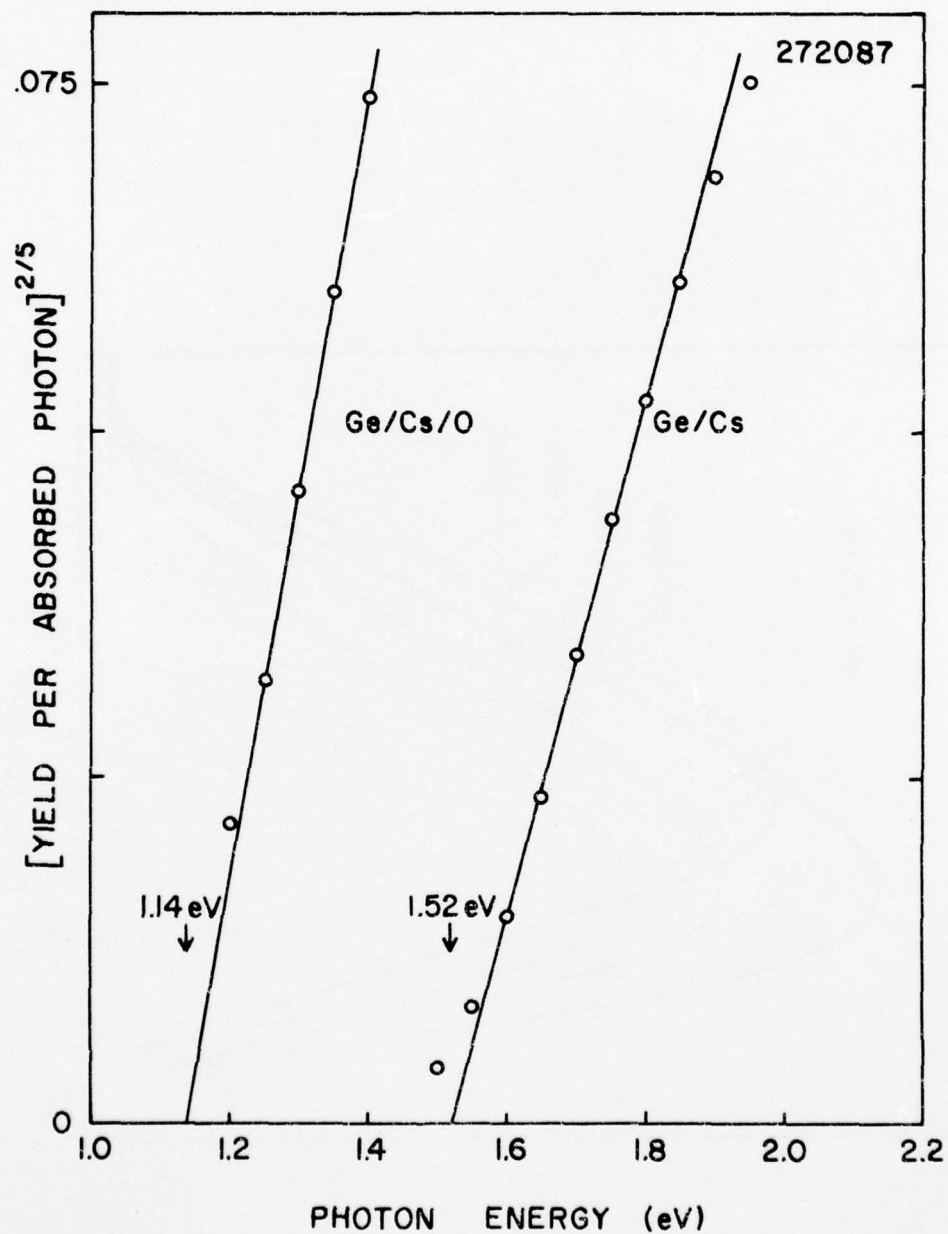
Figure 27 $Y^{2/5}$ plots of threshold spectral yields for Ge/Cs and Ge/Cs/0
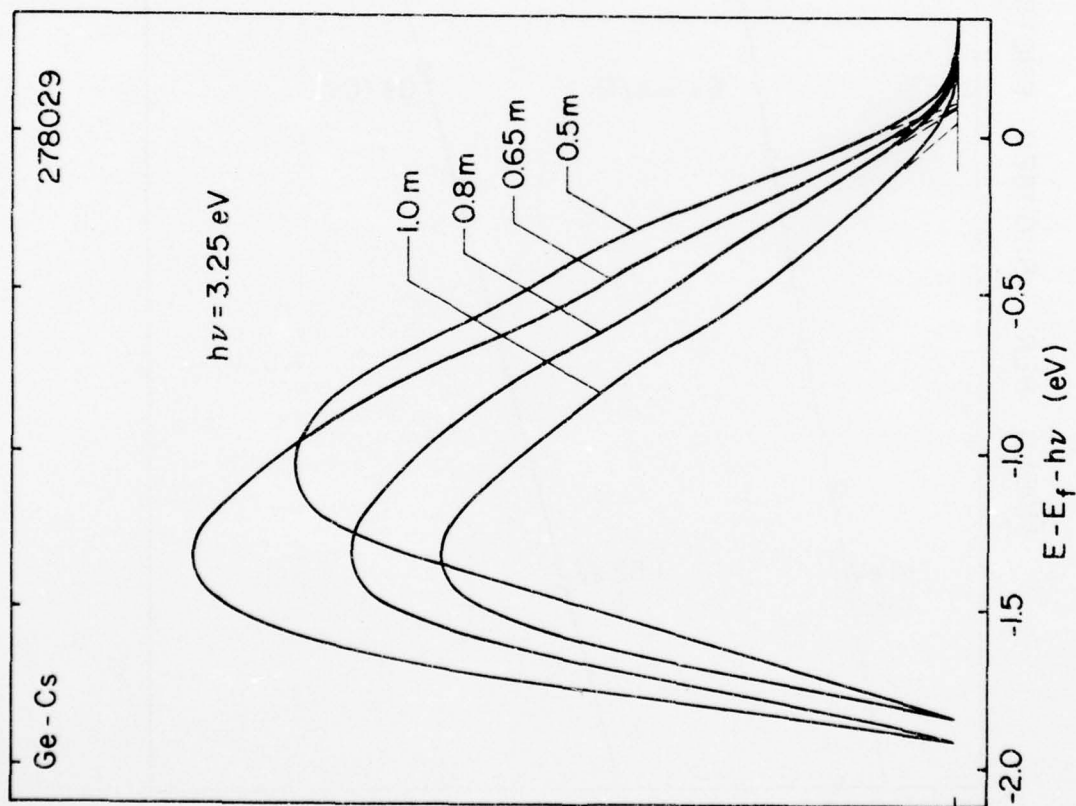
Figure 28   Ge(100)-Cs EDC's at θ=.5, .65, .8, and 1.0 m
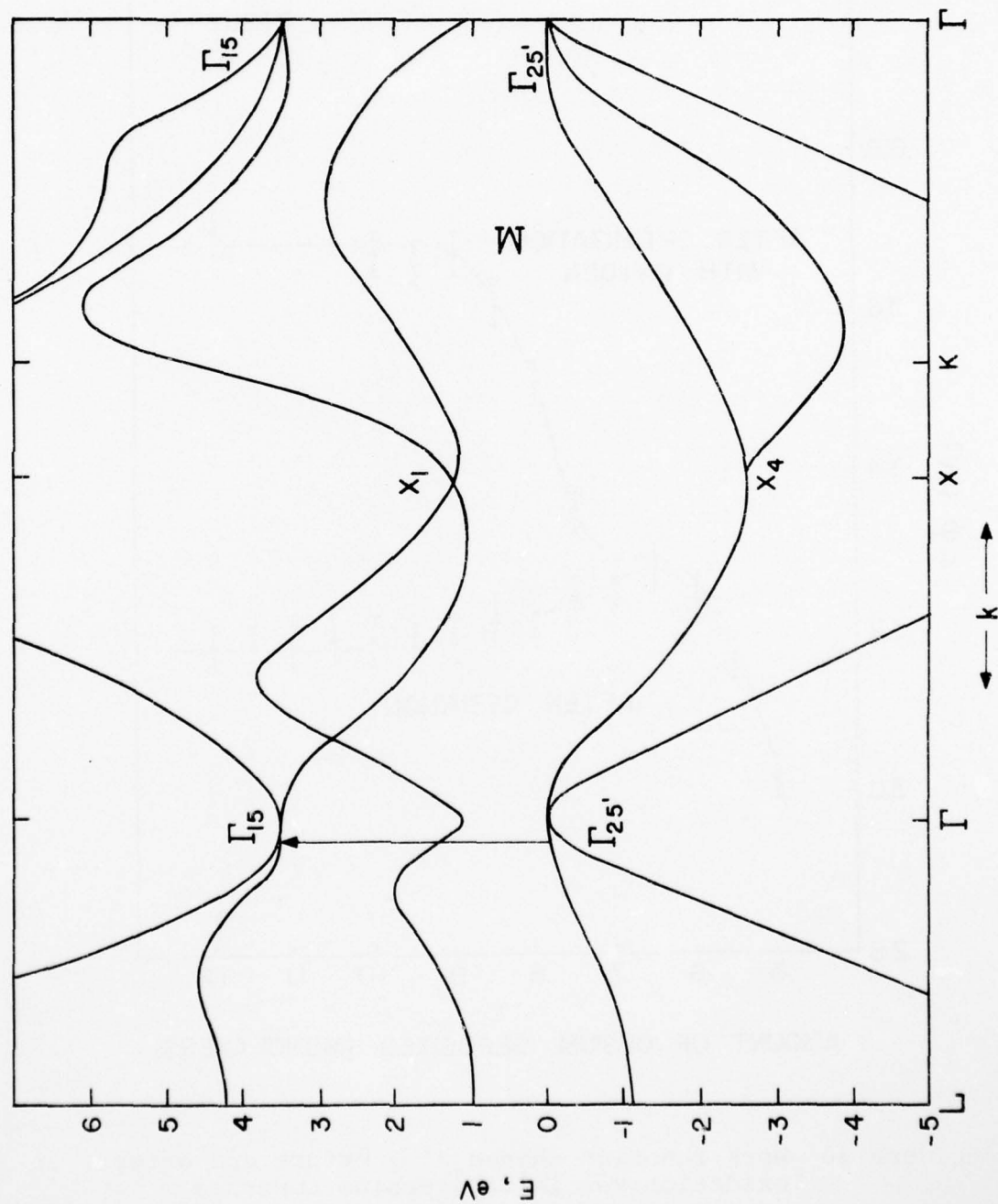
Figure 29 Band structure of germanium calculated by Cohen and Bergstresser

272029
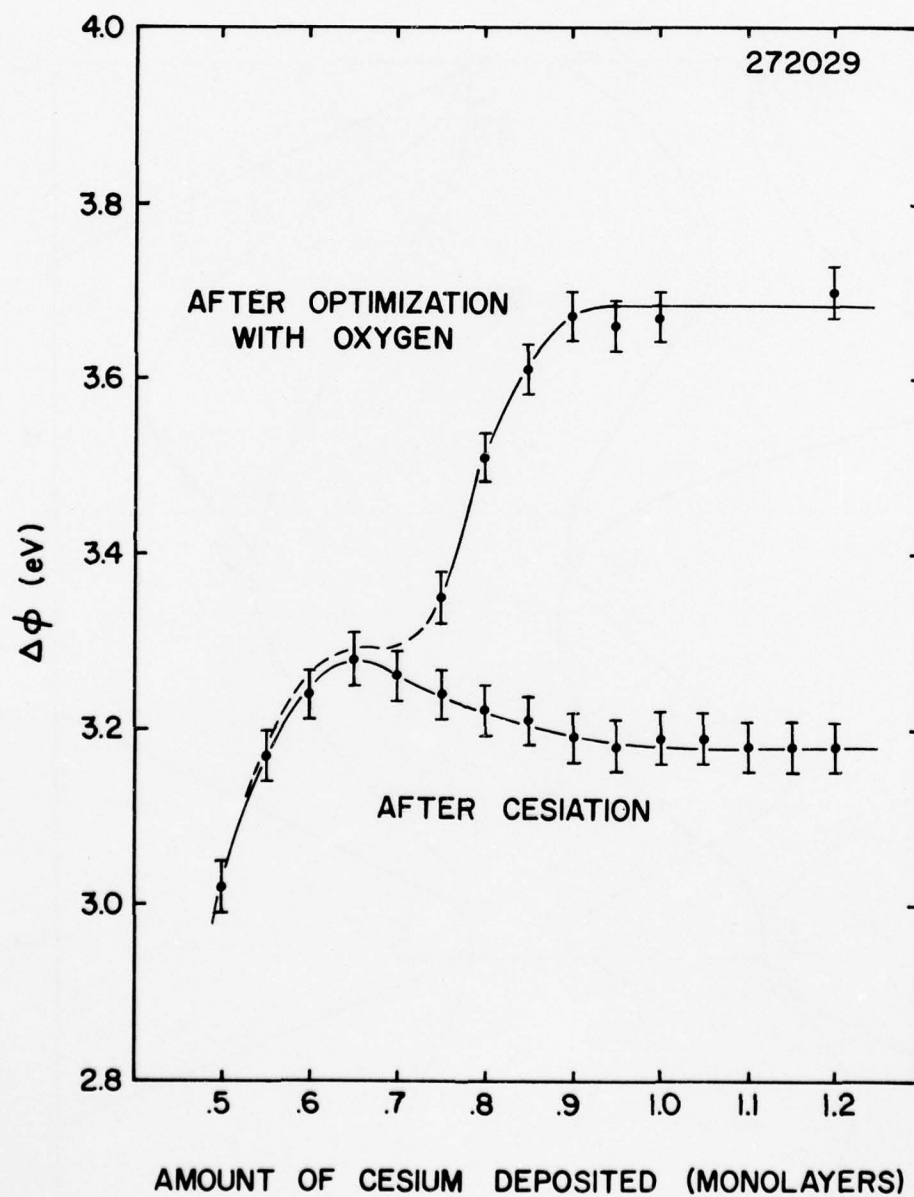
Figure 30   Work function change ($\Delta\varphi$) before and after
oxidation vs. initial cesium coverage
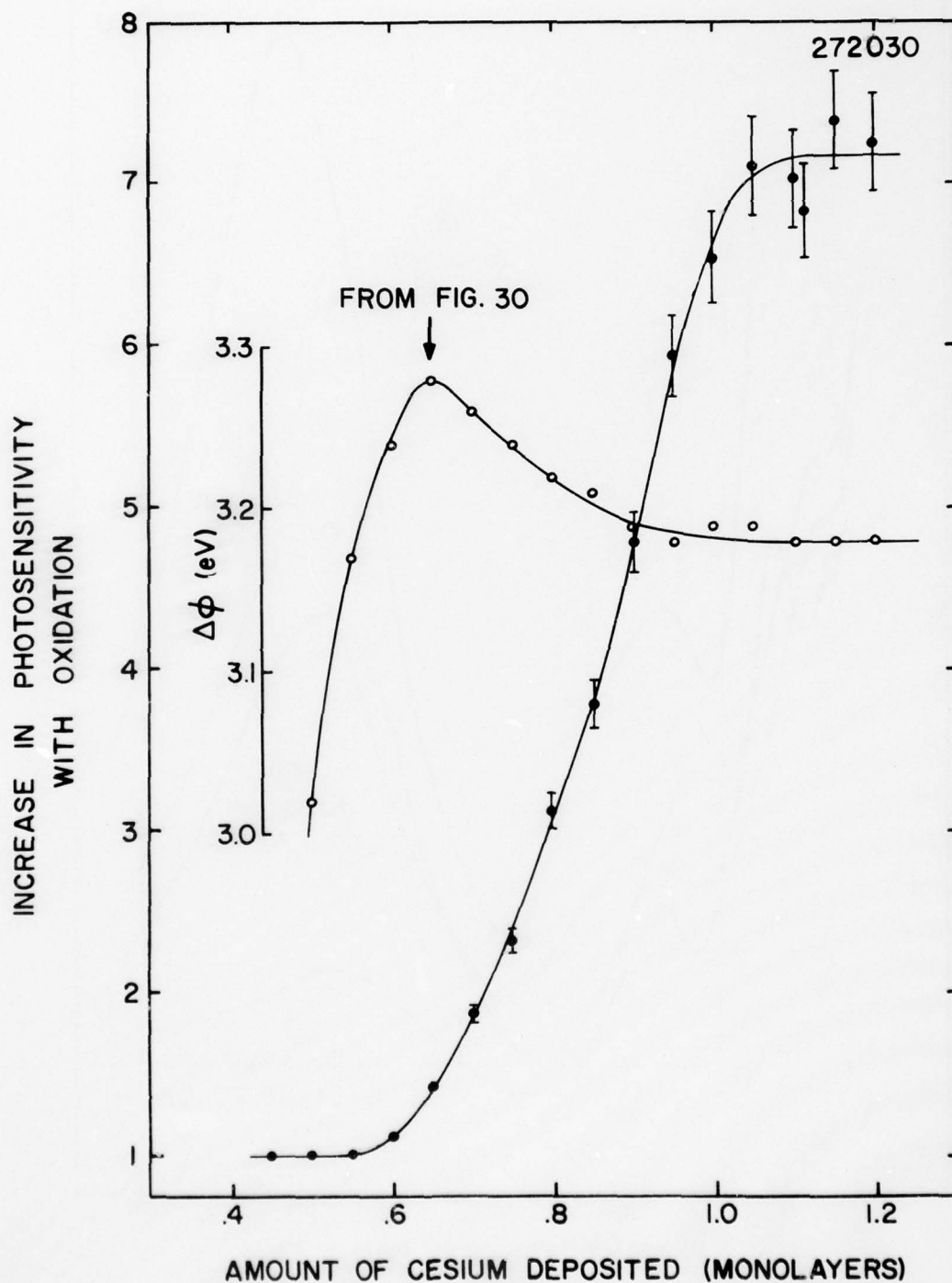
Figure 31   Increase in photosensitivity with oxidation
vs. initial cesium coverage
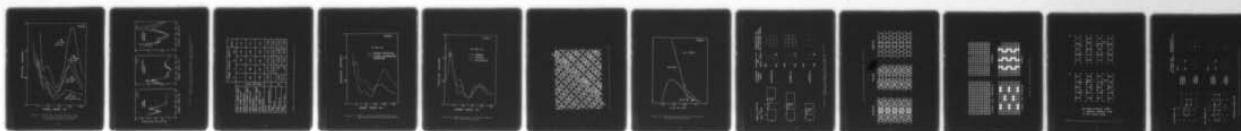
87
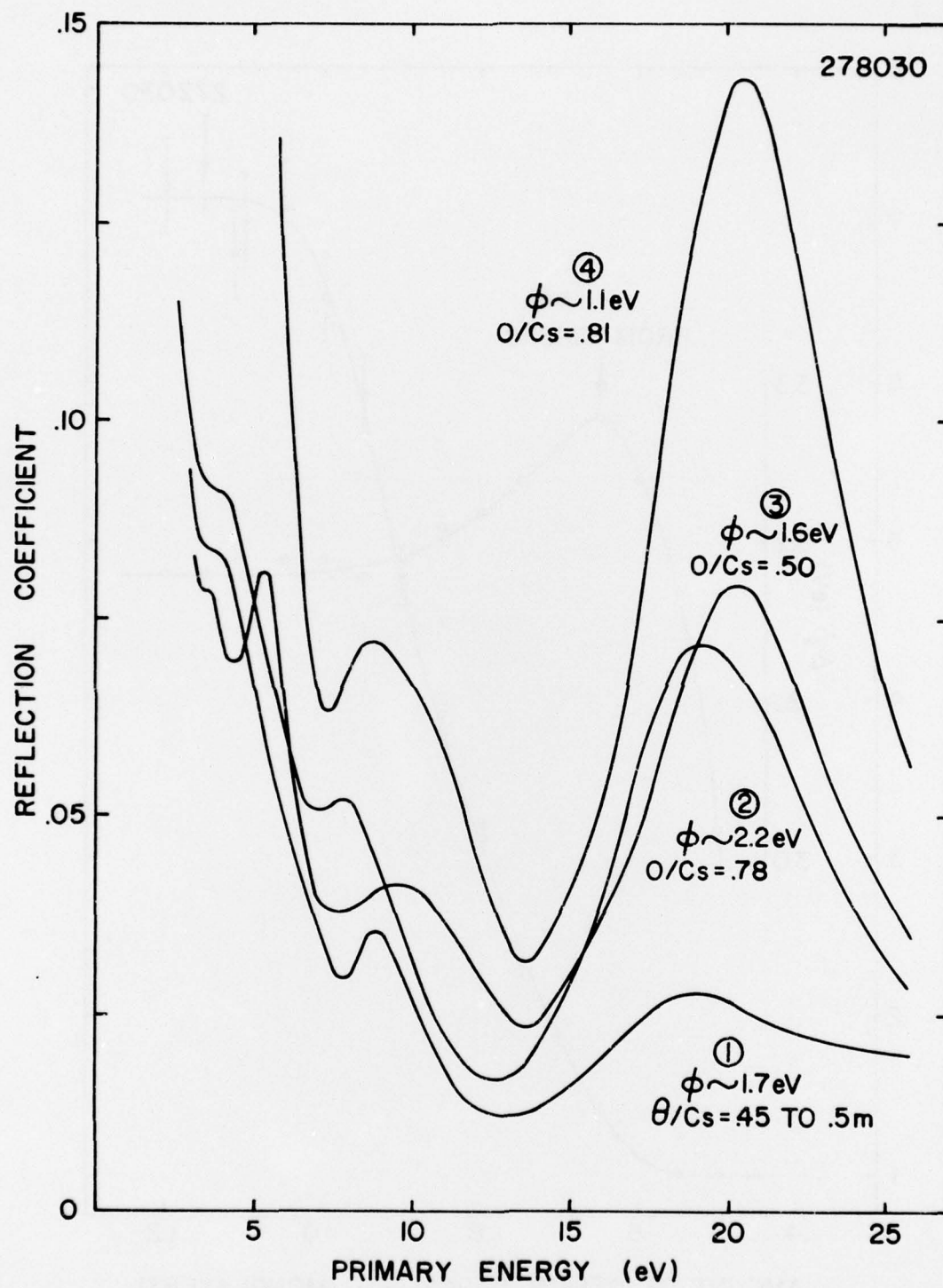
Figure 32   ESER, AES, and work function data
for a Ge/Cs/O surface produced by
a four-step activation process

88
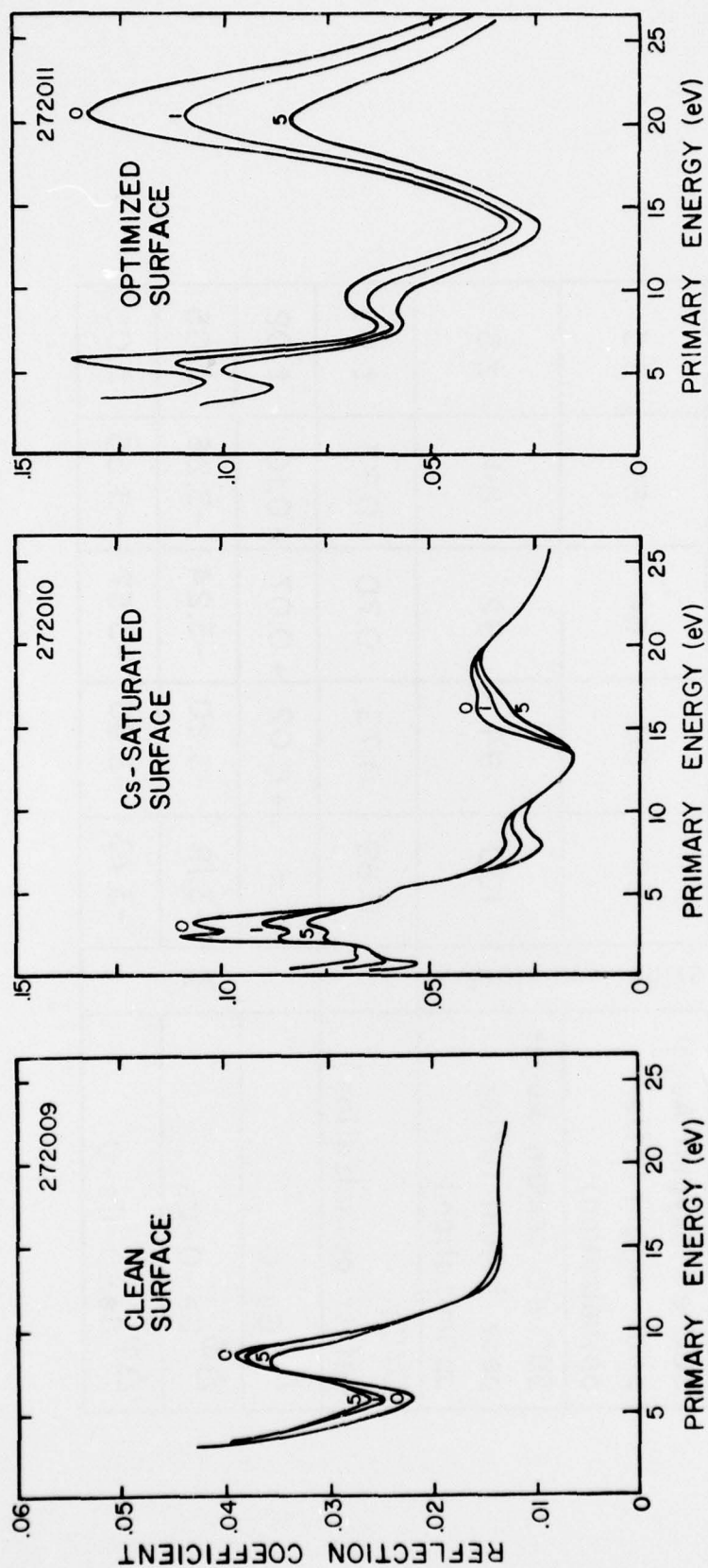
Figure 33 ESER for clean, cesium-saturated, and optimized surfaces of Ge(100) following various initial oxygen exposures

89

		Oxygen exposure relative				Error
		0	1	5	20	
520 eV oxygen Auger peak height (after initial oxidation)	Arbitrary units	–	7	16	22	±2
520 eV oxygen Auger peak height (after optimization)		69	68	64	62	±5
565 eV cesium Auger peak height (after optimization)		100	94	92	84	±5
O/Cs (after optimization)		0.69	0.73	0.70	0.73	±.05
$\Delta\phi_{Ge-O}$	eV	–	+0.02	+0.07	+0.10	±.02
$\Delta\phi_{Ge-O-Cs}$		-3.18	-3.20	-3.24	-3.26	±.05
$\Delta\phi_{Ge-O-Cs-O}$		-3.73	-3.65	-3.57	-3.56	±.05

FIGURE 34 Work function and AES data corresponding to Fig. 33
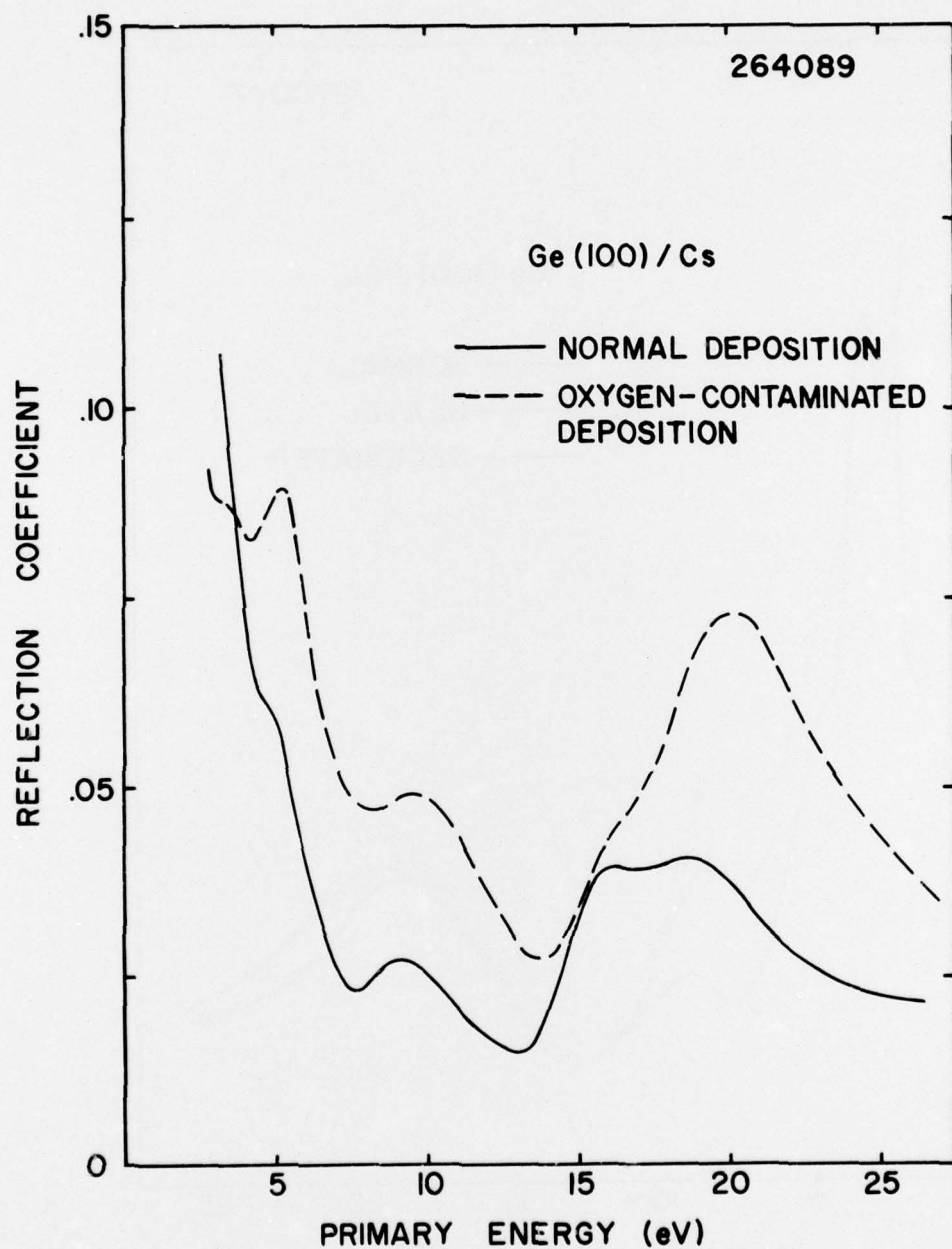
Figure 35   ESER for Ge/Cs following normal and
oxygen-contaminated cesium depositions
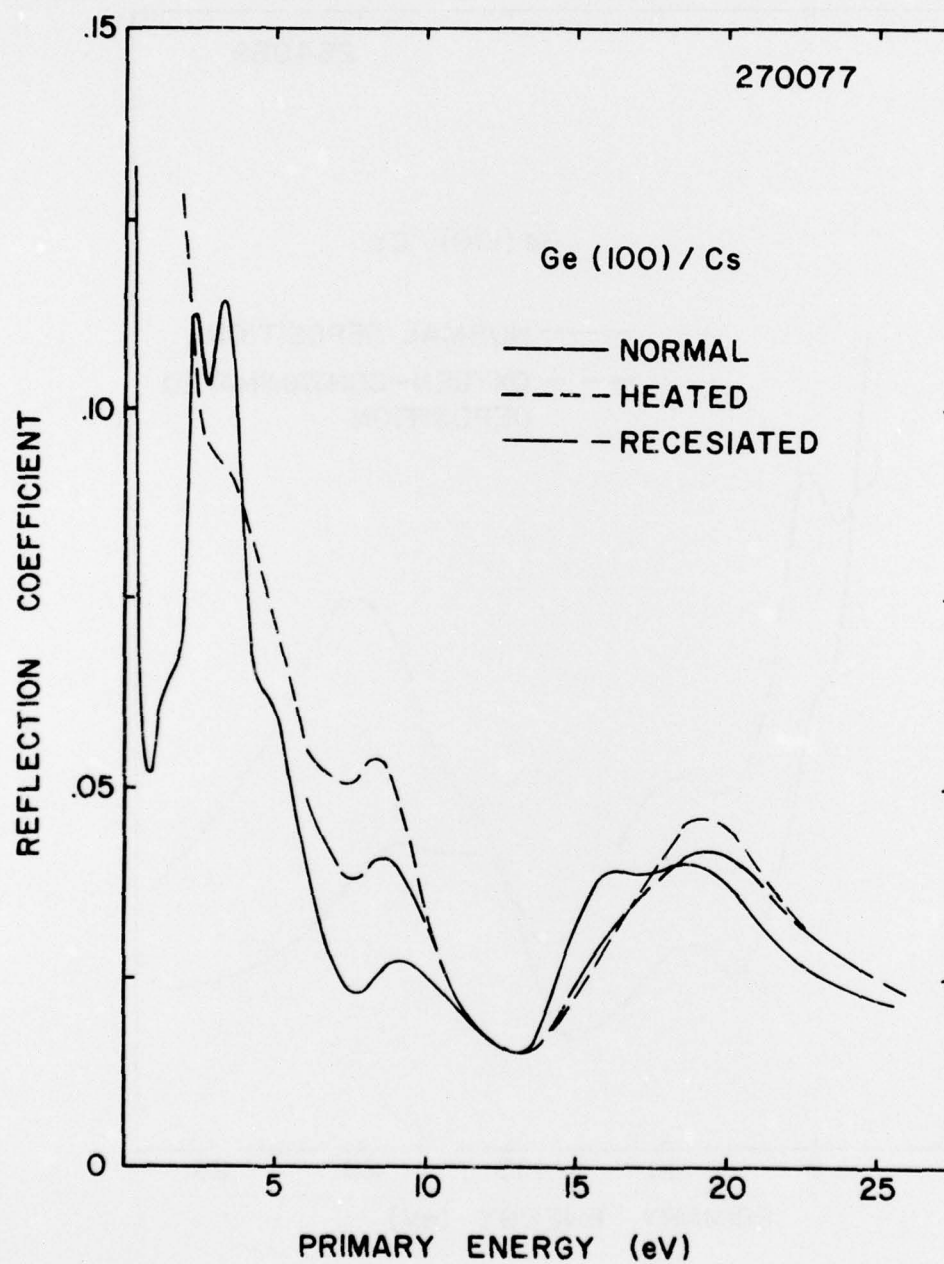
Figure 36   ESER from Ge/Cs for normal, heated
and recesiated surfaces

92
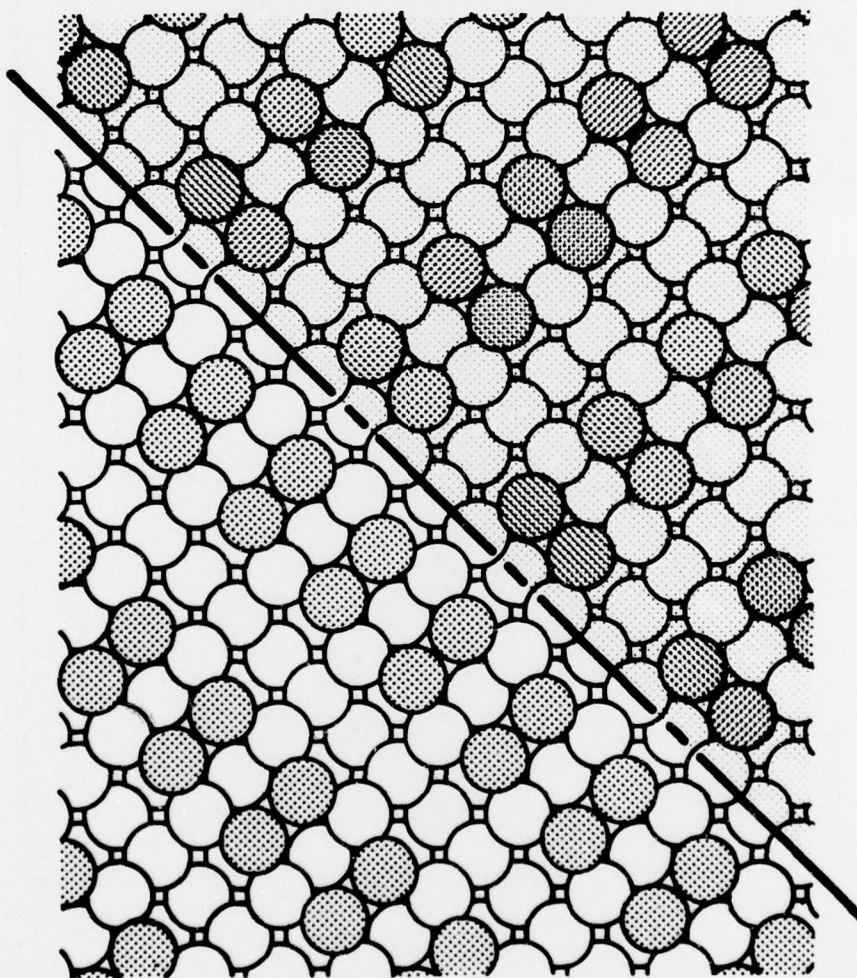
Figure 37 Schlier and Farnsworth structural model for Ge(100)

278029

hν = 3.00 eV

Ge/Cs/O

0.2 eV

E - E_f - hν (eV)
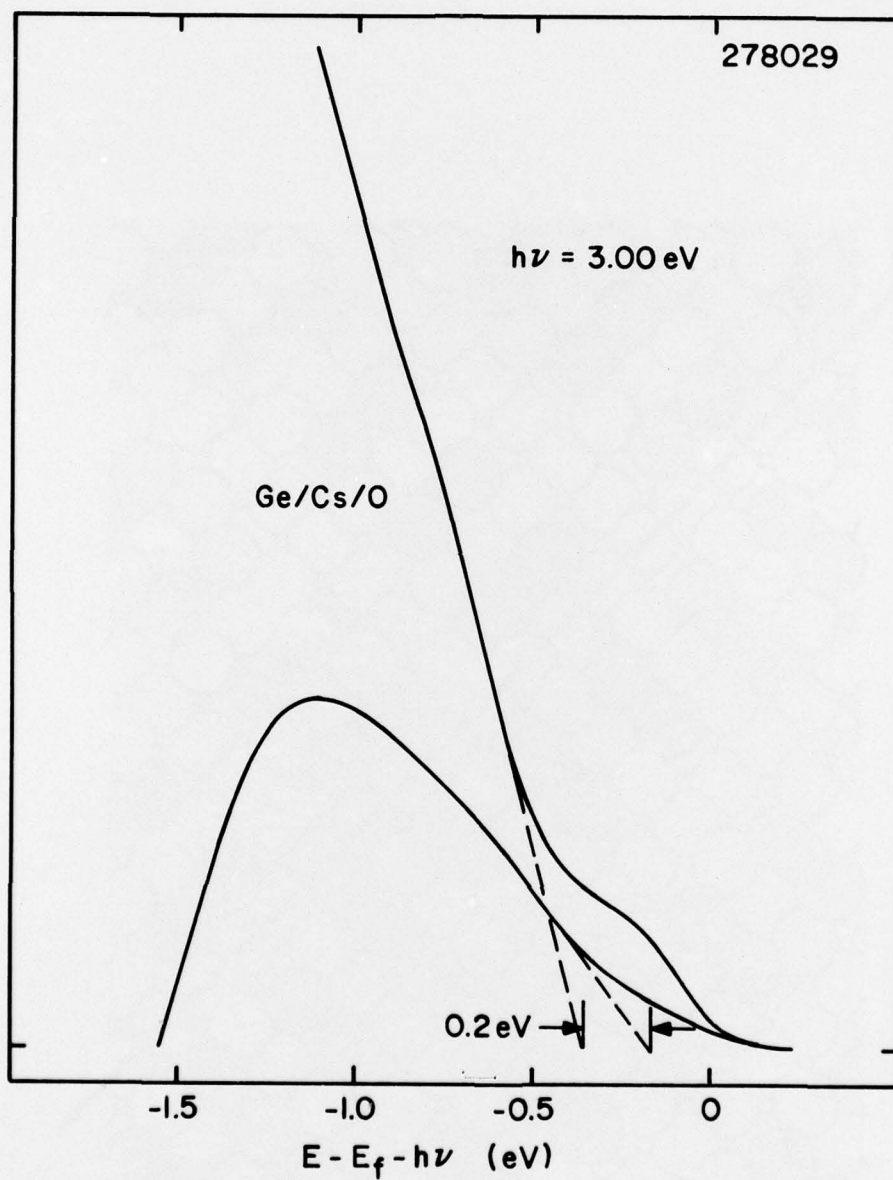
Figure 38   Comparison of Ge/Cs and Ge/Cs/O EDC's
at 3.00 eV photon energy

94
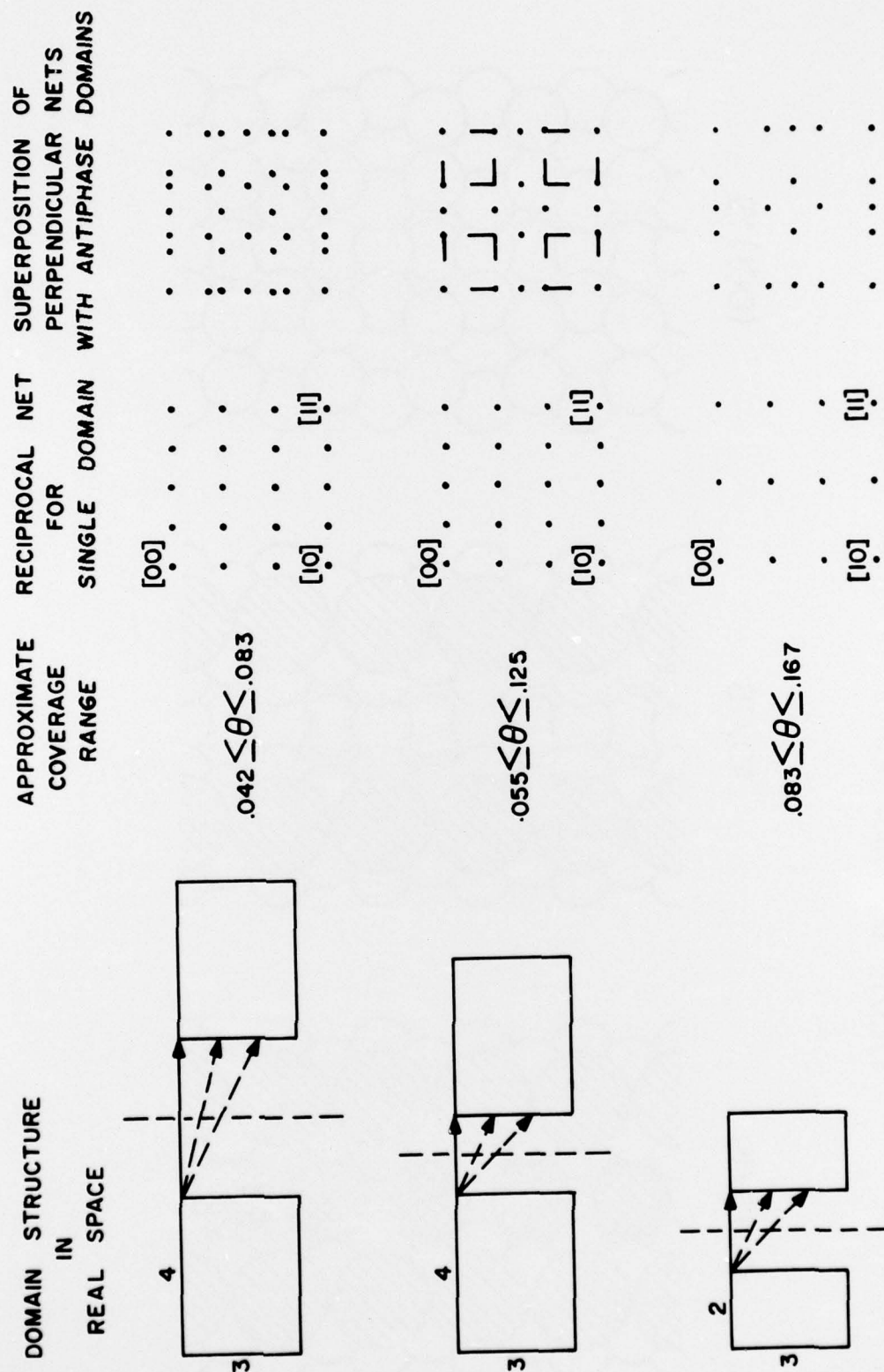
Figure 39   Effect of antiphase domains on the 4x3 and 2x3
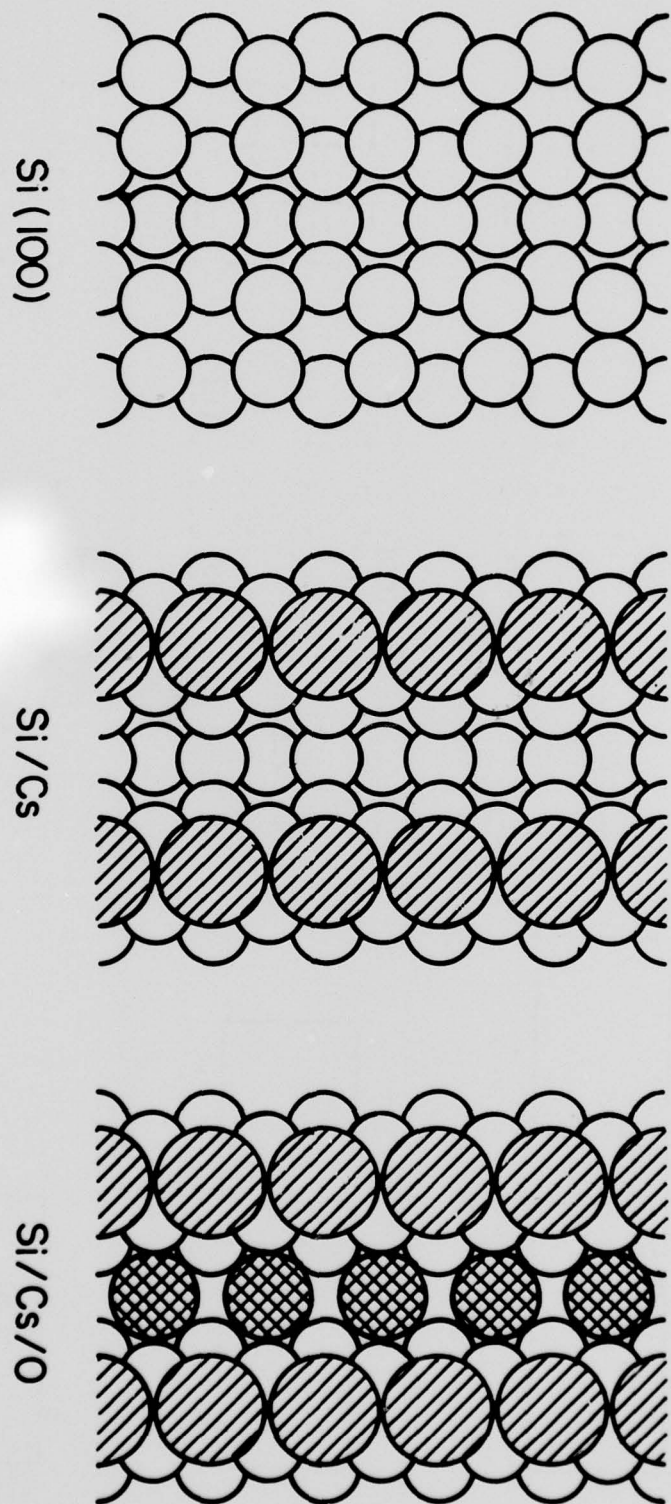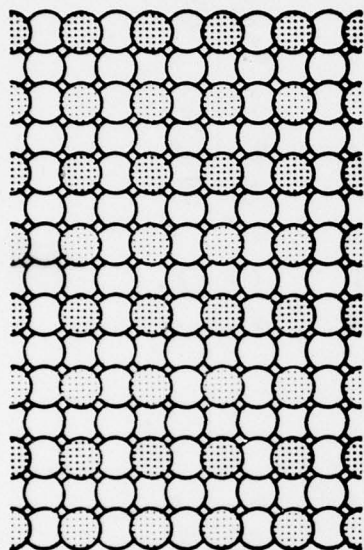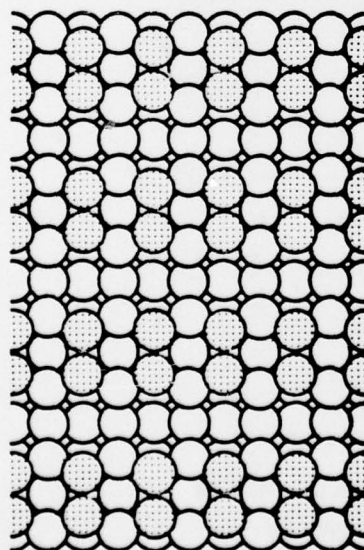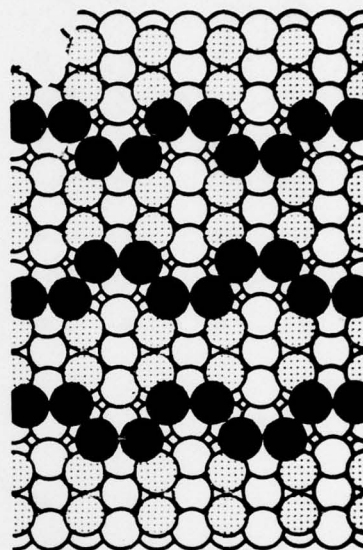LEED features observed for Ge(100)-Cs

Si (100)

Si / Cs

Si / Cs / 0

Figure 40   Levine structural model for Si/Cs/0
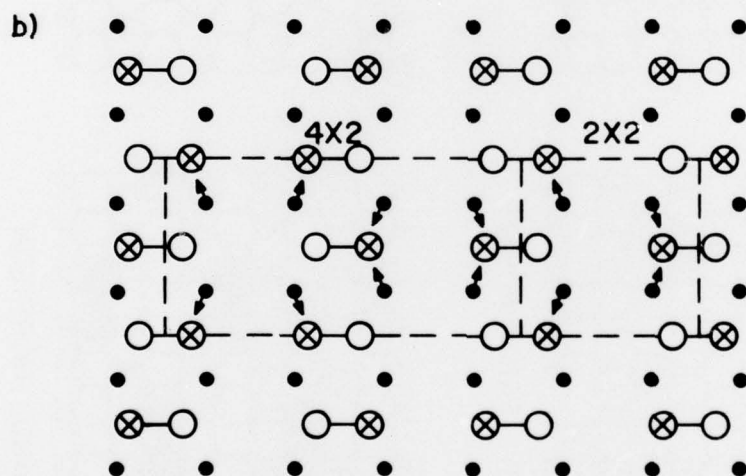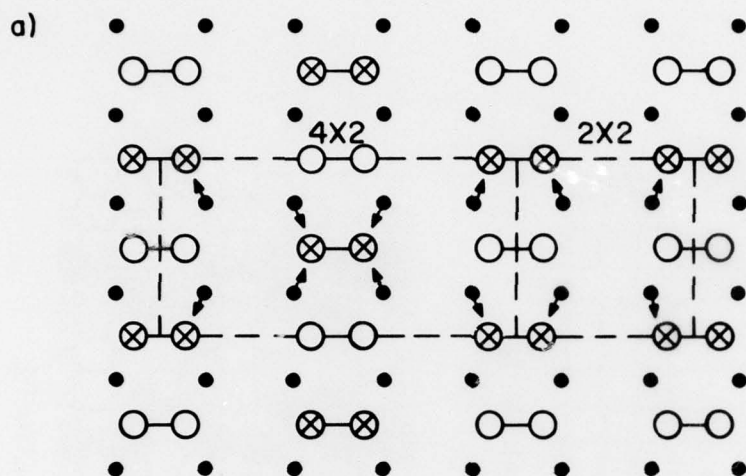
96

HANEMAN

SEIWATZ

SCHLIER AND FARNSWORTH
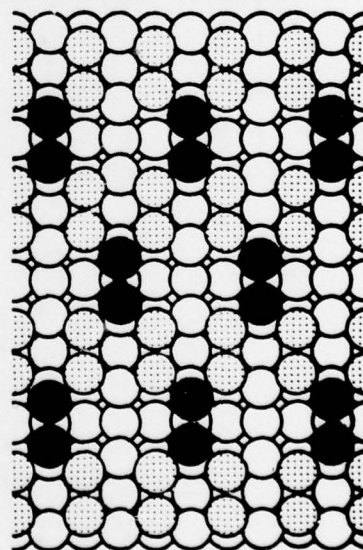
LANDER AND MORRISON

Figure 41   Ge(100) structural models

97

a)

4X2　　　2X2

b)

4X2　　　2X2

⊗ RAISED SURFACE ATOM
○ LOWERED SURFACE ATOM
• 2nd LAYER ATOM

FIGURE 42   Possible distortions of the Ge(100) surface

98

Figure 43   Effect of antiphase domains on the Ge(100) LEED pattern